# Economic Geology

BULLETIN OF THE SOCIETY OF ECONOMIC GEOLOGISTS

VOL. 99 December 2004 NO. 8

# Timing of Gold Mineralization at Red Lake, Northwestern Ontario, Canada: New Constraints from U-Pb Geochronology at the Goldcorp High-Grade Zone, Red Lake Mine, and the Madsen Mine*

B. DUBÉ,†

*Geological Survey of Canada, 880 Chemin Sainte-Foy, Quebec, Quebec, Canada G1S 2L2*

K. WILLIAMSON,

*INRS-ETE, 880 Chemin Sainte-Foy, Sainte-Foy, P.O. Box 7500, Canada G1V 4C7*

V. MCNICOLL,

*Geological Survey of Canada, 601 Booth Street, Ottawa, Ontario, Canada K1A 0E8*

M. MALO,

*INRS-ETE, 880 Chemin Sainte-Foy, Sainte-Foy, P.O. Box 7500, Canada G1V 4C7*

T. SKULSKI,

*Geological Survey of Canada, 601 Booth Street, Ottawa, Ontario, Canada K1A 0E8*

T. TWOMEY,

*Goldcorp Inc., Red Lake Mine, Balmertown, Ontario, Canada P0V 1C0*

AND M. SANBORN-BARRIE

*Geological Survey of Canada, 601 Booth Street, Ottawa, Ontario, Canada K1A 0E8*

**Abstract**

The Goldcorp High-Grade zone at the Red Lake mine has reserves (proven and probable) established at 1.775 million tons (Mt) at an average grade of 80.6 g/t Au. New U-Pb geochronologic data combined with detailed mapping and crosscutting relationships provide timing constraints and new insights into the formation of the exceptionally rich Goldcorp High-Grade zone. The results show that the main stage of the high-grade mineralization in the High-Grade zone formed before 2712 Ma and that a second stage of gold mineralization, much smaller in terms of total gold content but spectacular in terms of grade, formed after 2702 Ma. This second stage is attributed to gold remobilization caused by the enhanced thermal gradient and deformation associated with the emplacement of the Cat Island pluton (2699 Ma), approximately 7 km east of the deposit, or by the ca. 2.63 to 2.66 Ga postorogenic regional thermal event indicated by hornblende, muscovite, and biotite Ar-Ar cooling ages from the Uchi subprovince. It is proposed that the main stage of high-grade mineralization formed between ca. 2723 to 2712 Ma, possibly synchronous with emplacement of the Dome and McKenzie Island stocks, the Abino granodiorite, and Hammell Lake batholith, as well as with penetrative $D_2$ main-stage regional deformation.

*Geological Survey of Canada contribution 2003217

† Corresponding author: email, bdube@nrcan.gc.ca


, Vol. 99, pp. 1611–1641
0361-0128/01/3473/1611-31 $6.00

Lamprophyre dikes spatially associated with the deposit postdate main-stage mineralization by at least 10 m.y. A postore granodiorite dike from the Madsen mine, the second largest deposit in the district, was dated at 2698 ± 1 Ma. This age is similar to a postalteration and late-deformation diorite dike at the Creek zone showing near the former Starratt-Olsen mine, which was dated at 2696 ± 2 Ma. The crosscutting relationships confirm that the main stage of mineralization at the Madsen mine is pre-2698 Ma.

A folded and metamorphosed polymictic conglomerate located stratigraphically above the Campbell-Red Lake deposit, and deposited after ca. 2747 but before 2712 Ma, is correlated with the newly recognized Huston assemblage. Crosscutting and overprinting relationships between the conglomerate and the alteration indicate protracted multistage aluminous and iron-carbonate ± quartz veining and/or alteration event(s) before and after deposition of the conglomerate. The age of the conglomerate confirms that the Campbell-Red Lake deposit is proximal to a folded regional unconformity, consistent with the empirical relationship between large gold deposits and unconformities elsewhere in Archean greenstone belts. This paleosurface represents a key first-order exploration target, and it is proposed that areas of high potential for gold exploration in Red Lake occur in the Balmer assemblage rocks within 500 m to 1 km of the unconformity.

## Introduction

THE WORLD-CLASS Campbell-Red Lake deposit (Fig. 1) is actively mined by Placer Dome Inc. (Campbell mine) and Goldcorp Inc. (Red Lake mine) and represents one of the largest and richest Canadian Archean gold deposits (>20 Moz Au). The Goldcorp High-Grade zone at the Red Lake mine, formerly known as the A.W. White mine and the Dickenson mine, has produced 1.5 Moz at an impressive average grade of 88 g/t Au since the beginning of its extraction in 2001. Reserves (proven and probable) are established at 1.775 million tons (Mt) at an average grade of 80.6 g/t Au (Goldcorp Inc., 2003). The study of such high-grade mineralization has helped to define fundamental geologic parameters controlling the formation of high-grade ore and to develop exploration guidelines for such targets (Dubé et al., 2001a, b, 2002, 2003; Chi et al., 2002, 2003).

The Campbell-Red Lake deposit is a complex deposit and its genesis is the subject of debate. Penczak and Mason (1997, 1999) and Damer (1997) proposed a premetamorphic low-sulfidation epithermal origin, whereas other workers have proposed a synmetamorphic-syntectonic origin (Rigg and Helmsteadt, 1981; Mathieson and Hodgson, 1984; Andrews et al., 1986; Christie, 1986; Rogers, 1992; Zhang et al., 1997; Tarnocai, 2000; Dubé et al., 2001a, 2002, 2003; Twomey and McGibbon, 2001; M. O'Dea, unpub. rept. for Goldcorp Inc., 1999; N. Archibald and V. Wall, unpub. rept. for Goldcorp Inc., 2000). The Campbell-Red Lake deposit potentially

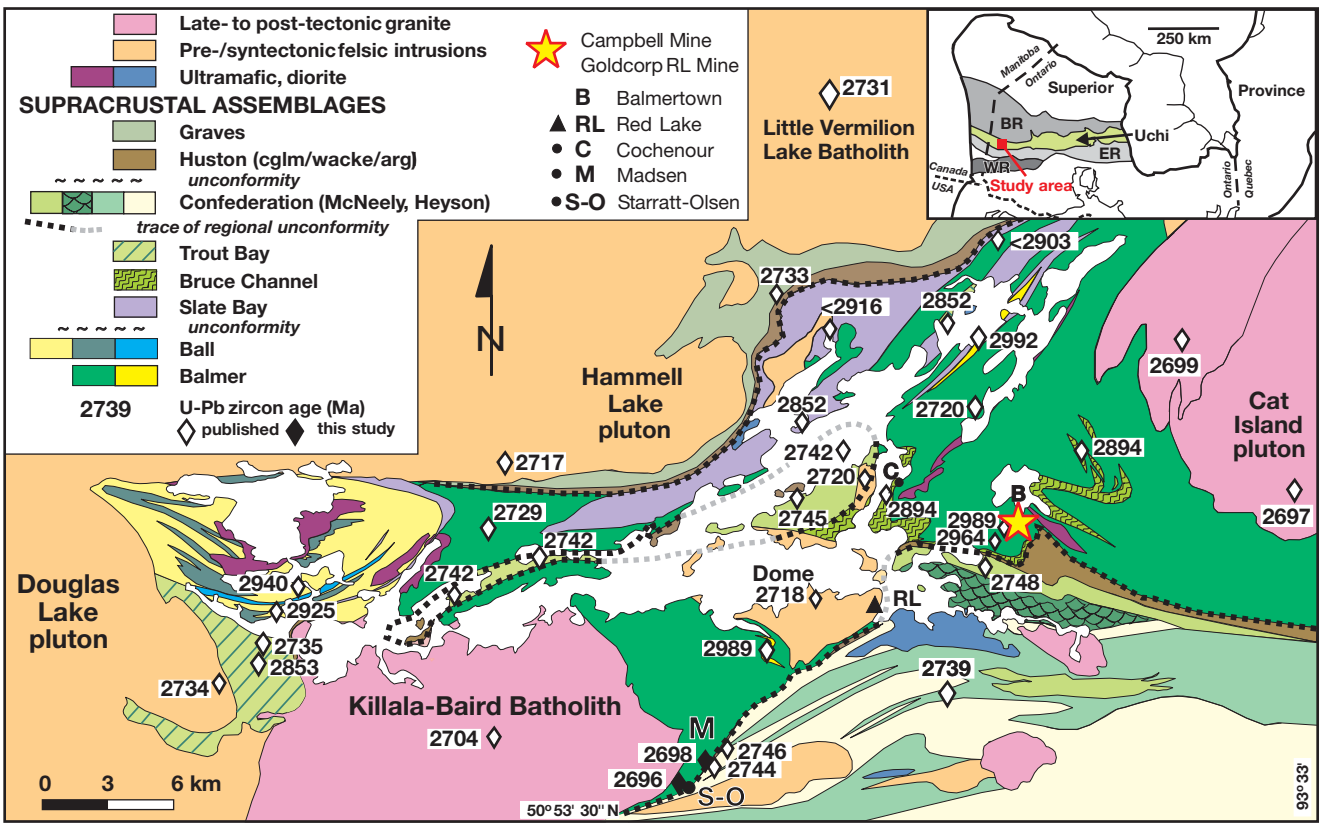


FIG. 1. Geology of the Red Lake greenstone belt (from Sanborn-Barrie et al., 2001; modified from Stott and Corfu, 1991). BR = Berens River subprovince (North Caribou terrane), ER = English River subprovince, WR = Winnipeg River terrane. See Figure 15 caption for reference to the ages displayed. Argl = argillite, cglm = conglomerate.

represents the end product of several stages of hydrothermal alteration, gold mineralization, and episodic brittle-ductile deformation (MacGeehan and Hodgson, 1982; Dubé et al., 2002). Dubé et al. (2003) concluded that gold mineralization was a result of multistage alteration and veining event(s) comprising pre- and early-$D_2$ iron-carbonate and aluminous alteration, followed by arsenopyrite-rich silicification and gold precipitation, as well as some late carbonatization and gold remobilization.

One of the keys to a better understanding of the formation of the deposit is the timing of the high-grade mineralization relative to the increments of deformation, metamorphism, and hydrothermal activity. This is one of the outstanding problems in the understanding of the formation of orogenic gold deposits (Groves et al., 2003). The interpretation of the age of gold mineralization in the Red Lake district has evolved from largely synvolcanic (Cowan, 1979; Kerrich et al., 1981; Kusmirski 1981; Pirie, 1981), to preregional deformation and metamorphism and associated with strike-slip faulting within the interval of 2722 to 2710 Ma (Penczak and Mason, 1997, 1999), to syndeformation, related to tectonomagmatism within the interval 2720 to 2700 Ma (Andrews et al., 1986; Corfu and Andrews, 1987; Parker, 2000), to late tectonic at ca. 2700 Ma (Tarnocai, 2000). MacGeehan and Hodgson (1982) proposed three periods of mineralization that include an early synvolcanic stage, followed by two younger syn-to late-deformation stages that predated emplacement of late mafic to felsic dikes. Menard et al. (1999) proposed two stages of gold mineralization, with the main stage corresponding to $D_2$ and occurring between 2720 to 2715 Ma and a subsequent but lesser event in terms of total gold content at around ca. 2700 Ma, represented by auriferous quartz-pyrite-tourmaline vein-type deposits (e.g., Buffalo mine) hosted by the ca. 2718 Ma Dome stock. A model age for galena calculated from samples of gold, chalcopyrite, pyrite, and galena using the western Superior province model indicated a first stage of gold mineralization in the Red Lake district responsible for the formation of the Campbell-Red Lake deposit at ca. 2865 Ma and a much younger stage for gold mineralization at the Madsen and Starratt-Olsen deposits at ca. 2715 to 2709 Ma (Gulson et al., 1993). The new U-Pb geochronologica data presented here provide additional timing constraints and new insights on the formation of the Goldcorp High-Grade zone based on detailed mapping and crosscutting relationships between high-grade ore and intrusive dikes. Our study indicates that (1) at least part of the carbonate alteration predated deposition of the conglomerate of the Huston assemblage, (2) main-stage gold mineralization in the High-Grade zone occurred before 2712 Ma, (3) second-stage gold mineralization occurred after 2702 Ma, and (4) the minimum age of the brittle-ductile regional deformation in the deposit area is $2699^{+2}_{-1}$ Ma, indicated by the age of unstrained shallowly dipping lamprophyre dikes.

## Regional Geologic Setting

The Red Lake greenstone belt is located in the Uchi subprovince of the Superior province (Fig. 1). The greenstone belt is dominated by Mesoarchean mafic-ultramafic volcanic rocks of the Balmer assemblage (2.99–2.96 Ga), intermediate to felsic calc-alkaline flows and pyroclastic rocks of the Ball assemblage (2.94–2.92 Ga), and intermediate calc-alkaline pyroclastic rocks overlain by clastic sedimentary rocks and banded iron-formation of the Bruce Channel assemblage (2.894 Ga; first volcanic cycle; Pirie, 1981; Andrews et al., 1986; Wallace et al., 1986; Corfu and Andrews, 1987; Parker 2000; Sanborn-Barrie et al., 2000, 2001, 2002, and references therein). The Bruce Channel assemblage appears to disconformably overlie the Balmer assemblage (Sanborn-Barrie et al., 2001). The Mesoarchean rocks were tilted by a pre-$D_1$ episode of deformation and a regional angular unconformity separates the Mesoarchean rocks from the Neoarchean (i.e., 2.8–2.5 Ga) volcanic rocks (Sanborn-Barrie et al., 2000, 2001). The unconformity is locally draped by polymictic conglomerate that gives way to a Neoarchean volcanic succession (second volcanic cycle of Pirie, 1981), including calc-alkaline and tholeiitic volcanic rocks of the ca. 2.75 to 2.73 Ga Confederation assemblage (McNeely and Heyson sequences, respectively) and calc-alkaline rocks of the ca. 2.732 Ga Graves assemblage (Fig. 1). Polymictic conglomerate and finer clastic sedimentary rocks of the Huston assemblage separate the Confederation and Graves assemblages on the north shore of Red Lake. In the vicinity of the Red Lake mine, the conglomerate of the Huston assemblage rests unconformably on a substrate of supracrustal rocks of the Balmer and Bruce Channel assemblages (Sanborn-Barrie et al., 2001, 2002).

Four stages of plutonism, at ca 2.74, 2.73, 2.72 to 2.71, and 2.7 to 2.698 Ga, are recorded in the belt (Fig. 1). Two main episodes of deformation ($D_1$, $D_2$) took place after ca. 2742 Ma volcanism (Sanborn-Barrie et al., 2001). The main stages of penetrative deformation produced two sets of folds ($F_1$ and $F_2$). A locally recognized northerly trending $S_1$ foliation is axial planar to north-northeast–trending $F_1$ folds. According to Sanborn-Barrie et al. (2001, 2002), $D_1$ coincided with the deposition of the polymictic conglomerate of the Huston assemblage and preceded the eruption of the Graves assemblages at ca. 2733 Ma (Sanborn-Barrie et al., 2001). $D_1$ deformation probably occurred between 2742 and 2733 Ma in response to east-directed shortening. A weakly to moderately developed $S_2$-$L_2$ fabric and associated southeast-trending $F_2$ folds are widespread in the eastern Red Lake area where the deposit is located. The main cleavage-forming stage of $D_2$ deformation and associated metamosphism predated 2718 Ma (i.e., the age of the Dome stock), but foliation coplanar with $S_2$ and amphibolite facies metamorphism outlasted emplacement of the Dome stock, indicating that $D_2$ shortening continued beyond its emplacement (Sanborn-Barrie et al., 2002, 2004). Sanborn-Barrie et al. (2004) suggest that $D_2$ strain across the Red Lake greenstone belt occurred between ca. 2720 to 2715 Ma and recorded the collisional stage of the Uchian phase of the Kenoran orogeny (cf. Stott et al., 1989; Stott and Corfu, 1991). Across the Red Lake belt, and elsewhere throughout the Uchi subprovince, the Uchian phase of the Kenoran orogeny was related to collision between the ca. 3.0 Ga North Caribou terrane to the north of the Red Lake greenstone belt and the ca. 3.4 Ga Winnipeg River terrane to the south (Fig. 1). Postcollisional $D_3$ strain is locally recorded in the Red Lake belt after 2700 ± 6 Ma, the maximum age of a deformed and metamorphosed conglomerate near the Madsen mine area that displays a penetrative foliation coplanar with $D_2$ fabrics (Sanborn-Barrie et al., 2004).

An orogenic setting has been proposed for arclike magmatism, deformation, hydrothermal alteration, and metamorphism in the Red Lake gold camp (Stott and Corfu, 1991; Sanborn-Barrie et al., 2000, 2001). In contrast previous studies proposed that gold mineralization and deformation in the district were directly related to the emplacement of granitoid batholiths marginal to the belt (Hugon and Schwerdtner, 1984; Andrews et al., 1986; Corfu and Wallace, 1986; Corfu and Andrews, 1987). Amphibolite facies metamorphism of supracrustal rocks at the margins of the belt was attributed to the thermal affect of batholithic emplacement, whereas rocks in the central part of the belt are of lower grade (Hugon and Schwerdtner, 1984; Andrews et al., 1986; Stott and Corfu, 1991; Menard and Pattison, 1998, Tarnocai, 2000). However, Thompson (2003) showed that the patterns of major metamorphic boundaries are cut by, and hence older than, several of the major batholiths. Menard et al. (1999) defined a sequence of four tectono-metamorphic events ($D_1$-$D_4$) throughout the Red Lake greenstone belt that occurred between 2740 to 2700 Ma. The first three are associated with plutonism, whereas $D_4$ is late (2680–2650 Ma) and characterized by brittle faulting. They further proposed that the regional $D_2$ stage of deformation described above could be divided into two distinct events, $D_2$-$M_2$ (2720–2715 Ma), which coincided with the thermal peak of metamorphism (amphibolite facies), and $D_3$-$M_3$ (2700 Ma).

The majority of the large gold deposits in the Red Lake district are hosted by the Mesoarchean Balmer assemblage and are proximal to the regional angular unconformity between the ca. 2.99 Ga Balmer and ca. 2.75 to 2.74 Ga Confederation assemblages (Sanborn-Barrie et al., 2001; Dubé et al., 2003). The deposits are either hosted by amphibolite facies rocks (Madsen mine) or the amphibolite-greenschist isograd occurs within the deposit (Campbell-Red Lake deposit; Mathieson and Hodgson, 1984; Andrews et al., 1986; Christie, 1986; Damer, 1997; Dubé et al., 2000; Parker, 2000; Tarnocai, 2000), suggesting an empirical relationship between major gold deposits and peak metamorphism in the district (Andrews et al., 1986; Menard et al., 1999; Tarnocai, 2000). More recently, Thompson (2003) proposed that the deposits generally occur in close proximity to the transition between the greenschist and amphibolite facies.

## Local Geologic Setting

A brief summary of the local geologic setting of the Campbell-Red Lake deposit is presented below. Readers are referred to MacGeehan and Hodgson (1982), Andrews et al. (1986), Rogers (1992), Penczak and Mason (1997, 1999), Zhang et al. (1997), Tarnocai (2000), Twomey and McGibbon (2001), and Dubé et al. (2001a, 2002, 2003), among others, for more detail.

The Campbell-Red Lake gold deposit is hosted mainly by tholeiitic basalt and locally by komatiitic basalt of the Mesoarchean Balmer assemblage. Peridotitic komatiite, variolitic basalt, rhyolite, and associated mafic intrusions of the ca. 2.99 to 2.96 Ga Balmer assemblage and felsic pyroclastic rocks with clastic and chemical sedimentary rocks of the ca. 2.984 Ga Bruce Channel assemblage complete the sequence in the mine (Penczak and Mason, 1997; Dubé et al., 2000a; Twomey and McGibbon, 2001; Fig. 2). The deposit occurs stratigraphically below a folded regional unconformity marking the contact between locally overturned rocks of the Balmer and Bruce Channel assemblages and overlying Neoarchean volcanic rocks of the Confederation assemblage (Fig. 1; Sanborn-Barrie et al., 2002; Dubé et al., 2003). In the deposit area, this contact is marked by a younger intravolcanic sequence of clastic rocks (Huston assemblage) that contains zircons derived almost exclusively from the 2.747 to 2.743 Ga Confederation age assemblage (McNeely sequence; Sanborn-Barrie et al., 2002; this paper). However, the conglomerate also contains a vast number of subangular to subrounded clasts derived from underlying Mesoarchean lithologies in and around the Red Lake mine (notably chemical sediments and chert of the Bruce Channel assemblage). On level 16 of the Red Lake mine, the conglomerate is in tectonic contact with basalt of the Balmer assemblage (Dubé et al., 2003). Therefore, the conglomerate of the Huston assemblage is probably contemporaneous with the early Neoarchean McNeely sequence but cuts farther down to the Bruce Channel and Balmer assemblages.

According to Christie (1986), the metamorphic conditions at the Campbell mine are constrained to middle to upper greenschist facies. In contrast, Damer (1997) interprets the metamorphism of host rocks at the Red Lake mine to have reached amphibolite facies, the product of contact metamorphism induced by the emplacement of the Cat Island pluton to the east (Fig.1). A new assessment of metamorphic assemblages across the belt (Thompson, 2003) supports Christie's (1986) work, placing the Campbell-Red Lake deposit close to the transition between middle and upper greenschist facies.

Based on relative chronology and U-Pb dating (see below), rocks of the mine sequence are affected by four generations of structures, $D_1$ through $D_4$, which we interpret as resulting from various increments of deformation. Their corresponding structures are described as $S_1$, $F_1$, $S_2$, $F_2$, etc. The terminology does not necessarily imply four different episodes of deformation. The mine sequence is located on the eastern limb of a regional north-northeast–trending $F_1$ anticline (Sanborn-Barrie et al., 2001, Dubé et al., 2003). All units have been tightly refolded by southeast-trending and southwest- or southeast-plunging (≈60°) $F_2$ folds forming antiform-synform pairs as illustrated by the geometry of the peridotitic komatiite in Figure 2. The superposition of $D_1$ and $D_2$ results locally in a type-2 interference fold pattern (Ramsay and Huber, 1987). The southeast-striking $S_2$ foliation represents the main fabric. The $F_2$ folds are disrupted by three subparallel, steeply dipping (70°–80°S), southeast-trending brittle-ductile structures, the Dickenson, New Mine (also known as Red Lake fault), and Campbell faults, which coincide with the transposed limbs of $F_2$ folds and can be traced along strike for more than 1,500 m (Fig. 2). The Campbell and New Mine faults have recorded a reverse-sinistral component of motion, whereas the Dickenson fault has an apparent dextral component of motion (MacGeehan and Hodgson, 1982; Mathieson and Hodgson, 1984; Rogers, 1992; Penczak and Mason, 1997; Dubé et al., 2001a, 2002; Twomey and McGibbon, 2001; N. Archibald and V. Wall, unpub. rept. for Goldcorp Inc., 2000). These faults coincide spatially with a large proportion of the ore zones in the Campbell-Red Lake deposit and with $D_2$ folds and fabrics, collectively defining a southeast deformation corridor known as the Red Lake mine trend (Cochenour-Gullrock deformation zone of Hugon and

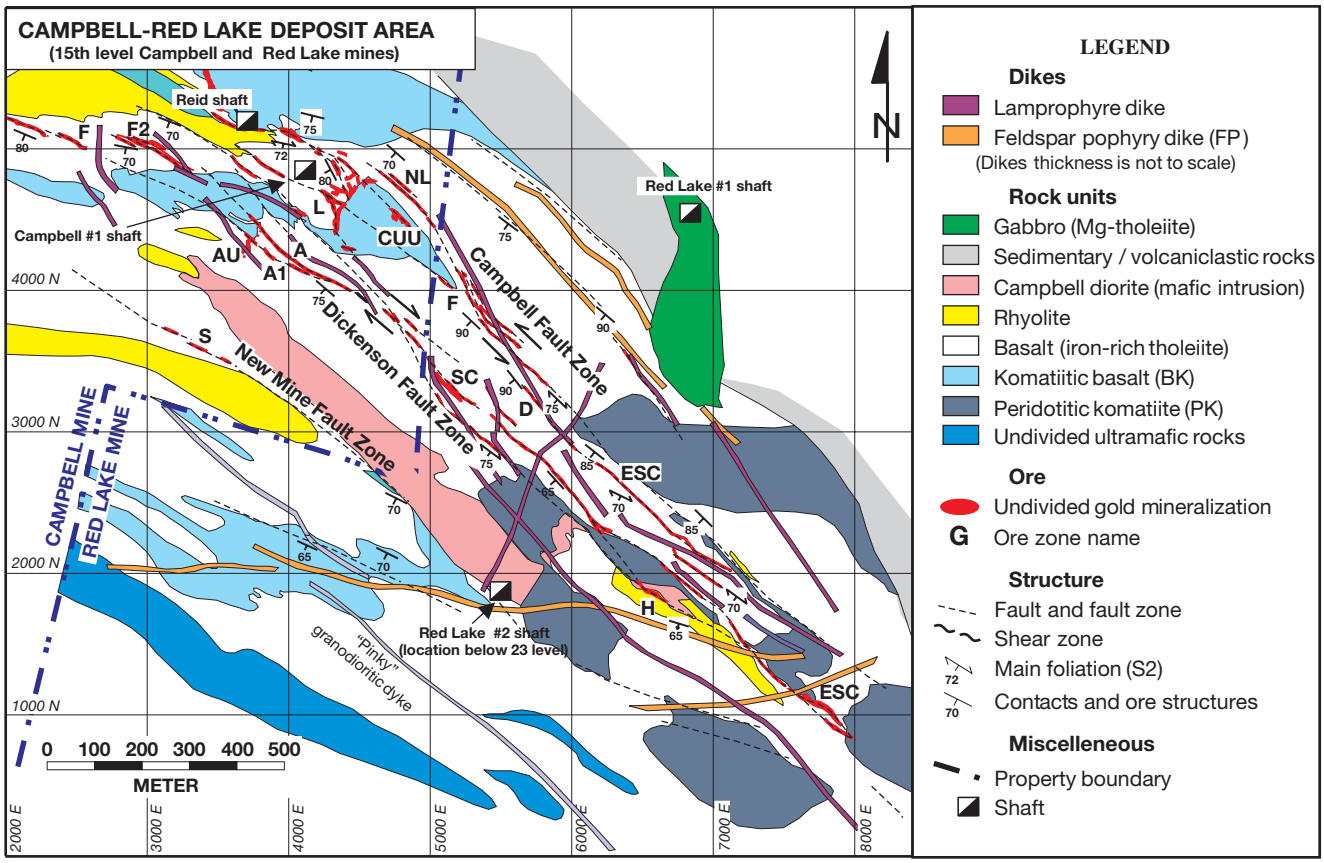


FIG. 2. Geology of level 34, Campbell-Red Lake deposit (from Dubé et al., 2001a; modified from Goldcorp Ltd. geologic data).

Schwerdtner, 1984, and Andrews et al., 1986), and have played a key role in the formation and/or deformation of the deposit (Rogers, 1992; Penczak and Mason, 1997; Tarnocai, 2000; Dubé et al., 2002, and references therein; N. Archibald and V. Wall, unpub. rept. for Goldcorp Inc., 2000). $S_3$ is a weakly to moderately developed foliation, coplanar with $S_2$ and recorded in various sets of feldspar porphyry granodiorite and lamprophyre dikes (see below) that crosscut both limbs of $F_2$ folds as well as the Red Lake mine trend structural corridor (Figs. 2–3A). A postdike, $S_3$ foliation also has been documented at the Campbell mine by Penczak (1996), Zhang et al. (1997), and Tarnocai (2000). $D_3$ is interpreted to be a result of northeast-oriented regional shortening but is significantly less intense than the predike $D_2$ deformation, as the dikes hosting the $S_3$ foliation and cutting across $F_2$ fold limbs and the Red Lake mine trend remain straight compared to the folded and faulted volcanic rocks. $D_3$ may represent a late increment of a continuous $D_2$ to $D_3$ regional shortening associated with the Uchian phase of the Kenoran orogeny. $D_4$ deformation is manifested as hairline brittle faults known as "black line faults" (Rogers, 1992; Penczak and Mason, 1997; Tarnocai, 2000). The black line faults are well developed in the Red Lake mine trend. They are barren, discrete, 2- to 5-mm slip planes containing fine quartz, tourmaline, and dark-colored chlorite that cut and displace the mineralization as well as the feldspar porphyry granodiorite and lamprophyre dikes over meters and more rarely a few tens of meters (Dubé et al., 2003).

The Campbell-Red Lake deposit is characterized by numerous barren to low-grade banded colloform-crustiform, cavity-filling carbonate (dolomite-ankerite) ± quartz veins and cockade breccias (MacGeehan and Hodgson, 1982; Penczak and Mason, 1997, 1999; Tarnocai, 2000; Dubé et al., 2001a, 2002). In addition, five different styles of gold mineralization are present: (1) sulfide-rich veins and replacement-style ore, mainly present at the Red Lake mine and spatially associated with the Dickenson and the Campbell faults (e.g., East South C-type); (2) carbonate ± quartz veins, better developed in the upper portion of the deposit at the Campbell mine; (3) magnetite-rich ore; (4) high-grade arsenopyrite-rich silicification present at both the Campbell and Red Lake mines and characterized by multiounce ore zones that typify the high-grade zone; (5) abundant visible gold coating and filling late fractures (MacGeehan and Hodgson., 1982; Andrews et al., 1986; Rogers, 1992; Penczak and Mason, 1997, 1999; Tarnocai, 2000, Dubé et al., 2001a, 2002; Twomey and McGibbon, 2001). The Goldcorp High-Grade zone is currently the best known example of styles 3, 4, and 5.

## Goldcorp High-Grade Zone

The Goldcorp High-Grade zone is currently defined and mined between levels 31 and 38 (1,350–1,700 m below surface) of the Red Lake mine. In the core of the High-Grade zone (i.e., from levels 31–34), gold mineralization is located within or near a southeast-plunging (≈60°) $F_2$ antiformal

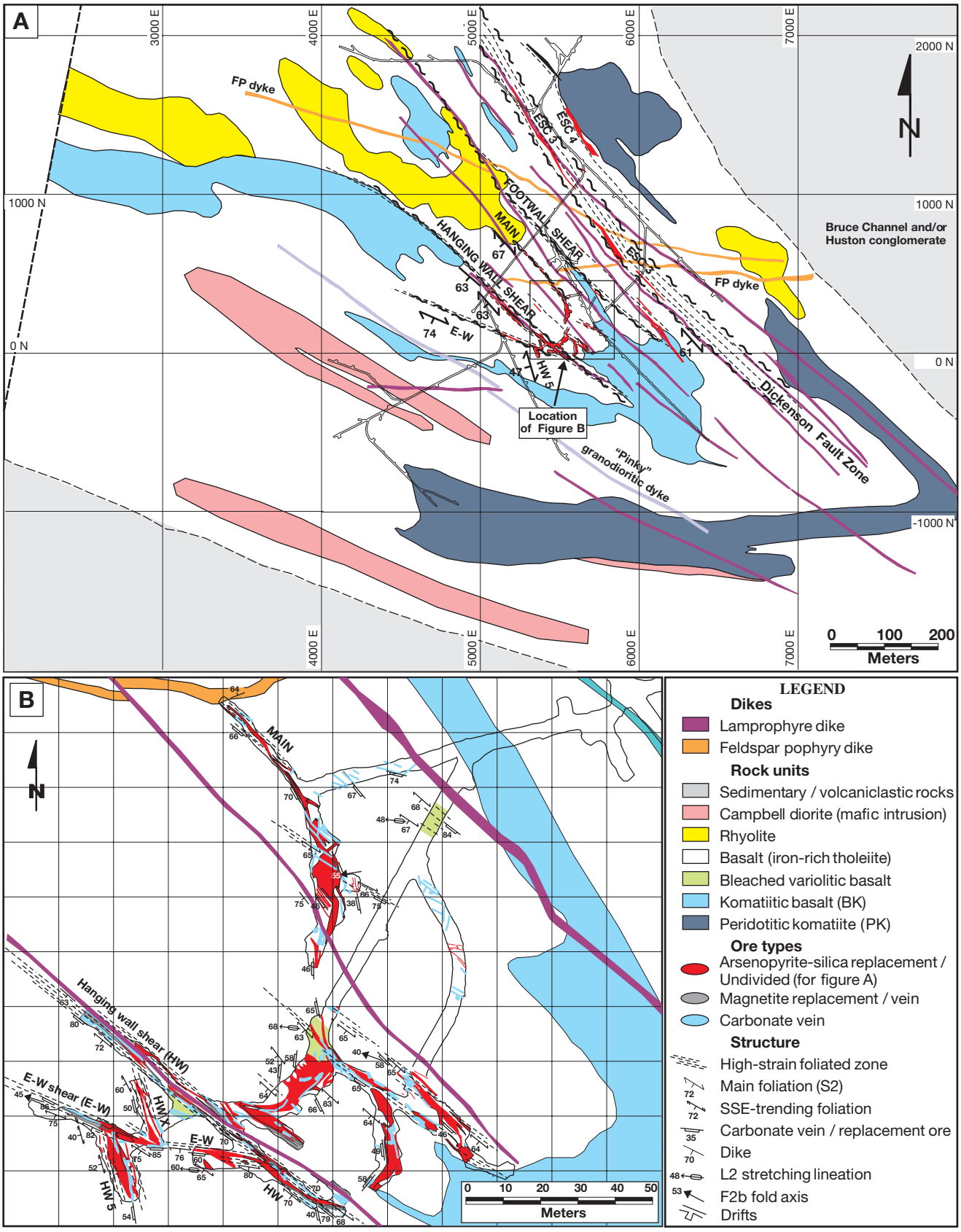


FIG. 3. A. Geology of level 34, Red Lake mine. B. Close-up of (A), showing the detailed geology of the High-Grade zone in cuts 2 and 4 (modified from Dubé et al., 2002, and from Goldcorp Ltd. geologic data). Grid spacing is 50 ft (15.2 m).

hinge zone and is hosted mainly by tholeiitic basalt of the Balmer assemblage near the folded contact with komatiitic basalt (Fig. 3A; Dubé et al., 2001a, 2002). Part of the high-grade ore is, however, also locally hosted by komatiitic basalt. One such zone is found on level 34 (stope 34-786-4E, cuts 4 and 5) where gold mineralization occurs in silicified iron-carbonate ± quartz veins with stibnite, arsenopyrite, visible gold, and associated green mica.

The ore zones have a known lateral and vertical extent of approximately 130 and 615 m, respectively. In the High-Grade zone, the association of southeast-trending and oblique carbonate ± quartz veins, high-grade ore zones, and an $F_2$ fold hinge defining the basalt-ultramafic contact suggests, at least in part, a local structural control on gold mineralization by $F_2$ folding (Dubé et al., 2001a, 2002; N. Archibald and V. Wall, unpub. rept. for Goldcorp Inc., 2000). However, below level 34, the number and size of the known mineralized zones diminish, are located progressively farther away from the hinge area, and essentially correspond to south-southeast–trending structures and veins. Gold mineralization also occurs in the hinge area close to the basalt and/or komatiitic basalt contact on level 37, but this zone is relatively small.

*Structure and veins*

The predike $S_2$ foliation is the main fabric in the High-Grade zone and defines local centimeter- to meter-wide southeast-trending (128°/63°) high-strain zones, which are especially well developed in the host basalt of the Balmer assemblage. Sulfide- and arsenopyrite-rich silicified carbonate ± quartz veins and wall rock are commonly spatially associated with these high-strain zones. The north limb of an $F_2$ antiform is transposed by a 5- to 10-m-wide ductile high-strain zone, known as the barren southeast-trending "Footwall Shear" (Fig. 3A), which is thought to be part of the New Mine fault (Dubé et al., 2002; N. Archibald and V. Wall, unpub. rept. for Goldcorp Inc., 2000). The High-Grade zone is located to the south (hanging-wall side) of the Footwall Shear and is characterized by the presence of three main sets of brittle-ductile structures, distinguished by their respective orientation (east-southeast, southeast, and south-southeast) and structural characteristics (Dubé et al., 2001a, 2002). The dominant sets of brittle-ductile structures strike southeast and east-southeast and are located toward the central part of the $F_2$ antiformal hinge zone. These structures include the east-southeast–striking "E-W shear" and the southeast-striking "Main" and "Hanging-Wall Shear" high-grade ore zones (Fig. 3B). On level 34 (Fig. 3A-B), a third set of smaller, subsidiary structures, oriented south-southeast, occurs southwest of the Hanging-Wall Shear and includes the extremely rich "HW5" zone (Dubé et al., 2001a, 2002). Below level 36, the south-southeast–oriented structures (HW5 and HWA) become the most important ore zones and may have acted as feeder zones. These different sets of structures contain centimeter- to meter-wide foliation-parallel and oblique extensional, barren to low-grade colloform-crustiform sheeted veins and cockade breccias of iron-carbonate ± quartz that are extensively developed in basalt but are also locally present in komatiitic basalt and rhyolite (Fig. 4A-B). The geometry of these iron-carbonate ± quartz veins and cockade breccias is, at least in part, related to a pre- or early increment of $D_2$ strain (Dubé et al., 2001a, 2002). They have been folded, faulted, and have undergone asymmetric boudinage during $D_2$ and/or $D_3$ and/or $D_4$.

High-grade gold mineralization, characterized by silicification with abundant arsenopyrite, follows a westerly plunging ore shoot (275°/45°) defined by the intersection of the different sets of structures and veins described above (Dubé et al., 2002; N. Archibald and V. Wall, unpub. rept. for Goldcorp Inc., 2000). The auriferous silica-rich fluid was, at least in part, focused into $F_2$ hinge zones due to competency contrast, tangential longitudinal strain, presence of carbonatized komatiitic basalt located above the ore zone and forming a low permeability cap, and local higher strain zones (Dubé et al. 2001a, 2002; N. Archibald and V. Wall, unpub. rept. for Goldcorp Inc., 2000). This was followed by further increment(s) of strain ($D_2$ and/or $D_3$) that resulted in attenuation and transposition of the $F_2$ fold limbs, deformation of the vein network, formation of new veins, and reverse-sinistral faulting along structures such as the Campbell fault (Dubé et al. 2001a , 2002; N. Archibald and V. Wall, unpub. rept. for Goldcorp Inc., 2000). The ore zones have been deformed and are cut by late- to post-$D_2$ foliation-parallel and foliation-oblique faults and high-strain zones. Postdike black line faults ($D_4$) also cut the veins and mineralized zones, but their occurrence and geometry are poorly constrained in the study area.

*Gold mineralization and alteration*

Gold mineralization in the High-Grade zone is related to syn-$D_2$ deformation, silicification and brecciation of preexisting colloform-crustiform, barren to low-grade, iron-carbonate ± quartz veins and breccias, and of enclosing wall-rock selvages (Dubé et al., 2001a, 2002; Twomey and McGibbon, 2001). The silicification is associated with variable amounts of fine-grained arsenopyrite (0–50%), sericite, rutile, and visible gold (Fig. 4C-D), as well as variable amounts of pyrite, pyrrhotite, and magnetite. Locally, trace amounts of sphalerite and chalcopyrite are also present, with stibnite occurring locally toward or at the contact with komatiitic basalt. The ore mineralogy varies from predominantely arsenopyrite to pyrrhotite-pyrite-arsenopyrite-magnetite-rich assemblages (sulfide-rich ore) or magnetite-dominated assemblages (magnetite-ore). The arsenopyrite is directly associated with high-grade gold, and its presence correlates with silicification of the iron-carbonate ± quartz veins and the Fe-rich basalt host rocks (Dubé et al., 2001a, 2002). The intensity of the silicification is highly variable (Fig. 4C-D). Commonly, silicification and associated arsenopyrite and/or pyrite occur only along the margins of carbonate ± quartz veins as glassy quartz with or without arsenopyrite-rich selvages (Fig. 4C). Significant high-grade arsenopyrite-rich mineralization associated with silicification is located at the intersection between the south-southeast–striking iron-carbonate ± quartz breccia veins and the east-southeast–striking iron-carbonate ± quartz veins and structures (Dubé et al., 2002). The High-Grade zone is characterized by spectacular visible gold in the silicified and sulfidized iron-carbonate ± quartz veins, as well as in late shallowly dipping fractures and fault planes that cut the ore zones and which are at high angle to the main foliation (Figs. 4E-F, 5A). A proximal centimeter- to meter-wide reddish-brown biotite-carbonate alteration with disseminated arsenopyrite,

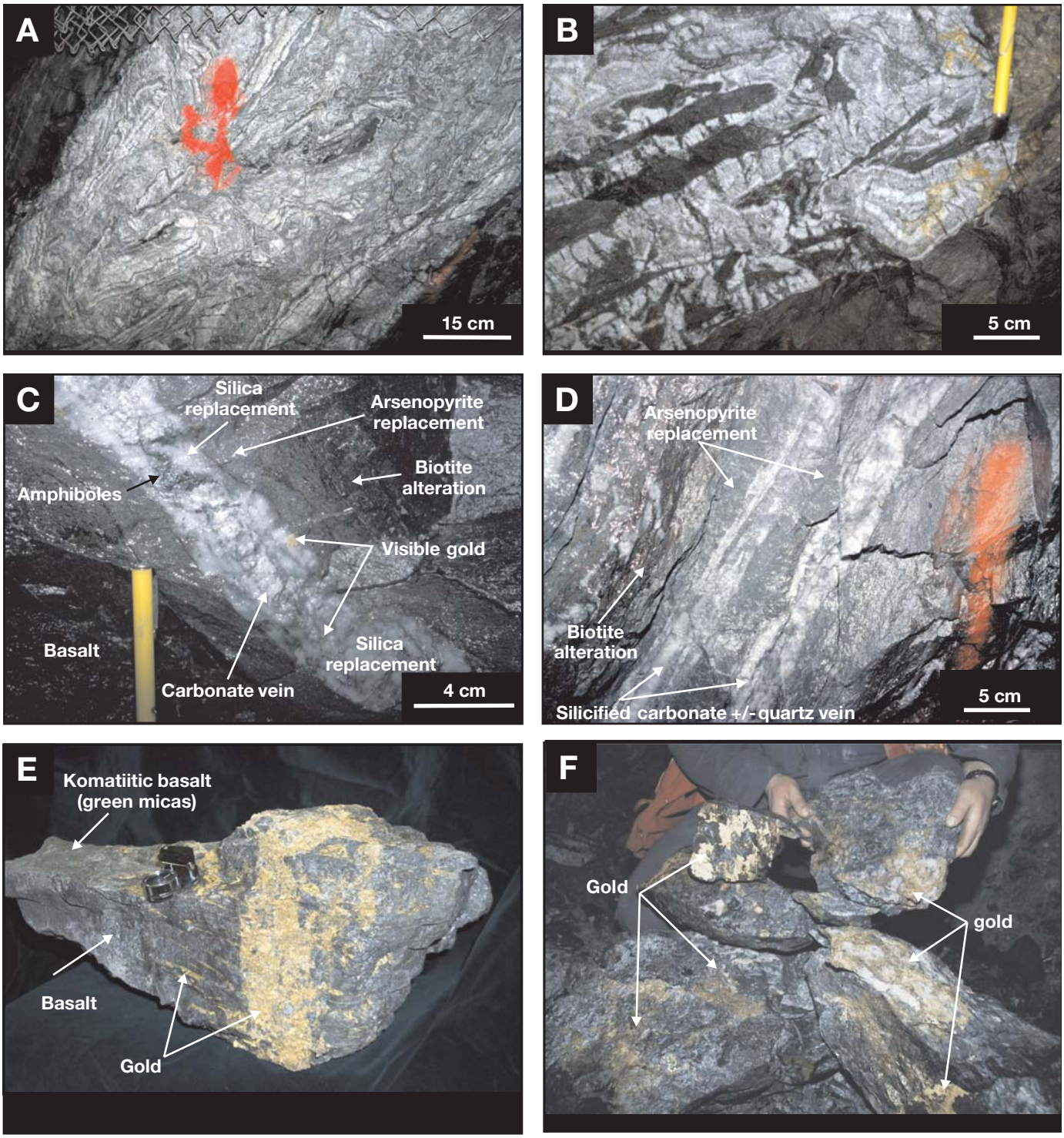


FIG. 4. A. Steeply dipping cockade carbonate ± quartz breccia vein with colloform-crustiform texture, section view (stope 37-756-1 cut 6). B. Close-up showing colloform-crustiform texture in a carbonate ± quartz cockade breccia vein, section view (stope 31-826-2 ramp). C. Gold-rich silicification of a barren to low-grade carbonate ± quartz vein with associated arsenopyrite-rich replacement of biotitized vein selvages, section view (HW5 zone, stope 34-806-5wdr). D. Au-rich silicification of barren to low-grade carbonate ± quartz veins with associated high-grade arsenopyrite-rich replacement of vein selvages, section view (HWX zone, stope 34-806-8). E. Example of spectacular high-grade mineralization, showing semimassive gold veins at high angle to the contact between basalts of the Balmer assemblage and komatiitic basalt or filling fractures subparallel to the contact. Sample weight is 37 kg and contains approximately 300 oz Au, equivalent to 7,284 oz/t Au (stope 32-826-1, hand lens is 6 cm long). F. Example of high-grade gold mineralization (stope 37-746-2).

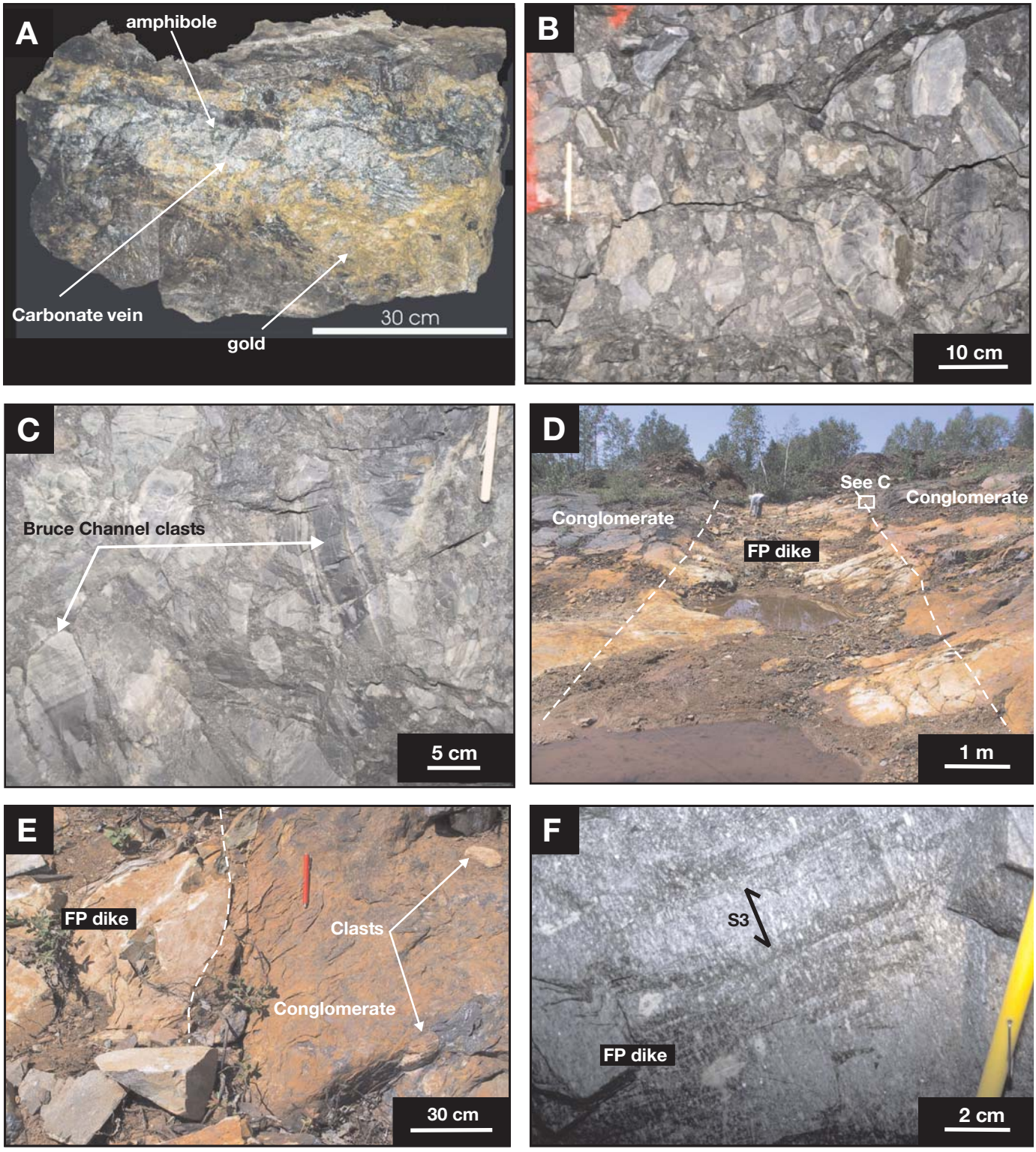


FIG. 5. A. Example of high-grade mineralization. Sample weight is 127 kg and contains approximately 630 oz Au, equivalent to 4,508 oz/t Au (stope 37-746-2, cut 9). B. Proximal polymictic Huston assemblage conglomerate containing numerous laminated chert clasts of the Bruce Channel assemblage, section view (drift 16-007-1 EDR). C. Subangular to subrounded clasts in conglomerate of the Bruce Channel assemblage, section view (drift 16-007-1 EDR). D. Feldspar porphyry granodiorite dike (FP) cutting across the conglomerate of the Huston assemblage (surface outcrop in Goldcorp mine property). E. Close-up of a crosscutting relationship between a feldspar porphyry dike and conglomerate. F. Tectonic foliation within the feldspar porphyry granodiorite dike that cuts the high-grade ore (see Fig. 6C), section view (stope 32-826-8).

pyrite, pyrrhotite, and variable amounts of sericite, quartz, and amphibole in well foliated basalt is commonly associated with the silicified high-grade zones and represents a key megascopic visual alteration vector to the high-grade mineralization (Fig. 4D; Dubé et al., 2001a, b, 2002; Twomey and McGibbon, 2001).

*Relative timing of carbonate alteration*

The colloform-crustiform iron-carbonate ± quartz veins and cockade breccias associated with gold mineralization are typically barren to low grade and are characteristic of the Red Lake district. Their timing and genesis are uncertain (MacGeehan and Hodgson, 1982). Dubé et al. (2002, 2003) presented evidence that iron-carbonate ± quartz veins and breccias have accommodated a significant part of the $D_2$ strain and are either early-$D_2$ or pre-$D_2$. However, evidence found at the Red Lake mine supports a protracted history of multistage events, including pre-, early-, and late- to postmain-stage deformation ($D_2$) iron carbonate ± quartz veining. A colloform-cockade iron-carbonate ± quartz breccia vein cuts pyrrhotite-rich sulfide veins and replacement-style gold mineralization (referred to locally as ESC style) on level 23, suggesting that some iron-carbonate ± quartz veining is late to postsulfide-rich veins and replacement-style mineralization. Important timing relationships come from an exploration drift on level 16 of the Red Lake mine, which exposes a section through polymictic conglomerate correlated with the Huston assemblage (Fig. 5B). Here, the conglomerate contains numerous subangular to subrounded laminated chert clasts interpreted to be part of the underlying Bruce Channel assemblage (Fig. 5C). More importantly, the conglomerate contains clasts of andalusite-rich altered basalt in an unaltered matrix and a few clasts of layered (sheeted?) carbonate material with small crustiform banding and cockade texture (Fig. 6A-B). The conglomerate also is locally strongly altered, as indicated by abundant sericite, quartz, local green micas, and andalusite both in the matrix and the clasts. Regionally, this conglomerate displays local evidence for postdepositional iron-carbonate alteration (Dubé et al., 2003). On level 16, the clasts are locally flattened and the matrix contains $S_2$ foliation. The conglomerate is cut by a mesocratic lamprophyre dike and by a feldspar porphyry granodiorite dike at surface (Fig. 5D-E). Together, these relationships indicate protracted pre- to postconglomerate aluminous alteration and iron-carbonate alteration and/or veining (Dubé et al., 2003).

*Relative timing of gold mineralization*

The timing of the silicification and associated arsenopyrite is critical for the understanding of the formation of the High-Grade zone, since the high-grade mineralization is directly related to this alteration. Dubé et al. (2001a, 2002) presented evidence for multiple stages of gold deposition, silicification, and carbonate ± quartz veining and also showed that the main gold-related silicification of the carbonate ± quartz veins coincided with or postdated development of the asymmetric boudinage of the iron-carbonate ± quartz veins. They proposed a progressive and dynamic syndeformation mineralization event(s) dominated by the silicification of carbonate ± quartz veins with some local late gold-bearing colloform carbonate-quartz veinlets cutting across the high-grade siliceous ore.

*Postore intrusive rocks*

All rock units, including the carbonate ± quartz veins and the high-grade mineralization, are cut by feldspar porphyry granodiorite dikes and lamprophyre dikes (Figs. 2–3; Dubé et al., 2001a, 2002; Twomey and McGibbon, 2001). The feldspar porphyry granodiorite dikes are a few meters wide, strike east to east-southeast, dip steeply, and contain abundant feldspar phenocrysts (3–5 mm) with a few percent of quartz (1–2 mm) and disseminated biotite. They have an intermediate composition and are barren (Table 1). One such east-striking massive and unfoliated feldspar porphyry granodiorite dike (KG-03-17) cuts the conglomerate of the Huston assemblage exposed at surface (Fig. 5D-E). Locally, the postore feldspar porphyry granodiorite dikes are weakly to moderately foliated (N140°/55°; Fig. 5F). This postdike foliation is interpreted to be an $S_3$ foliation because the east-striking feldspar porphyry granodiorite dikes cut across both limbs of an $F_2$ fold (Fig. 2). These barren dikes are chilled against and cut the high-grade ore (Fig. 6C). On level 34, the Footwall Shear (New Mine fault zone) cuts a feldspar porphyry granodiorite dike with an apparent reverse-sinistral component of displacement (7–8 m). This minor displacement is interpreted as a reactivation of the Footwall Shear, as the map pattern suggests up to 800 m of sinistral displacement of the komatiitic basalts by the Footwall Shear (N. Archibald and V. Wall, unpub. rept. for Goldcorp Inc., 2000; Fig. 2).

Lamprophyre dikes, as defined by Rock (1991), containing grayish-brown to black biotite and amphibole are also chilled against and clearly cut iron-carbonate ± quartz veins (Fig. 6D) and gold mineralization (Penczak and Mason, 1997, Zhang et al., 1997; Tarnocai, 2000, Dubé et al., 2001a, 2002; Twomey and McGibbon, 2001, and references therein). At the Red Lake mine, four sets of such lamprophyre dikes (≤3 m wide) are present (Figs. 2, 3A-B). Three sets are mesocratic and calc-alkaline in composition, one set is subparallel to the main southeast-trending foliation (130°/70°), a second set is west-striking and dips steeply to the north, and a third less common set is oriented N220°/30°. The dikes contain abundant plagioclase with biotite and variable proportions of hornblende and/or tschermakite and traces to a few percent of carbonate. Sample KG-03-32B contains up to 70 percent hornblende and tschermakite. These dikes have been interpreted as spessartite lamprophyres at the Campbell and Red Lake mines (Christie, 1986; Penczak and Mason, 1997, Tarnocai, 2000; Twomey and McGibbon, 2001). The compositions of some of these mesocratic intermediate dikes are shown in Table 1 and are consistent with this interpretation. In contrast, a fourth set is melanocratic and strikes north-south with a shallow dip to the west. The melanocratic dikes are less abundant but cut across a large section of the Red Lake mine. They are meter-thick, extensive and massive, and contain biotite with plagioclase phenocrysts. Compared to the mesocratic dikes, they contain more titanium, zirconium, and barium (Table 1). The composition of the melanocratic dikes corresponds to kersantite, a member of the calc-alkaline lamprophyre clan (Rock, 1991). The three sets of mesocratic dikes cut the feldspar porphyry granodiorite dikes and high-grade ore (Figs. 6E-F, 7A-B). The steeply dipping mesocratic lamprophyre dikes are weakly foliated ($S_3$) and commonly

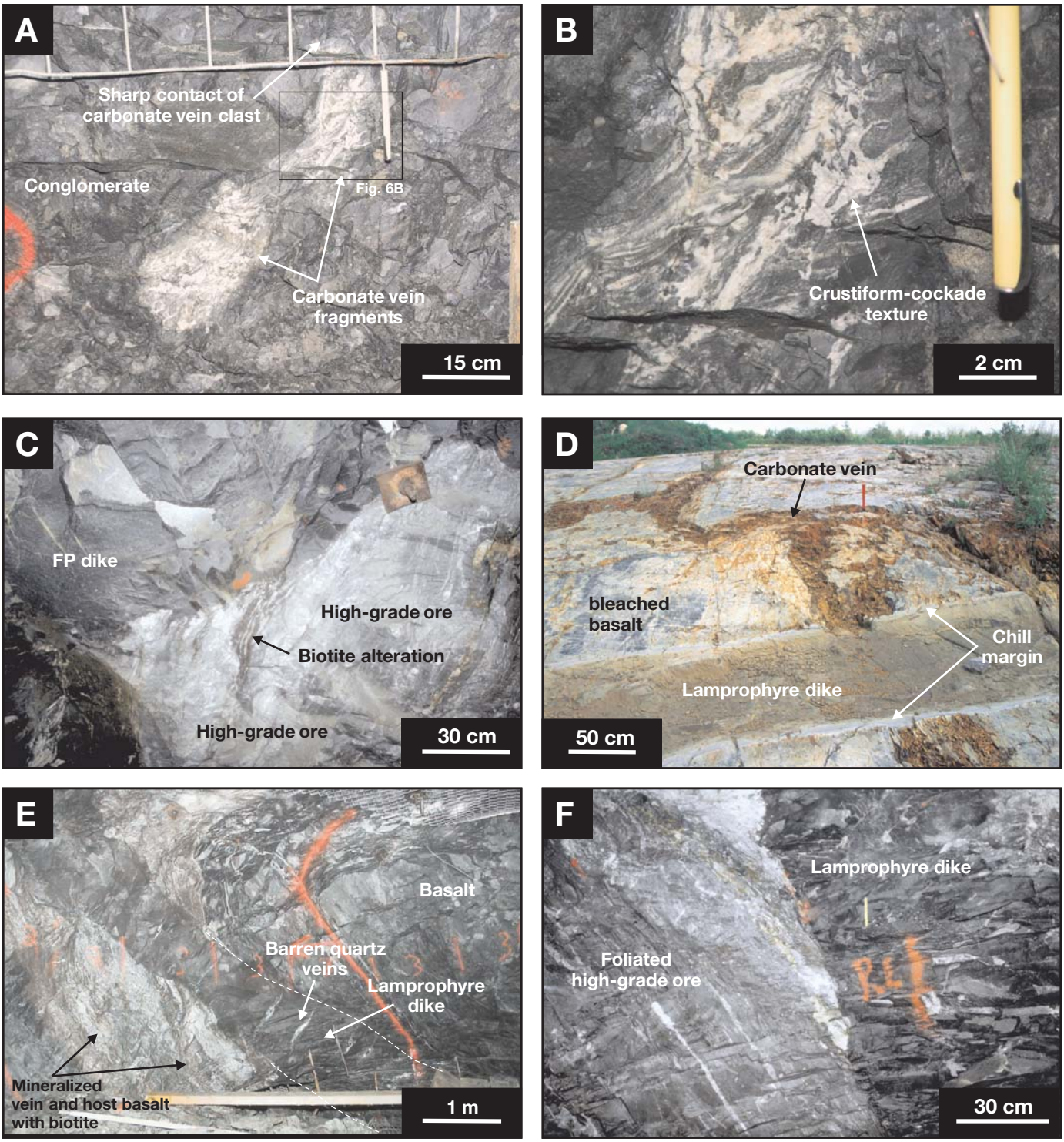


FIG. 6. A. Two carbonate vein clasts within conglomerate of the Huston assemblage, section view (drift16-007-1 EDR). B. Close-up of (A), showing crustiform-cockade texture in a carbonate vein clast (drift16-007-1 EDR). C. Feldspar porphyry granodiorite dike (FP) cutting across multiounce arsenopyrite-rich and silicified carbonate ± quartz vein hosting foliated biotite-rich mafic clasts, view toward back (stope 32-826-8). D. Lamprophyre dike cutting a carbonate vein and bleached basalt on surface outcrop of the Campbell mine. Note the presence of chill margins all along the dike. E. Moderately dipping mesocratic barren lamprophyre dike hosting barren extensional quartz ladder veins and cutting across high-grade mineralization, section view (stope 37-746-2 cut 1). F. Close-up of a south-southeast–trending, moderately dipping mesocratic lamprophyre dike cutting across foliated multiounce high-grade ore, section view (stope 37-746-2 cut 1). Late faulting along the dike walls has induced the local apparent dragging of the foliation in the ore.

TABLE 1. Chemical Composition of Dated Intrusives Rocks

| Sample no. | $SiO_2$ (%) | $TiO_2$ (%) | $Al_2O_3$ (%) | $Fe_2O_3^{(T)}$ (%) | MnO (%) | MgO (%) | CaO (%) | $Na_2O$ (%) | $K_2O$ (%) | $P_2O_5$ (%) | LOI (%) | Total (%) | $CO_2$ (%) | S (%) | Y (ppm) | Zr (ppm) | Au ppb | As (ppm) | Sb (ppm) | Ag (ppm) | Cu (ppm) | Zn (ppm) | Pb (ppm) | Ba (ppm) |
|---|---|---|---|---|---|---|---|---|---|---|---|---|---|---|---|---|---|---|---|---|---|---|---|---|
| Feldspar porphyry granodiorite dike (FP) | | | | | | | | | | | | | | | | | | | | | | | | |
| KG-2000-40B[1] | 66.84 | 0.47 | 14.72 | 3.30 | 0.04 | 0.97 | 3.42 | 3.69 | 2.14 | 0.10 | 3.44 | 99.13 | 2.12 | < 0.01 | 4.8 | 130.7 | 12 | 14.9 | 8.8 | 0.6 | 12.6 | 63.7 | 15 | 605 |
| KG-03-17BC[1] | 67.64 | 0.50 | 14.78 | 3.49 | 0.05 | 1.08 | 3.57 | 3.63 | 2.05 | 0.10 | 3.21 | 100.09 | 1.87 | 0.02 | 5.2 | 142.7 | 2.5 | 16.7 | 2.7 | 0.1 | 7.5 | 56.9 | 7 | 541 |
| M22104[2,3] | 69.38 | 0.35 | 15.01 | 2.33 | 0.04 | 0.70 | 2.37 | 4.23 | 2.26 | 0.07 | 2.55 | 99.29 | | | 4.0 | 116.0 | | | | | | | | 610 |
| M22507[2,3] | 66.68 | 0.49 | 15.16 | 3.32 | 0.05 | 1.04 | 3.48 | 3.41 | 2.28 | 0.11 | 3.38 | 99.40 | | | 6.0 | 124.0 | | | | | | | | 615 |
| M39680[2,3] | 66.33 | 0.49 | 15.29 | 3.45 | 0.05 | 1.20 | 3.47 | 3.90 | 2.08 | 0.10 | 3.59 | 99.95 | 2.70 | 0.06 | 6.0 | 129.5 | | | | 0.5 | 55.0 | 65.0 | 15 | 585 |
| M39681[2,3] | 67.50 | 0.37 | 15.12 | 2.37 | 0.04 | 0.94 | 2.62 | 4.56 | 2.26 | 0.10 | 2.93 | 98.81 | 2.00 | 0.02 | 3.5 | 128.0 | | | | 0.5 | 25.0 | 60.0 | 10 | 600 |
| M39684[2,3] | 69.49 | 0.35 | 15.00 | 2.20 | 0.04 | 0.71 | 2.80 | 4.34 | 1.84 | 0.08 | 2.86 | 99.71 | 1.70 | 0.06 | 3.5 | 126.0 | | | | 0.5 | 20.0 | 40.0 | 5 | 487 |
| M39686[2,3] | 69.56 | 0.33 | 15.36 | 2.14 | 0.03 | 0.73 | 2.93 | 3.57 | 1.85 | 0.10 | 2.97 | 99.57 | 1.60 | 0.04 | 3.5 | 121.5 | | | | 0.5 | 25.0 | 60.0 | 25 | 547 |
| Avg | 67.93 | 0.42 | 15.06 | 2.82 | 0.04 | 0.92 | 3.08 | 3.92 | 2.09 | 0.10 | 3.12 | 99.49 | 2.00 | 0.04 | 4.6 | 127.3 | 7.25 | 15.8 | 5.8 | 0.5 | 24.2 | 57.6 | 13 | 574 |
| Std. deviation | 1.35 | 0.08 | 0.23 | 0.61 | 0.01 | 0.19 | 0.46 | 0.41 | 0.18 | 0.01 | 0.35 | 0.43 | 0.39 | 0.02 | 1.1 | 7.8 | 6.718 | 1.3 | 4.3 | 0.2 | 16.6 | 9.1 | 7 | 45 |
| Mesocratic lamprophyres | | | | | | | | | | | | | | | | | | | | | | | | |
| KG-2000-86C[1] | 60.54 | 0.40 | 15.75 | 4.32 | 0.06 | 2.50 | 6.05 | 2.36 | 1.95 | 0.15 | 2.80 | 96.88 | 2.22 | 0.09 | 12.2 | 107.1 | 3 | 18.0 | 10.9 | 0.8 | 28.2 | 72.5 | 14 | 504 |
| KG-03-32B[1] | 45.55 | 0.63 | 11.50 | 8.66 | 0.16 | 8.60 | 10.22 | 2.21 | 1.41 | 0.25 | 8.90 | 98.09 | 6.86 | 0.54 | 15.8 | 98.5 | 10 | 30.2 | 16.3 | 1.1 | 72.9 | 79.6 | 20 | 572 |
| GC1758-1[3,4] | 54.90 | 0.85 | 15.80 | 7.59 | 0.10 | 3.56 | 7.80 | 1.82 | 1.62 | 0.29 | 4.35 | 98.68 | 3.80 | | 15.0 | 163.0 | | | | | | | | 508 |
| GC-GD-12[3,4] | 56.20 | 0.51 | 14.50 | 6.18 | 0.09 | 4.97 | 6.28 | 4.00 | 0.62 | 0.18 | 6.05 | 99.58 | 4.60 | | 13.0 | 116.0 | | | | | | | | 312 |
| M39682[2,3] | 58.51 | 0.55 | 15.42 | 6.55 | 0.10 | 5.37 | 6.84 | 3.72 | 1.03 | 0.19 | 1.48 | 99.76 | 0.70 | 0.18 | 15.0 | 112.0 | | | | 0.5 | 65.0 | 75.0 | | 337 |
| M39688[2,3] | 56.66 | 0.59 | 14.23 | 7.45 | 0.12 | 6.85 | 7.44 | 3.36 | 0.61 | 0.20 | 1.50 | 99.01 | 0.80 | 0.14 | 16.5 | 108.0 | 2.5 | | | 0.5 | 65.0 | 85.0 | 10 | 197 |
| M39699[2,3] | 52.70 | 0.90 | 14.98 | 7.79 | 0.11 | 3.69 | 8.47 | 3.30 | 0.59 | 0.21 | 6.21 | 98.95 | 5.40 | 0.07 | 18.5 | 106.5 | 2.5 | | | 0.5 | 70.0 | 80.0 | 5 | 259 |
| Avg | 55.01 | 0.63 | 14.60 | 6.93 | 0.11 | 5.08 | 7.59 | 2.97 | 1.12 | 0.21 | 4.47 | 98.71 | 3.48 | 0.20 | 15.1 | 115.9 | 5 | 24.1 | 13.6 | 0.7 | 60.2 | 78.4 | 12 | 384 |
| Std. deviation | 4.86 | 0.18 | 1.49 | 1.41 | 0.03 | 2.10 | 1.44 | 0.83 | 0.55 | 0.05 | 2.76 | 0.98 | 2.34 | 0.19 | 2.1 | 21.5 | 4.33 | 8.6 | 3.8 | 0.3 | 18.2 | 4.8 | 6 | 143 |
| Melanocratic lamprophyres | | | | | | | | | | | | | | | | | | | | | | | | |
| KG-2000-48B[1] | 55.24 | 1.88 | 14.75 | 8.91 | 0.11 | 2.72 | 5.34 | 3.81 | 2.63 | 1.16 | 1.60 | 98.15 | 0.54 | 0.20 | 28.9 | 428.5 | 9 | 16.1 | 2.0 | 0.5 | 34.3 | 165.0 | 17 | 1260 |
| M39693[2,3] | 53.32 | 2.26 | 14.11 | 9.82 | 0.12 | 3.52 | 6.57 | 3.54 | 2.57 | 1.60 | 1.35 | 98.78 | 0.80 | 0.24 | 27.0 | 355.0 | 2.5 | | | 0.5 | 55.0 | 180.0 | 30 | 1135 |
| M39698[2,3] | 54.25 | 2.05 | 14.20 | 9.07 | 0.11 | 3.16 | 5.86 | 3.97 | 2.88 | 1.23 | 1.80 | 98.58 | 1.20 | 0.23 | 25.5 | 358.0 | 2.5 | | | 0.5 | 50.0 | 180.0 | 25 | 1205 |
| Avg | 54.27 | 2.06 | 14.35 | 9.27 | 0.11 | 3.13 | 5.92 | 3.77 | 2.69 | 1.33 | 1.58 | 98.50 | 0.85 | 0.22 | 27.1 | 380.5 | 4.667 | 16.1 | 2.0 | 0.5 | 46.4 | 175.0 | 24 | 1200 |
| Std. deviation | 0.96 | 0.19 | 0.35 | 0.49 | 0.01 | 0.40 | 0.62 | 0.22 | 0.16 | 0.24 | 0.23 | 0.32 | 0.33 | 0.02 | 1.7 | 41.6 | 3.753 | <0.1 | <0.1 | <0.1 | 10.8 | 8.7 | 7 | 63 |
| "Pinky" granodiorite dikes | | | | | | | | | | | | | | | | | | | | | | | | |
| KG-03-21B[1] | 66.91 | 0.20 | 16.19 | 3.13 | 0.08 | 0.38 | 3.62 | 3.58 | 1.92 | 0.08 | 2.29 | 98.37 | 0.84 | < 0.01 | 15.3 | 191.4 | 10 | 6.7 | 5.3 | 0.4 | 8.4 | 68.5 | 13 | 484 |
| KG-00-55C[1] | 68.01 | 0.20 | 16.53 | 3.18 | 0.08 | 0.40 | 3.91 | 3.58 | 1.48 | 0.09 | 2.06 | 99.51 | 0.79 | < 0.01 | 15.3 | 190.9 | 2.5 | 5.9 | 4.7 | 0.9 | 4.3 | 76.6 | 12 | 455 |
| D0004014[2,3] | 64.96 | 0.25 | 16.96 | 3.56 | 0.12 | 0.51 | 4.43 | 2.67 | 2.40 | 0.12 | 2.71 | 98.69 | 1.00 | 0.11 | 14.5 | 166.0 | 8 | | | 0.5 | 10.0 | 35.0 | 30 | 432 |
| M22113[2,3] | 66.49 | 0.21 | 16.82 | 3.29 | 0.11 | 0.48 | 3.70 | 3.80 | 1.71 | 0.10 | 2.12 | 98.83 | | | 14.0 | 174.0 | | | | | | | | 515 |
| M38103[2,3] | 66.80 | 0.22 | 17.10 | 3.21 | 0.10 | 0.42 | 3.74 | 3.24 | 1.80 | 0.09 | 2.36 | 99.08 | 0.80 | 0.03 | 14.5 | 182.0 | 2.5 | | | 0.5 | 2.5 | 85.0 | 5 | 476 |
| M38104[2,3] | 66.96 | 0.20 | 16.87 | 3.21 | 0.11 | 0.35 | 3.95 | 3.29 | 1.76 | 0.10 | 1.94 | 98.74 | 1.00 | 0.08 | 14.5 | 183.0 | 2.5 | | | 0.5 | 2.5 | 70.0 | 15 | 439 |
| M38105[2,3] | 66.02 | 0.24 | 17.20 | 3.47 | 0.09 | 0.56 | 3.76 | 3.81 | 1.64 | 0.12 | 2.12 | 99.03 | 0.80 | 0.10 | 15.0 | 184.5 | 2.5 | | | 0.5 | 2.5 | 50.0 | 20 | 448 |
| M39687[2,3] | 66.29 | 0.21 | 16.75 | 3.01 | 0.11 | 0.40 | 3.40 | 4.05 | 2.18 | 0.11 | 2.31 | 98.82 | 1.20 | 0.03 | 14.0 | 166.0 | 2.5 | | | 0.5 | 5.0 | 105.0 | 10 | 540 |
| Avg | 66.55 | 0.22 | 16.80 | 3.26 | 0.10 | 0.44 | 3.81 | 3.50 | 1.86 | 0.10 | 2.24 | 98.88 | 0.92 | 0.07 | 14.6 | 179.7 | 4.357 | 6.3 | 5.0 | 0.5 | 5.0 | 70.0 | 15 | 474 |
| Std. deviation | 0.88 | 0.02 | 0.32 | 0.18 | 0.02 | 0.07 | 0.30 | 0.43 | 0.30 | 0.01 | 0.24 | 0.33 | 0.16 | 0.04 | 0.5 | 10.1 | 3.224 | 0.6 | 0.4 | 0.2 | 3.0 | 22.8 | 8 | 38 |

[1] XRAL (Don Mills, Ontario) and INRS-ETE (Quebec City)

[2] CHEMEX (Vancouver)

[3] Data provided by R. Penczak (Goldcorp Inc.); samples GC-1758-1 and GC-GD-12 from Campbell mine, all others from Red Lake mine

[4] XRAL = INRS assays, ICP-AES = XRAL and CHEMEX assays, majors elements by XRF, $CO_2$ by coulometry, S by LECO, Au by lead fire assay, As-Sb by ICP fusion, Y-Zr-Ag-Cu-Zn-Pb-Ba by ICP80

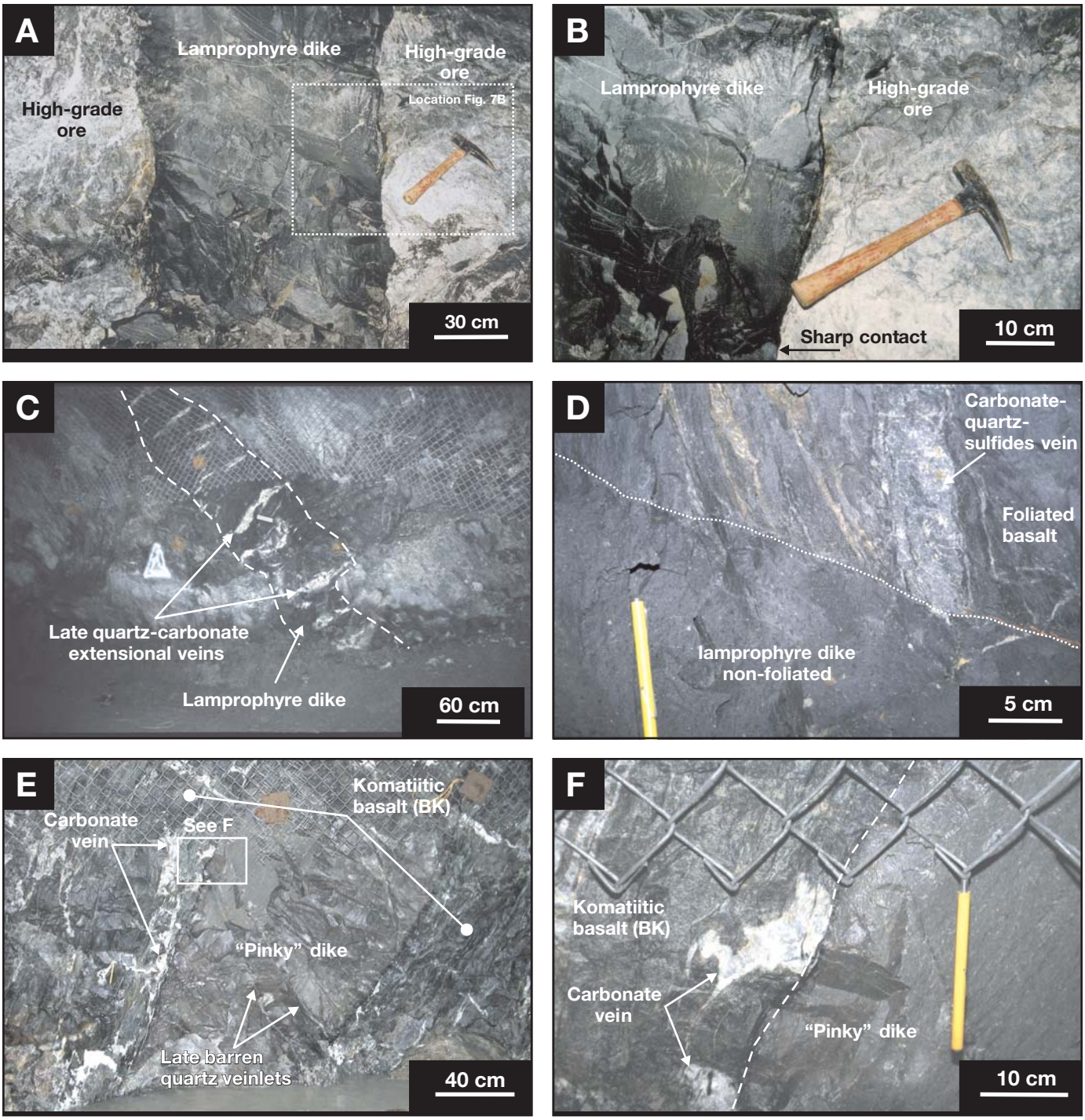


FIG. 7. A. East-southeast–trending, steeply dipping mesocratic lamprophyre dike cutting across high-grade ore zone, section view (stope 37-786-1 SXC drift). B. Close-up of (A), showing the sharp contact between the barren lamprophyre dike and the multiounce ore zone. C. Mesocratic lamprophyre dike hosting shallowly dipping, barren quartz-carbonate extension ladder veins, section view (stope 32-786-8 WDR). D. Shallowly dipping, melanocratic nonfoliated barren lamprophyre dike cutting across well-foliated basalt and a carbonate-quartz-sulfides vein, section view (intersection between the 30-844-1 SCX and 30-S959 WDR drifts). E. "Pinky" granodiorite dike cutting across the komatiitic basalt and carbonate veins. The pinky dike contains late barren quartz veinlets. F. Close-up showing the sharp crosscutting relationship between the pinky granodiorite dike and deformed carbonate veins hosted by the komatiitic basalt.

contain arrays of north-south–striking and shallowly to moderately dipping (N360°/45°–350°/35°) barren quartz-carbonate ± tourmaline extensional ladder veins, which record dilation due to oblique-vertical elongation (Figs. 6E, 7C). The dikes are locally cut by late brittle faults, and the presence of west-southwest–plunging striations (254°/28°) with steps, locally developed along the walls of the steep east-southeast–trending lamprophyre dikes, record a late oblique sinistral-reverse sense of motion. At the Campbell mine, these mesocratic lamprophyre dikes are foliated, boudinaged, and locally cut by late brittle black line faults (Zhang et al., 1997; Tarnocai, 2000). Shallowly dipping melanocratic lamprophyre dikes are nonfoliated but may locally contain a few quartz-carbonate extensional veinlets (Fig. 7D). Although they cut sulfide-rich veins and replacement-style gold mineralization, their relationship to high-grade ore is unknown, as they occur at a higher elevation in the mine.

A southeast-striking and steeply south dipping "pinky" granodiorite dike is present at depth in the southwest part of the deposit (Fig. 2). The dike is 1.5 m wide and contains disseminated feldspar phenocrysts (2–3 mm) in a quartz-feldspar matrix with 5 percent biotite and traces of quartz phenocrysts. The dike is commonly bleached due to the variable replacement of feldspar by sericite. Traces of garnet are locally present. The dike has an intermediate composition and is barren (Table 1). It contains less titanium and significantly more zirconium and yttrium than the feldspar porphyry granodiorite dikes. It cuts across all lithological units and commonly displays a weak to moderate southeast-striking $S_3$ foliation defined by elongated biotite (≤5%) and sericite. On level 34, the pinky granodiorite dike cuts altered basalt of the Balmer assemblage containing abundant andalusite but is itself devoid of such andalusite, whereas on level 37 the dike cuts carbonate veins hosted by strongly carbonatized komatiitic basalt (Fig. 7E-F). There, the dike is devoid of carbonate veinlets but locally contains extensional quartz veinlets at an angle to the foliation. Its relationship to gold mineralization is unknown, as the dike does not occur adjacent to mineralized zones.

*Late-stage gold mineralization*

Late fractures contain extremely rich ore zones with spectacular visible gold. Late-$D_2$ gold remobilization has been proposed at the Red Lake mine (Dubé et al. 2001a, b, 2002; Twomey and McGibbon, 2001) and at the Campbell mine (Tarnocai, 2000) to explain this phenomenon. At the Red Lake mine, late-stage gold mineralization is represented by coatings of gold on late shallowly dipping fractures at a high angle to $S_2$ (Dubé et al. 2001a, b). Spectacular fillings or coatings of visible gold occur in fractures within both east- and west-striking and moderately north-dipping postore mesocratic lamprophyre dikes cutting across preexisting orebodies in the High-Grade zone (stope 32-826-1 cut 1, see fig. 3A of Dubé et al., 2001a; stope 37-746-2; Fig. 8A-D). It is proposed that this late-stage gold mineralization is related to post-$D_2$ strain and metamorphism, which appears to have partly remobilized gold from the main arsenopyrite-rich siliceous ore.

## U-Pb Geochronology: Age of Gold Mineralization

Radiometric ages were determined for a suite of seven samples by U-Pb geochronology to independently constrain the age of hydrothermal activity, gold mineralization, and remobilization in the High-Grade zone of the Red Lake mine. Two additional samples from the south-central part of the belt (Madsen and Starratt-Olsen mines) were analyzed to test existing constraints on deformation and mineralization elsewhere in the belt (cf. Corfu and Andrews, 1987). Five samples were included from the High-Grade zone (KG-2000-39, KG-2000-86, KG-03-32A, KG-2000-47, and KG-02-81).

The maximum age of a conglomerate or breccia (debris flow) exposed on level 16 in the Red Lake mine that contains clasts of carbonate vein material (KG-02-50; Dubé et al., 2003) was determined using the sensitive high resolution ion microprobe (SHRIMP) to analyze detrital zircon (Figs. 5B, 6A-B). This analysis helps to constrain the timing of protracted carbonate and aluminous alteration event(s) in the district and to test correlations with the conglomerate of the Huston assemblage, recognized elsewhere in the belt (Sanborn-Barrie et al., 2002). We also dated a feldspar porphyry dike (KG-03-17B), which cuts the conglomerate, using both SHRIMP and TIMS (thermal ionization mass spectometry) to determine the minimum age of the conglomerate (Figs. 5D-E, 9A). It has been previously established that the gold mineralization at the Red Lake mine predated 2714 ± 4 Ma, the age of a foliated quartz-feldspar porphyry dike that cuts magnetite-rich gold mineralization (avg grade 10 g/t Au over 0.5 m; Corfu and Andrews, 1987). The dated dike was interpreted to have been emplaced in the late ductile deformation stage related to the Red Lake mine trend, postdating gold mineralization by a relatively small time interval (Corfu and Andrews, 1987; Rogers, 1992). Tarnocai (2000) proposed that the dike predates mineralization, thus providing a maximum age for the timing of mineralization. In this study, we independently test the minimum age of main-stage arsenopyrite-rich siliceous replacement-style mineralization in the High-Grade zone by dating zircon from a feldspar porphyry dike (KG-2000-39) that cuts high-grade mineralization (Figs. 6C, 9B). In order to determine the maximum age of the late-stage gold mineralization, the ages of south-southeast–striking and east-west–striking and steeply dipping mesocratic lamprophyre dikes (KG-2000-86, KG-03-32A) of the type that cut high-grade mineralization and contain abundant visible gold (KG-03-32A; Figs. 7A-B, 8A-C, 9C-D), also have been determined by TIMS analysis of zircon from the dike. The age of zircon from a shallowly dipping melanocratic lamprophyre dike (KG-2000-47) that postdates sulfide-rich veins and replacement-style gold mineralization and ductile strain (Figs. 7D, 9E) has been determined by TIMS in order to define the minimum age of gold mineralization and ductile deformation. To help constrain the age of hydrothermal alteration, a pinky granodiorite dike (KG-02-81) that cuts carbonate veins hosted by komatiitic basalt and aluminous alteration in basalt (Figs. 7E-F, 9F) has been dated by TIMS analysis of zircon. A sample of weakly deformed granodiorite dike (MD-39-99) that cuts economic gold mineralization hosted by the highly foliated Austin tuff (Figs. 8E, 10) also was collected underground at the Madsen mine (Fig. 1) in order to gain a broader regional perspective on the timing of gold mineralization. The age of a similar dike (2699 ± 4 Ma, titanite age) was previously established using a surface sample by Corfu and Andrews (1987). Finally, the age of an unaltered and weakly deformed

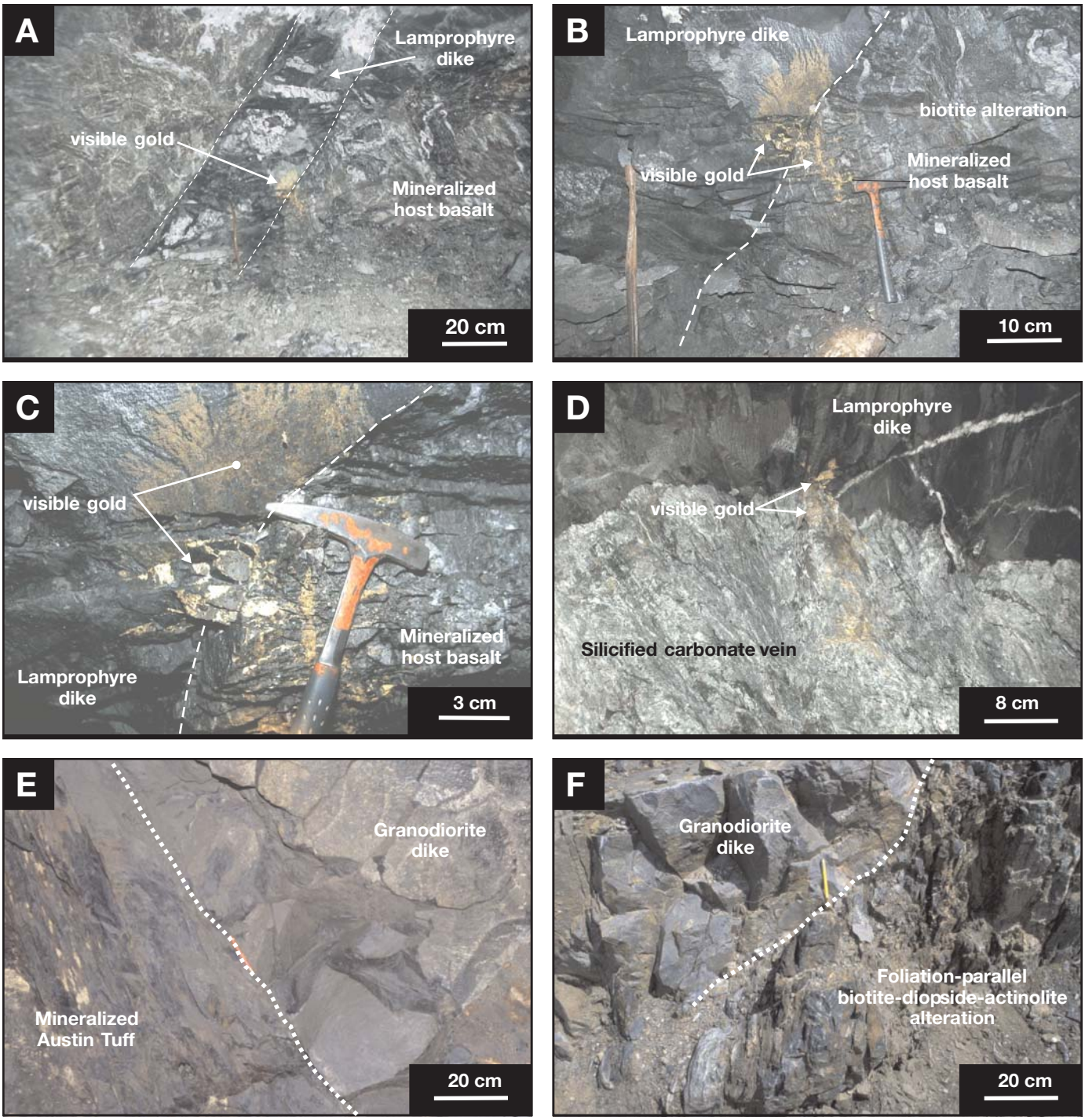


FIG. 8. A. Steeply dipping, east-west–trending mesocratic lamprophyre dike cutting across high-grade ore and hosting second-stage visible gold coating and filling late brittle fractures (stope 32-826-1E, cut 1). B. Close-up of Figure 7A. C. Close-up of Figure 7B. D. Visible gold in shallowly dipping mesocratic lamprophyre dike cut by late veinlets, section view (stope 37-746-2 cut 1). E. Section view showing a barren massive granodiorite dike cutting the foliated Austin tuff ore zone. The contact is partly masked by rust. F. Weakly foliated massive granodiorite dike cutting across quartz-sericite schists and foliation parallel biotite-diopside-actinote-epidote metasomatic layering, Creek zone, Starratt-Olsen area.

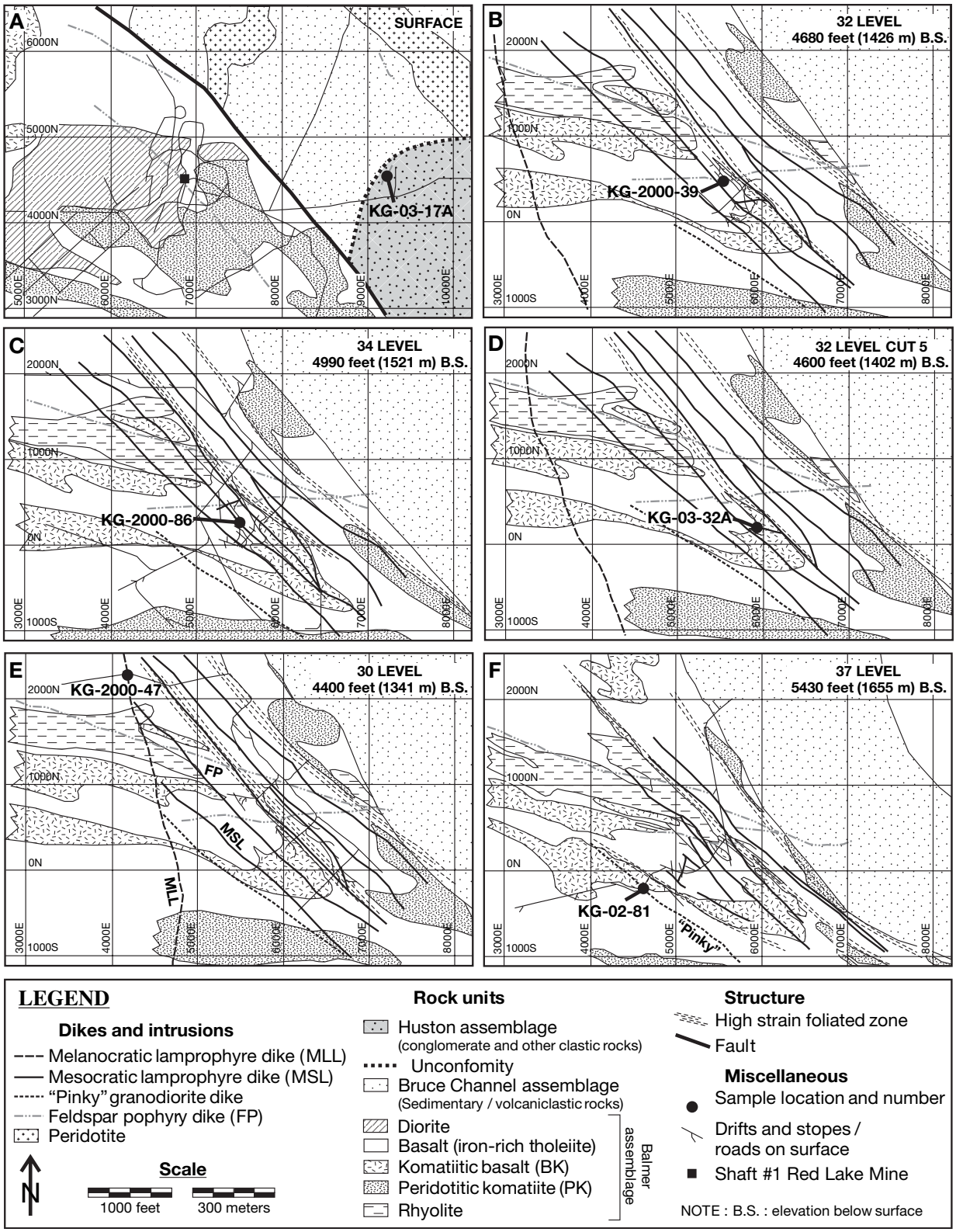


FIG. 9. A. Surface map showing sample location of dated feldspar porphyry granodiorite dike (FP) which cuts the conglomerate of the Huston assemblage. B. Level 32 map showing the location of the dated feldspar porphyry granodiorite dike (FP) that cuts high-grade ore. C. Level 34 map showing the location of the dated southeast-trending mesocratic lamprophyre dike that cuts high-grade ore. D. Level 32 (cut 5) map showing the location of the dated east-striking mesocratic lamprophyre dike hosting visible gold. E. Level 30 map showing the location of the dated melanocratic lamprophyre dike (MLL). F. Level 37 map showing the location of the dated pinky granodiorite dike, (dike thickness is exaggerated). Geology from Goldcorp's 3D model. Mine grid is in feet.

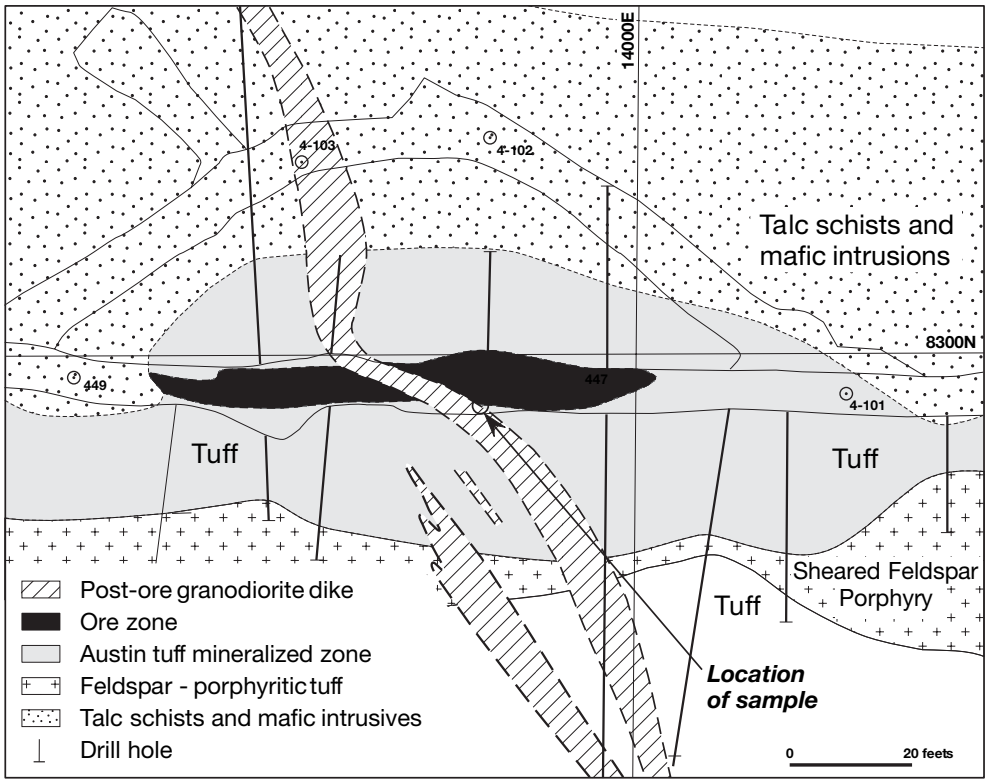


FIG. 10. Level plan showing a granodiorite dike cutting across an ore zone hosted by the mineralized Austin tuff at the Madsen mine (modified from Claude Resources).

granodiorite dike (SNB00-5130A; Fig. 8F) that cuts across well-foliated and altered pillowed basalt of the Balmer assemblage, gabbro and rhyolite from the gold-bearing Creek zone showing on the Starratt-Olsen property in the Madsen area (Fig. 1), has been determined. This dike postdates alteration and is late with respect to ductile deformation. The results for the nine U-Pb analyses are presented below.

*Analytical techniques*

SHRIMP II analyses were conducted at the Geological Survey of Canada, using analytical and data reduction procedures described by Stern (1997) and Stern and Amelin (2003) and briefly summarized here. Zircons from the samples and fragments of a laboratory zircon standard (z6266 zircon = 559 Ma) were cast in epoxy grain mounts (mount IP284 for sample KG-02-50, z7502, and mount IP312 for sample KG-03-17, z7803), polished with diamond compound to reveal the grain centers, and photographed in transmitted light. The mounts were evaporatively coated with ~10 nm of high-purity Au, and the internal features of the zircons were characterized by backscattered electron imaging (BSE), utilizing a scanning electron microscope (SEM). Analyses were conducted using an $O^-$ primary beam projected onto the zircons with elliptical spot sizes ranging between 16 and 12 $\mu$m (in the longest dimension). The count rates of ten isotopes of $Zr^+$, $U^+$, $Th^+$, and $Pb^+$ in zircon were measured sequentially with a single electron multiplier. Off-line data processing was accomplished using customized in-house software. The SHRIMP analytical data are presented in Table 2. Common-Pb corrected ratios and ages are reported with 1$\sigma$ analytical errors, which incorporate an external uncertainty of 1.0 percent in calibrating the standard zircon (see Stern and Amelin, 2003). The data are plotted in concordia diagrams with errors at the 2$\sigma$ level, using Isoplot v. 2.49 (Ludwig, 2001) to generate the concordia plots (Fig. 11A-B). Data from the conglomerate sample (KG-02-50) is also presented in a cumulative probability plot. Only data that are ≤5 percent discordant are included in the cumulative probability plot.

TIMS analytical methods utilized in this study are outlined in Parrish et al. (1987) and Davis et al. (1997). Heavy mineral concentrates were prepared by standard crushing, grinding, and concentration on a Wilfley™ table and by heavy liquid techniques. Mineral separates were sorted by magnetic susceptibility using a Frantz™ isodynamic separator. Single and multigrain zircon fractions chosen for analysis were very strongly air abraded following the method of Krogh (1982). Multigrain fractions of titanite also were lightly air abraded. Treatment of analytical errors follows Roddick et al. (1987), with errors on the ages reported at the 2$\sigma$ level (Table 2). Concordia diagrams showing the results of these analyses are presented in Figures 11D and 12.

*Results*

*Sample KG-02-50 (z7502), conglomerate:* Sample KG-02-50 was collected in exploration drift 16-007-1 EDR on level 16 of the Red Lake mine. It is a polymictic proximal

TABLE 2. U/Pb SHRIMP Analytical Data1

| Spot name | U (ppm) | Th (ppm) | Th/U | Pb* (ppm) | $^{204}$Pb (ppb) | $^{204}$Pb/$^{206}$Pb | ± $^{204}$Pb/$^{206}$Pb | f(206)$^{204}$ | $^{208}$Pb/$^{206}$Pb | ± $^{208}$Pb/$^{206}$Pb | $^{207}$Pb/$^{235}$U | ± $^{207}$Pb/$^{235}$U | $^{206}$Pb/$^{238}$U | ± $^{206}$Pb/$^{238}$U | Corr Coeff | $^{207}$Pb/$^{206}$Pb | ± $^{207}$Pb/$^{206}$Pb | Ages (Ma)[1] $^{206}$Pb/$^{238}$U | ± | $^{207}$Pb/$^{206}$Pb | ± | Disc. (%) |
|---|---|---|---|---|---|---|---|---|---|---|---|---|---|---|---|---|---|---|---|---|---|---|
| KG-02-50 (z7502): Conglomerate | | | | | | | | | | | | | | | | | | | | | | |
| 7502-71.1 | 346 | 177 | 0.527 | 209 | 2 | 0.000015 | 0.000008 | 0.0003 | 0.1468 | 0.0011 | 13.7702 | 0.1727 | 0.5250 | 0.0058 | 0.928 | 0.1902 | 0.0009 | 2720 | 25 | 2744 | 8 | 0.9 |
| 7502-10.1 | 275 | 134 | 0.503 | 163 | 2 | 0.000015 | 0.000008 | 0.0003 | 0.1414 | 0.0013 | 13.4691 | 0.1764 | 0.5176 | 0.0058 | 0.908 | 0.1888 | 0.0010 | 2689 | 25 | 2731 | 9 | 1.6 |
| 7502-5.1 | 105 | 60 | 0.590 | 64 | 0 | 0.000001 | 0.000017 | 0.0000 | 0.1645 | 0.0023 | 13.9012 | 0.2518 | 0.5228 | 0.0073 | 0.838 | 0.1928 | 0.0019 | 2711 | 31 | 2766 | 16 | 2.0 |
| 7502-16.1 | 454 | 182 | 0.414 | 271 | 2 | 0.000011 | 0.000005 | 0.0002 | 0.1130 | 0.0008 | 13.9216 | 0.1908 | 0.5323 | 0.0067 | 0.952 | 0.1897 | 0.0008 | 2751 | 28 | 2740 | 7 | –0.4 |
| 7502-58.1 | 265 | 170 | 0.663 | 158 | 2 | 0.000016 | 0.000009 | 0.0003 | 0.1768 | 0.0024 | 13.1866 | 0.2253 | 0.5074 | 0.0078 | 0.944 | 0.1885 | 0.0011 | 2645 | 34 | 2729 | 9 | 3.1 |
| 7502-4.1 | 71 | 38 | 0.548 | 42 | 2 | 0.000051 | 0.000147 | 0.0009 | 0.1554 | 0.0062 | 13.6520 | 0.2975 | 0.5131 | 0.0070 | 0.715 | 0.1930 | 0.0030 | 2670 | 30 | 2768 | 25 | 3.5 |
| 7502-67.1 | 408 | 174 | 0.440 | 240 | 4 | 0.000023 | 0.000022 | 0.0004 | 0.1250 | 0.0017 | 13.7850 | 0.2286 | 0.5179 | 0.0069 | 0.865 | 0.1930 | 0.0016 | 2691 | 29 | 2768 | 14 | 2.8 |
| 7502-62.1 | 324 | 183 | 0.584 | 196 | 5 | 0.000033 | 0.000041 | 0.0006 | 0.1607 | 0.0022 | 13.6710 | 0.1916 | 0.5205 | 0.0060 | 0.887 | 0.1905 | 0.0013 | 2701 | 26 | 2747 | 11 | 1.7 |
| 7502-61.1 | 2142 | 1253 | 0.604 | 1424 | 8 | 0.000007 | 0.000004 | 0.0001 | 0.1695 | 0.0012 | 15.0470 | 0.2634 | 0.5670 | 0.0089 | 0.936 | 0.1925 | 0.0012 | 2895 | 37 | 2763 | 10 | –4.8 |
| 7502-60.1 | 275 | 115 | 0.431 | 164 | 7 | 0.000053 | 0.000042 | 0.0009 | 0.1197 | 0.0078 | 13.8620 | 0.1975 | 0.5265 | 0.0062 | 0.883 | 0.1910 | 0.0013 | 2727 | 26 | 2751 | 11 | 0.9 |
| 7502-78.1 | 217 | 97 | 0.464 | 128 | 10 | 0.000102 | 0.000046 | 0.0018 | 0.1214 | 0.0025 | 13.6210 | 0.2331 | 0.5258 | 0.0069 | 0.833 | 0.1879 | 0.0018 | 2724 | 29 | 2724 | 16 | 0.0 |
| 7502-50.1 | 888 | 483 | 0.562 | 556 | 6 | 0.000015 | 0.000009 | 0.0003 | 0.1542 | 0.0010 | 14.2990 | 0.1739 | 0.5401 | 0.0061 | 0.961 | 0.1920 | 0.0007 | 2784 | 25 | 2760 | 6 | –0.9 |
| 7502-17.1 | 1274 | 901 | 0.730 | 806 | 10 | 0.000017 | 0.000015 | 0.0003 | 0.2000 | 0.0018 | 13.8520 | 0.2278 | 0.5282 | 0.0070 | 0.866 | 0.1902 | 0.0016 | 2734 | 29 | 2744 | 14 | 0.4 |
| 7502-11.1 | 326 | 132 | 0.418 | 189 | 6 | 0.000042 | 0.000027 | 0.0007 | 0.1136 | 0.0017 | 13.5860 | 0.1938 | 0.5155 | 0.0060 | 0.875 | 0.1911 | 0.0013 | 2680 | 26 | 2752 | 11 | 2.6 |
| 7502-13.1 | 327 | 127 | 0.400 | 194 | 5 | 0.000034 | 0.000031 | 0.0006 | 0.1117 | 0.0026 | 13.9245 | 0.2157 | 0.5302 | 0.0073 | 0.933 | 0.1905 | 0.0011 | 2742 | 31 | 2746 | 9 | 0.1 |
| 7502-8.1 | 236 | 114 | 0.497 | 140 | 14 | 0.000137 | 0.000061 | 0.0024 | 0.1395 | 0.0028 | 13.5592 | 0.2001 | 0.5179 | 0.0060 | 0.853 | 0.1899 | 0.0015 | 2690 | 26 | 2741 | 13 | 1.9 |
| 7502-9.1 | 248 | 205 | 0.852 | 162 | 18 | 0.000161 | 0.000072 | 0.0028 | 0.2329 | 0.0042 | 13.9103 | 0.2390 | 0.5344 | 0.0071 | 0.837 | 0.1888 | 0.0018 | 2760 | 30 | 2732 | 16 | –1.0 |
| 7502-21.1 | 329 | 113 | 0.355 | 192 | 3 | 0.000021 | 0.000057 | 0.0004 | 0.0995 | 0.0031 | 13.9704 | 0.2524 | 0.5265 | 0.0059 | 0.713 | 0.1924 | 0.0025 | 2727 | 25 | 2763 | 21 | 1.3 |
| 7502-31.1 | 222 | 92 | 0.426 | 130 | 1 | 0.000010 | 0.000010 | 0.0002 | 0.1150 | 0.0024 | 13.7215 | 0.3028 | 0.5223 | 0.0092 | 0.861 | 0.1905 | 0.0022 | 2709 | 39 | 2747 | 19 | 1.4 |
| 7502-30.1 | 685 | 290 | 0.438 | 421 | 4 | 0.000014 | 0.000011 | 0.0002 | 0.1199 | 0.0010 | 14.3759 | 0.2626 | 0.5443 | 0.0077 | 0.839 | 0.1916 | 0.0019 | 2801 | 32 | 2756 | 17 | –1.7 |
| 7502-47.1 | 453 | 210 | 0.479 | 274 | 6 | 0.000030 | 0.000035 | 0.0005 | 0.1304 | 0.0030 | 13.8541 | 0.1978 | 0.5316 | 0.0067 | 0.930 | 0.1890 | 0.0010 | 2748 | 28 | 2734 | 9 | –0.5 |
| 7502-45.1 | 1413 | 1026 | 0.751 | 938 | 11 | 0.000017 | 0.000009 | 0.0003 | 0.2066 | 0.0024 | 14.4006 | 0.1854 | 0.5527 | 0.0064 | 0.937 | 0.1890 | 0.0009 | 2837 | 26 | 2733 | 8 | –3.8 |
| 7502-77.1 | 399 | 149 | 0.386 | 236 | 2 | 0.000013 | 0.000015 | 0.0002 | 0.1060 | 0.0018 | 13.9242 | 0.1912 | 0.5307 | 0.0061 | 0.894 | 0.1903 | 0.0012 | 2745 | 26 | 2745 | 10 | 0.0 |
| 7502-42.1 | 322 | 214 | 0.687 | 202 | 6 | 0.000040 | 0.000050 | 0.0007 | 0.1852 | 0.0028 | 13.8766 | 0.2340 | 0.5308 | 0.0069 | 0.836 | 0.1896 | 0.0018 | 2745 | 29 | 2739 | 15 | –0.2 |
| 7502-55.1 | 908 | 583 | 0.663 | 580 | 5 | 0.000011 | 0.000007 | 0.0002 | 0.1820 | 0.0012 | 14.1682 | 0.1880 | 0.5406 | 0.0058 | 0.875 | 0.1901 | 0.0012 | 2786 | 24 | 2743 | 11 | –1.6 |
| 7502-57.1 | 2106 | 1028 | 0.504 | 1353 | 17 | 0.000017 | 0.000005 | 0.0003 | 0.1337 | 0.0007 | 14.8185 | 0.1818 | 0.5635 | 0.0066 | 0.984 | 0.1907 | 0.0004 | 2881 | 27 | 2749 | 4 | –4.8 |
| 7502-15.1 | 312 | 129 | 0.428 | 184 | 3 | 0.000024 | 0.000026 | 0.0004 | 0.1195 | 0.0021 | 13.8416 | 0.1923 | 0.5225 | 0.0063 | 0.916 | 0.1921 | 0.0011 | 2710 | 27 | 2761 | 9 | 1.8 |
| 7502-51.2 | 497 | 198 | 0.412 | 298 | 8 | 0.000034 | 0.000016 | 0.0006 | 0.1115 | 0.0013 | 14.0953 | 0.2254 | 0.5345 | 0.0072 | 0.899 | 0.1913 | 0.0014 | 2760 | 30 | 2753 | 12 | –0.3 |
| KG-03-17 (z7803): Feldspar porphyry granodiorite dike | | | | | | | | | | | | | | | | | | | | | | |
| 7803-8.1 | 165 | 86 | 0.536 | 97 | 10 | 0.000140 | 0.000036 | 0.0024 | 0.1466 | 0.0028 | 13.0795 | 0.2492 | 0.5149 | 0.0081 | 0.881 | 0.1842 | 0.0017 | 2677 | 34 | 2691 | 15 | 0.5 |
| 7803-45.1 | 118 | 51 | 0.444 | 66 | 15 | 0.000291 | 0.000062 | 0.0050 | 0.1302 | 0.0032 | 12.8002 | 0.2342 | 0.4954 | 0.0063 | 0.776 | 0.1874 | 0.0022 | 2594 | 27 | 2719 | 19 | 4.6 |
| 7803-43.1 | 72 | 60 | 0.855 | 44 | 7 | 0.000246 | 0.000157 | 0.0043 | 0.2494 | 0.0089 | 12.4263 | 0.2870 | 0.4891 | 0.0074 | 0.737 | 0.1843 | 0.0029 | 2567 | 32 | 2692 | 26 | 4.6 |
| 7803-26.1 | 261 | 61 | 0.240 | 145 | 9 | 0.000082 | 0.000025 | 0.0014 | 0.0673 | 0.0014 | 13.3812 | 0.2015 | 0.5147 | 0.0063 | 0.878 | 0.1885 | 0.0014 | 2677 | 27 | 2729 | 12 | 1.9 |
| 7803-29.1 | 203 | 136 | 0.694 | 117 | 6 | 0.000076 | 0.000034 | 0.0013 | 0.1860 | 0.0024 | 12.5590 | 0.2295 | 0.4867 | 0.0080 | 0.939 | 0.1872 | 0.0012 | 2556 | 35 | 2717 | 10 | 5.9 |
| 7803-12.1 | 164 | 79 | 0.497 | 93 | 8 | 0.000107 | 0.000051 | 0.0019 | 0.1365 | 0.0030 | 12.8431 | 0.1805 | 0.4981 | 0.0057 | 0.875 | 0.1870 | 0.0013 | 2606 | 25 | 2716 | 11 | 4.1 |
| 7803-11.1 | 181 | 99 | 0.562 | 108 | 13 | 0.000160 | 0.000033 | 0.0028 | 0.1535 | 0.0043 | 13.3153 | 0.2321 | 0.5176 | 0.0069 | 0.836 | 0.1866 | 0.0018 | 2689 | 29 | 2712 | 16 | 0.9 |
| 7803-10.1 | 303 | 147 | 0.499 | 177 | 9 | 0.000070 | 0.000023 | 0.0012 | 0.1375 | 0.0019 | 13.0926 | 0.1837 | 0.5112 | 0.0062 | 0.917 | 0.1858 | 0.0011 | 2662 | 27 | 2705 | 9 | 1.6 |
| 7803-18.1 | 91 | 50 | 0.561 | 52 | 9 | 0.000227 | 0.000110 | 0.0039 | 0.1489 | 0.0056 | 12.9125 | 0.3759 | 0.4987 | 0.0102 | 0.782 | 0.1878 | 0.0034 | 2608 | 44 | 2723 | 30 | 4.2 |
| 7803-46.1 | 208 | 126 | 0.625 | 125 | 23 | 0.000245 | 0.000047 | 0.0042 | 0.1657 | 0.0027 | 13.1609 | 0.1975 | 0.5162 | 0.0066 | 0.902 | 0.1849 | 0.0012 | 2683 | 28 | 2697 | 11 | 0.5 |

Notes: f206$^{204}$ refers to mole fraction of total $^{206}$Pb that is due to common Pb, calculated using the $^{204}$Pb method; common Pb composition used is the surface blank
Pb* = radiogenic Pb; Disc (%) refers to discordance relative to origin = 100 * (1-($^{206}$Pb/$^{238}$U age)/($^{207}$Pb/$^{206}$Pb age))
[1] Uncertainties reported at 1$\sigma$ (absolute) and are calculated by numerical propagation of all known sources of error (see Stern, 1997)

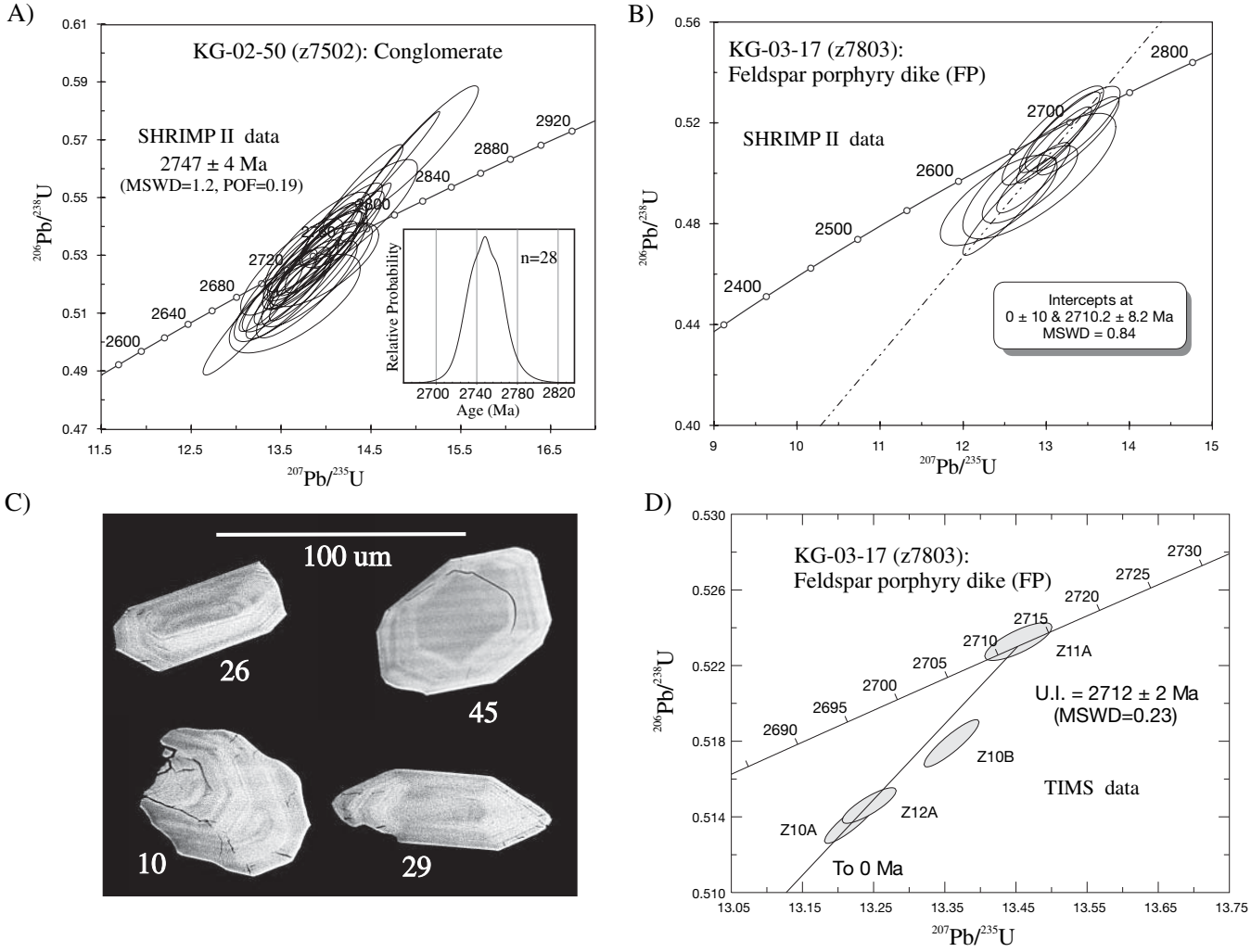


FIG. 11. A. U-Pb concordia diagram and inset cumulative probability plot of SHRIMP detrital zircon analyses from conglomerate, sample KG-02-50. B. U-Pb concordia diagram of SHRIMP analyses from crosscutting feldspar porphyry granodiorite dike, sample KG-03-17. C. Representative backscatter electron images of zircons showing fine oscillatory zoning (from feldspar porphyry granodiorite dike, sample KG-03-17). Numbers refer to zircons analyzed by SHRIMP (see Table 1). D. U-Pb concordia diagram of TIMS analyses of zircon from feldspar porphyry granodiorite dike, sample KG-03-17. MSWD = mean square of weighted deviates; POF = probability of fit.

conglomerate that contains detrital zircons with a range of morphologies, including well-faceted crystals varying from equant to prismatic as well as subrounded grains and fragments of crystals. The size of zircons recovered from the sample is consistently quite small (ranging from about 50 to <100 $\mu$m in the longest dimension, with many around 50 $\mu$m). The conglomerate contains zircons with abundant inclusions and fractures, as well as high-quality, optically clear grains.

Twenty-eight detrital grains from the conglomerate were analyzed on the SHRIMP (Table 2). The data are plotted in a concordia diagram (Fig. 11A) and in a cumulative probability plot of the $^{207}Pb/^{206}Pb$ ages (inset of Fig. 11A). The analyses of detrital zircon from the conglomerate define a single statistical population with an age of 2747 ± 4 Ma (mean square of weighted deviates (MSWD) = 1.2, probability of fit (POF) = 0.19, $n$ = 28). This dataset constrains the age of the conglomerate to be less than 2747 Ma. Its zircons are most likely derived from the felsic-intermediate (silica-saturated) rocks of the Confederation assemblage.

*Sample KG-03-17 (Z7803), feldspar porphyry granodiorite dike:* Sample KG-03-17 is a 7-m-wide nonfoliated barren feldspar porphyry granodiorite dike, which cuts the conglomerate (KG-02-50, z7502, described above). The sample was collected on surface at the Red Lake mine property (UTM: 449 396E, 5 656 868N; Fig. 9A). The composition of the dike is shown in Table 1 (KG-03-17BC).

The sample contains abundant small zircon, which in transmitted light appeared to contain either very strong growth zoning or core-rim relationships. As a result, zircon from this sample was selected, put on a grain mount, and analyzed on the SHRIMP (Table 2, Fig. 11B). Backscatter imaging of the zircons reveals that most of the grains have well-defined fine oscillatory zoning, interpreted to be magmatic in origin (Fig. 11C). Core-rim relationships were rarely observed. A linear

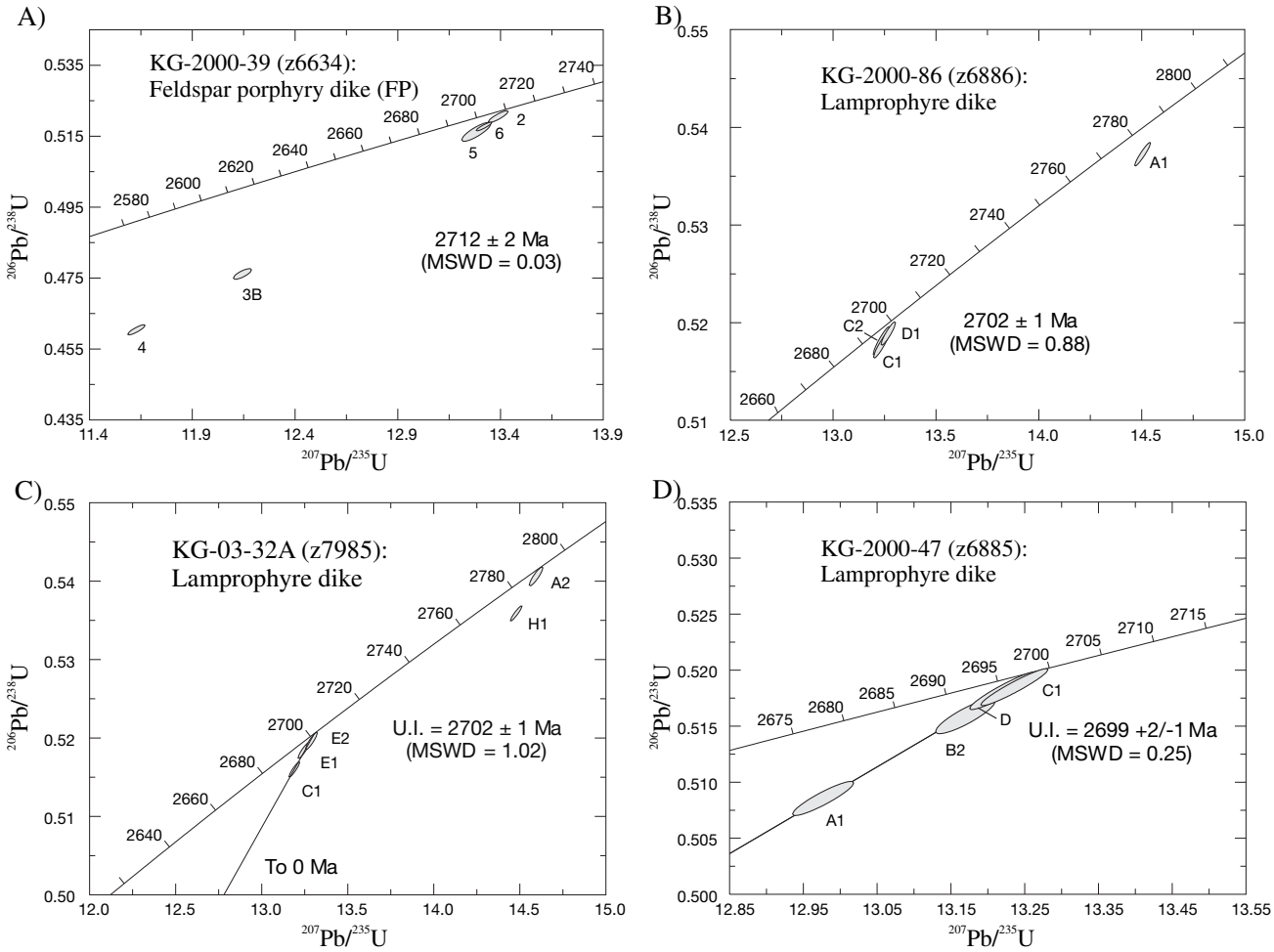


FIG. 12. A. U-Pb concordia diagram of single and multigrain zircon TIMS analyses from feldspar porphyry dike, sample KGOLD-2000-39. B. U-Pb concordia diagram of single and multigrain zircon TIMS analyses from lamprophyre dike, sample KGOLD-2000-86. C. U-Pb concordia diagram of single and multigrain zircon TIMS analyses from lamprophyre dike, sample KG-03-32A. D. U-Pb concordia diagram of single and multigrain zircon TIMS analyses from lamprophyre dike, sample KGOLD-2000-47. E. U-Pb concordia diagram of single and multigrain zircon TIMS analyses from feldspar porphyry dike, sample KG-02-81. F. U-Pb concordia diagram of zircon and titanite TIMS analyses from granodiorite dike, sample MD-39-99. G. U-Pb concordia diagram of TIMS titanite analyses from granodiorite dike, sample SNB00-5130A.

regression anchored at the origin and including all of the SHRIMP analyses has an upper intercept of 2710 ± 8 Ma (MSWD = 0.84). As the SEM imaging did not reveal much evidence for inheritance, follow-up TIMS work on four multigrain zircon fractions was conducted (Fig. 11D, Table 3). Fraction Z11a is concordant at 2711 ± 4 Ma. A linear regression that is anchored at the origin and including fractions Z10A, Z11a, and Z12a has an upper intercept of 2712 ± 2 Ma (MSWD = 0.23, POF = 0.63). This upper intercept age is in agreement with the age obtained from the SHRIMP analyses. Fraction Z10B, comprised of 4 grains, is not collinear with the other analyses and may contain a minor inherited component and/or may have experienced a different Pb-loss pattern than the other analyses. The crystallization age of the feldspar porphyry dike is interpreted to be 2712 ± 2 Ma. The depositional age of the polymictic conglomerate (KG-02-50, z7502) is therefore between ca. 2747 and 2712 Ma.

*Sample KG-2000-39 (Z6634), steeply dipping feldspar porphyry granodiorite dike:* Sample KG-2000-39 (Fig. 6C) is a 1- to 2-m-wide foliated feldspar porphyry dike chilled against and cutting a multiounce ore zone from the High-Grade zone (up to 2671 g/t or 78 oz/t Au in chip samples). The sample was taken in stope 32-826-8 cut 0 (mine grid: 5508E, 497N, elevation 5,324 ft; Fig. 9B). The high-grade ore zone shows a sinistral displacement along the dike. Figure 13A, C-E show the relationship between the dated feldspar porphry dike and the high-grade ore, as well as drill hole assays of both the dike and the ore. The geochemical analysis of the dated dike (KG-2000-40B) demonstrates that it is barren, has not been silicified, and is sulfide-free (<0.01 wt % S; Table 1). Accordingly, the age of the dike provides a minimum age on main-stage high-grade gold mineralization from the High-Grade zone.

The dike contains abundant fair to good quality euhedral zircon ranging from stubby prismatic to elongated in morphology. Backscatter and cathodoluminescence (CL) images of zircons from this sample reveal well-defined oscillatory zoning interpreted to be magmatic in origin. A representative

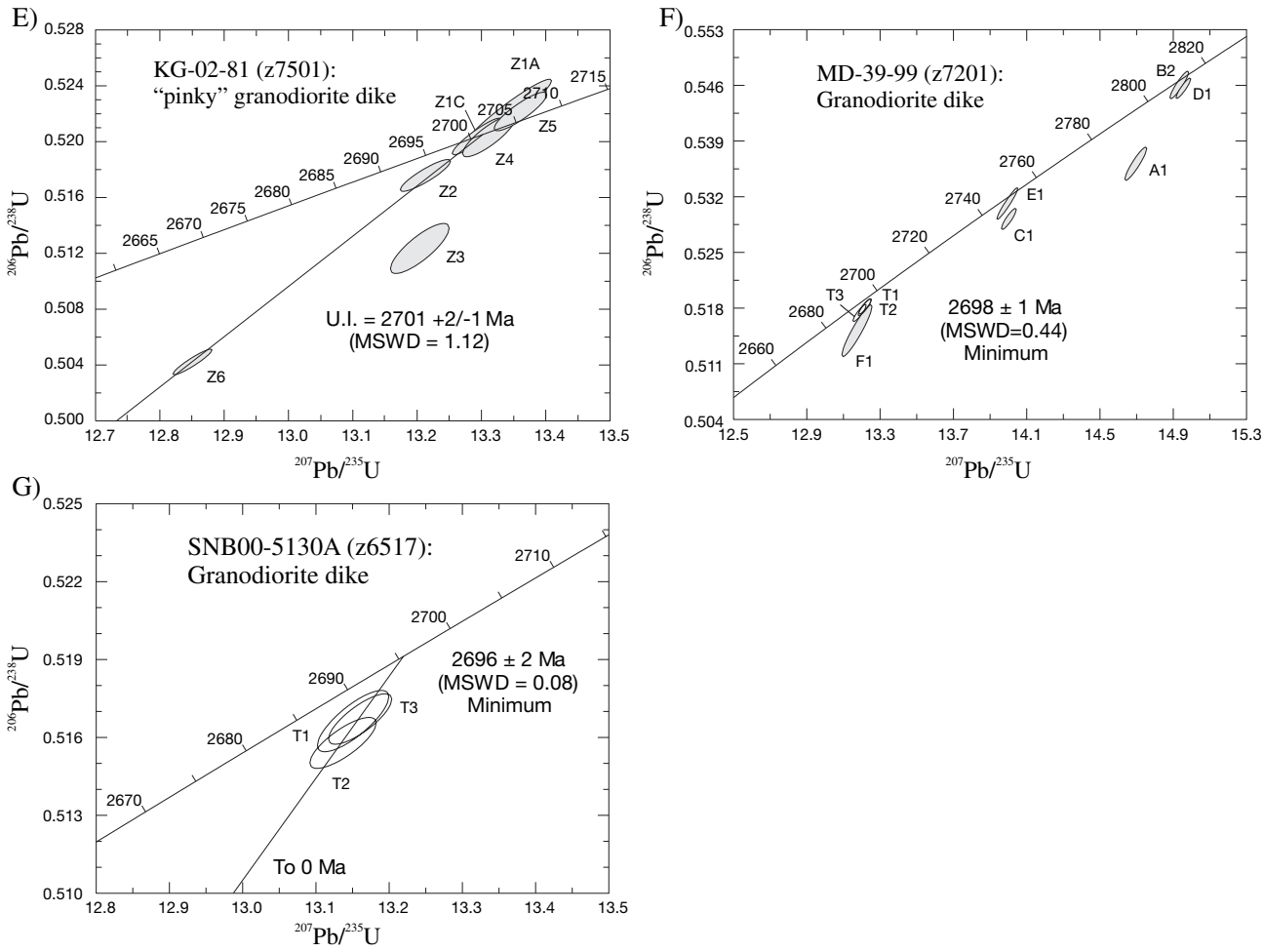


FIG. 12. *(Cont.)*

zircon from this sample is shown in Figure 14A. No apparent inherited cores or overgrowths were observed. Six zircon fractions, with one to six grains, were analyzed by TIMS from this sample. Data from one of the fractions is not included because of high analytical procedural Pb blanks. Five analyses ranged between 0.5 to 10.8 percent discordant and indicate varying amounts of Pb loss (Fig. 12A, Table 3). A linear regression including all five analyses has an upper intercept of $2715^{+4}_{-3}$ Ma and a lower intercept of 528 ± 95 Ma but has significant scatter (MSWD = 3.5, POF = 0.02). If the two most discordant analyses, zircon fractions 3B and 4 (8.4% and 10.8% discordant, respectively; Table 2, Fig. 12A) are not included, a weighted average of the $^{207}Pb/^{206}Pb$ ages of the three most concordant analyses (2, 5, and 6) is 2712 ± 2 Ma (MSWD = 0.03, POF = 0.97), which is interpreted to be the crystallization age of the dike. This age is in agreement with the age of the feldspar porphyry granodiorite dike sample KG-03-17 above.

*Sample KG-2000-86 (z6886), steeply dipping mesocratic lamprophyre dike:* Sample KG-2000-86 is a 60-cm-wide, south-southeast– striking, medium dark-gray, foliated mesocratic lamprophyre dike, containing an $S_3$ foliation defined by closely spaced biotite. The sample was collected in the Red Lake mine on level 34, in the 34-786-1 cut 0 SXC drift (mine grid: 5495E, 245N, elevation: 5,010 ft; Fig. 9C). Narrow fractures and joints (285°/70° and 030°/20°), locally coated by muscovite and/or biotite, cut the dike. The dike is chilled against and cuts foliated high-grade arsenopyrite-rich silicified carbonate ± quartz veins and wall-rock selvages (Fig. 7A-B). Figure 13B, F-I illustrate the relationships between the dated dike and the high-grade ore based on mapping and drill holes. The sample contains only 3 ppb Au and 18 ppm As (Table 1), which, together with the above relationships, demonstrate that the dated dike is barren and postore.

The sample contains a moderate amount of fair- to good-quality zircon and four zircon fractions were analyzed by TIMS (Fig. 12B, Table 3). Fraction A1 is comprised of three elongated prismatic grains. BSE and CL images of prismatic to elongated zircons from this sample reveal the presence of possible inherited cores and overgrowths with oscillatory zoning (Fig. 14B-C). Fraction A1 has a $^{207}Pb/^{206}Pb$ age of 2792 Ma and is interpreted to include an inherited component. Fractions C1, C2, and D1 comprise stubby prismatic to equant grains. SEM images of zircons of these morphologies are unzoned (Fig 14D) or show fine-scale oscillatory zoning (Fig. 14E), interpreted to be magmatic in origin. Inherited cores or overgrowths were not observed. Analyses C1, C2, and D1 overlap and are slightly discordant (0.6–0.4%). A

TABLE 3. U-Pb Thermal Ionization Mass Spectrometry (TIMS) Analytical Data

| | | | | | | | | Isotopic ratios[6] | | | | | | | Ages (Ma)[8] | | | | | | |
|---|---|---|---|---|---|---|---|---|---|---|---|---|---|---|---|---|---|---|---|---|---|
| Frac.[1] | Description[2] | Wt (ug) | U (ppm) | Pb[3] (ppm) | $^{206}Pb/^{204}Pb$ | Pb[5] (pg) | $^{208}Pb/^{206}Pb$ | $^{207}Pb/^{235}U$ | ±1SE Abs | $^{206}Pb/^{238}U$ | ±1SE Abs | Corr.[7] Coeff. | $^{207}Pb/^{206}Pb$ | ±1SE Abs | $^{206}Pb/^{238}U$ | ± 2SE | $^{207}Pb/^{235}U$ | ± 2SE | $^{207}Pb/^{206}Pb$ | ± 2SE | % Disc |
| (2) KG-03-17 (Z7803): Feldspar porphyry granodiorite dike | | | | | | | | | | | | | | | | | | | | | |
| Z10A (4) | Z,Co,Clr,rIn,Pr,Osc | 2 | 147 | 88 | 1199 | 8 | 0.16 | 13.21739 | 0.01823 | 0.51374 | 0.00057 | 0.890 | 0.18660 | 0.00012 | 2672.6 | 4.8 | 2695.3 | 2.6 | 2712.4 | 2.1 | 1.8 |
| Z10B (4) | Z,Co,Clr,fIn,fFr,Pr, Osc | 2 | 125 | 75 | 1145 | 8 | 0.15 | 13.35945 | 0.01937 | 0.51789 | 0.00062 | 0.896 | 0.18709 | 0.00012 | 2690.2 | 5.3 | 2705.4 | 2.7 | 2716.8 | 2.1 | 1.2 |
| Z11A (8) | Z,Z,Co,Clr,fFr,Pr | 3 | 120 | 73 | 624 | 22 | 0.16 | 13.45342 | 0.02364 | 0.52327 | 0.00050 | 0.770 | 0.18647 | 0.00022 | 2713.0 | 4.2 | 2712.0 | 3.3 | 2711.3 | 3.9 | –0.1 |
| Z12A (10) | Z,Co,Clr,rIn,fFr,El | 3 | 180 | 110 | 968 | 20 | 0.20 | 13.24377 | 0.01898 | 0.51460 | 0.00047 | 0.840 | 0.18665 | 0.00015 | 2676.2 | 4.0 | 2697.2 | 2.7 | 2712.9 | 2.7 | 1.7 |
| (3) KG-2000-39 (Z6634): Feldspar porphyry granodiorite dike | | | | | | | | | | | | | | | | | | | | | |
| 2 (1) | Z,Co,Clr,fFr,fIn,St, Osc | 1 | 123 | 74 | 893 | 5 | 0.16 | 13.38884 | 0.02404 | 0.52052 | 0.00083 | 0.8749 | 0.18655 | 0.00016 | 2701.4 | 7.1 | 2707.5 | 3.4 | 2712.0 | 2.9 | 0.5 |
| 3B (1) | Z,Co,Clr,fFr,fIn,St, Osc | 1 | 184 | 103 | 805 | 8 | 0.19 | 12.14400 | 0.02203 | 0.47616 | 0.00075 | 0.7742 | 0.18497 | 0.00021 | 2510.5 | 6.5 | 2615.6 | 3.4 | 2698.0 | 3.8 | 8.4 |
| 4 (2) | Z,Co,Clr,fFr,fIn,Pr, Osc | 2 | 100 | 53 | 1241 | 4 | 0.15 | 11.62795 | 0.02097 | 0.46041 | 0.00071 | 0.8667 | 0.18317 | 0.00016 | 2441.4 | 6.3 | 2574.9 | 3.4 | 2681.8 | 3.0 | 10.8 |
| 5 (3) | Z,Co,Clr,fFr,fIn,Pr, Osc | 2 | 200 | 121 | 512 | 25 | 0.17 | 13.28262 | 0.03534 | 0.51621 | 0.00133 | 0.841 | 0.18662 | 0.00028 | 2683.1 | 11.3 | 2699.9 | 5.0 | 2712.6 | 4.9 | 1.3 |
| 6 (6) | Z,Co,Clr,rFr,fIn,Pr, Osc | 3 | 121 | 74 | 2036 | 6 | 0.19 | 13.31961 | 0.01885 | 0.51774 | 0.00061 | 0.9091 | 0.18659 | 0.00011 | 2689.6 | 5.2 | 2702.6 | 2.7 | 2712.3 | 2.0 | 1.0 |
| (4) KG-2000-86 (Z6886): Lamprophyre dike | | | | | | | | | | | | | | | | | | | | | |
| A1 (3) | Z,pBr,Clr,rIn,El | 5 | 134 | 80 | 9334 | 3 | 0.10 | 14.50432 | 0.01928 | 0.53726 | 0.00061 | 0.942 | 0.19580 | 0.00009 | 2772.0 | 5.1 | 2783.3 | 2.5 | 2791.5 | 1.5 | 0.9 |
| C1 (1) | Z,pBr,Clr,St | 4 | 124 | 67 | 6275 | 3 | 0.03 | 13.23553 | 0.01943 | 0.51774 | 0.00069 | 0.927 | 0.18541 | 0.00010 | 2689.6 | 5.8 | 2696.6 | 2.8 | 2701.9 | 1.8 | 0.6 |
| C2 (3) | Z,pBr,Clr,St | 2 | 180 | 97 | 8603 | 2 | 0.03 | 13.23554 | 0.02038 | 0.51814 | 0.00074 | 0.924 | 0.18526 | 0.00011 | 2691.3 | 6.3 | 2696.6 | 2.9 | 2700.6 | 2.0 | 0.4 |
| D1 (2) | Z,pBr,Clr,rFr,Eq | 5 | 138 | 75 | 9986 | 2 | 0.03 | 13.26846 | 0.01757 | 0.51890 | 0.00060 | 0.917 | 0.18545 | 0.00010 | 2694.5 | 5.1 | 2698.9 | 2.5 | 2702.3 | 1.7 | 0.4 |
| (5) KG-03-32A (Z7985): Lamprophyre dike | | | | | | | | | | | | | | | | | | | | | |
| A2 (3) | Z,Co,Clr,rIn,Fg | 5 | 66 | 40 | 1238 | 9 | 0.10 | 14.59417 | 0.01982 | 0.54061 | 0.00061 | 0.900 | 0.19579 | 0.00012 | 2786.0 | 5.1 | 2789.2 | 2.6 | 2791.5 | 2.0 | 0.2 |
| C1 (1) | Z,pBr,Clr,rIn,Tip | 2 | 396 | 210 | 4678 | 7 | 0.01 | 13.18956 | 0.01552 | 0.51599 | 0.00049 | 0.929 | 0.18539 | 0.00009 | 2682.1 | 4.1 | 2693.3 | 2.2 | 2701.7 | 1.5 | 0.9 |
| E1 (1) | Z,pBr,Clr,St | 2 | 225 | 130 | 2185 | 8 | 0.11 | 13.24354 | 0.01617 | 0.51840 | 0.00051 | 0.915 | 0.18528 | 0.00009 | 2692.4 | 4.3 | 2697.2 | 2.3 | 2700.8 | 1.7 | 0.4 |
| E2 (1) | Z,pBr,Clr,rIn,St | 1 | 483 | 257 | 2282 | 3 | 0.01 | 13.28912 | 0.01700 | 0.51963 | 0.00056 | 0.913 | 0.18548 | 0.00010 | 2697.6 | 4.8 | 2700.4 | 2.4 | 2702.5 | 1.7 | 0.2 |
| H1 (2) | Z,pBr,Clr,Pr | 1 | 406 | 239 | 4948 | 4 | 0.08 | 14.47850 | 0.01679 | 0.53589 | 0.00049 | 0.941 | 0.19595 | 0.00008 | 2766.2 | 4.1 | 2781.6 | 2.2 | 2792.8 | 1.4 | 1.2 |
| (6) KG-2000-47 (Z6885): Lamprophyre dike | | | | | | | | | | | | | | | | | | | | | |
| A1 (2) | Z,Co,Clr,fFr,Pr | 3 | 138 | 84 | 4711 | 2 | 0.21 | 12.97676 | 0.02069 | 0.50855 | 0.00076 | 0.911 | 0.18507 | 0.00012 | 2650.4 | 6.5 | 2678.0 | 3.0 | 2698.8 | 2.2 | 2.2 |
| B2 (1) | Z,Co,Clr,fIn,St | 2 | 236 | 147 | 5926 | 2 | 0.22 | 13.16972 | 0.02021 | 0.51588 | 0.00077 | 0.868 | 0.18515 | 0.00014 | 2681.7 | 6.6 | 2691.9 | 2.9 | 2699.6 | 2.6 | 0.8 |
| C1 (1) | Z,Co,Clr,Eq | 3 | 147 | 92 | 5257 | 2 | 0.22 | 13.23604 | 0.02273 | 0.51848 | 0.00082 | 0.950 | 0.18515 | 0.00010 | 2692.7 | 7.0 | 2696.6 | 3.2 | 2699.6 | 1.8 | 0.3 |
| D (8) | Z,Co,Clr,cIn,St | 5 | 249 | 154 | 7065 | 6 | 0.20 | 13.22149 | 0.02301 | 0.51817 | 0.00085 | 0.939 | 0.18506 | 0.00011 | 2691.4 | 7.2 | 2695.6 | 3.3 | 2698.7 | 2.0 | 0.3 |
| (7) KG-02-81 (Z7501): "pinky" granodiorite dike | | | | | | | | | | | | | | | | | | | | | |
| Z1A (1) | Z,Co,Clr,El | 1 | 226 | 138 | 2978 | 3 | 0.17 | 13.34277 | 0.03308 | 0.52215 | 0.00116 | 0.9537 | 0.18533 | 0.00014 | 2708.3 | 9.8 | 2704.2 | 4.7 | 2701.2 | 2.5 | –0.3 |
| Z1C (1) | Z,Co,Clr,fIn,El | 1 | 271 | 169 | 2783 | 4 | 0.21 | 13.29253 | 0.01892 | 0.52037 | 0.00065 | 0.9233 | 0.18526 | 0.00010 | 2700.8 | 5.5 | 2700.7 | 2.7 | 2700.6 | 1.8 | 0.0 |
| Z2 (1) | Z,Co,Clr,fIn,Pr | 3 | 173 | 102 | 4610 | 3 | 0.14 | 13.21291 | 0.01952 | 0.51758 | 0.00057 | 0.8889 | 0.18515 | 0.00013 | 2688.9 | 4.8 | 2695.0 | 2.8 | 2699.5 | 2.3 | 0.5 |
| Z3 (11) | Z,Co,Clr,fIn,El | 2 | 107 | 63 | 2002 | 3 | 0.16 | 13.20414 | 0.02280 | 0.51235 | 0.00089 | 0.8136 | 0.18692 | 0.00020 | 2666.6 | 7.6 | 2694.4 | 3.3 | 2715.2 | 3.5 | 2.2 |
| Z4 (1) | Z,Co,Clr,Pr | 1 | 159 | 96 | 1314 | 4 | 0.17 | 13.31173 | 0.02053 | 0.52041 | 0.00075 | 0.8469 | 0.18552 | 0.00015 | 2700.9 | 6.3 | 2702.0 | 2.9 | 2702.8 | 2.8 | 0.1 |
| Z5 (3) | Z,Co,Clr,St | 1 | 122 | 76 | 988 | 5 | 0.19 | 13.36071 | 0.02047 | 0.52216 | 0.00069 | 0.8757 | 0.18558 | 0.00014 | 2708.3 | 5.8 | 2705.5 | 2.9 | 2703.4 | 2.4 | –0.2 |
| Z6 (2) | Z,Co,Clr,St | 2 | 688 | 420 | 3812 | 9 | 0.22 | 12.85075 | 0.01516 | 0.50422 | 0.00046 | 0.9343 | 0.18484 | 0.00009 | 2631.9 | 4.0 | 2668.8 | 2.2 | 2696.8 | 1.5 | 2.9 |
| (8) MD-39-99 (Z7201): Granodiorite dike | | | | | | | | | | | | | | | | | | | | | |
| A1 (1) | Z,Co,Clr,fIn,Pr | 1 | 171 | 107 | 1395 | 5 | 0.16 | 14.69547 | 0.02982 | 0.53615 | 0.00105 | 0.920 | 0.19879 | 0.00016 | 2767.3 | 8.8 | 2795.7 | 3.9 | 2816.3 | 2.6 | 2.1 |
| B2 (1) | Z,pBr,Clr,St | 3 | 75 | 47 | 1499 | 6 | 0.13 | 14.93284 | 0.02555 | 0.54605 | 0.00087 | 0.918 | 0.19834 | 0.00013 | 2808.7 | 7.2 | 2811.0 | 3.3 | 2812.6 | 2.2 | 0.2 |

TABLE 3. *(Cont.)*

| | | | | | | | | Isotopic ratios[6] | | | | | | | Ages (Ma)[8] | | | | | | |
|---|---|---|---|---|---|---|---|---|---|---|---|---|---|---|---|---|---|---|---|---|---|
| Frac.[1] | Description[2] | Wt (ug) | U (ppm) | Pb[3] (ppm) | $\frac{^{206}Pb}{^{204}Pb}$ | Pb[5] (pg) | $\frac{^{208}Pb}{^{206}Pb}$ | $\frac{^{207}Pb}{^{235}U}$ | ±1SE Abs | $\frac{^{206}Pb}{^{238}U}$ | ±1SE Abs | Corr.[7] Coeff. | $\frac{^{207}Pb}{^{206}Pb}$ | ±1SE Abs | $\frac{^{206}Pb}{^{238}U}$ | ± 2SE | $\frac{^{207}Pb}{^{235}U}$ | ± 2SE | $\frac{^{207}Pb}{^{206}Pb}$ | ± 2SE | % Disc |
| C1 (5) | Z,Co,Clr,fIn,St | 3 | 127 | 74 | 1435 | 8 | 0.09 | 14.00279 | 0.02031 | 0.52921 | 0.00066 | 0.894 | 0.19190 | 0.00012 | 2738.1 | 5.6 | 2749.9 | 2.7 | 2758.5 | 2.2 | 0.9 |
| D1 (1) | Z,pBr,Clr,rFr,El | 9 | 62 | 39 | 4192 | 4 | 0.14 | 14.95484 | 0.02009 | 0.54563 | 0.00064 | 0.913 | 0.19879 | 0.00011 | 2807.0 | 5.4 | 2812.4 | 2.6 | 2816.3 | 1.8 | 0.4 |
| E1 (10) | Z,Co,Clr,rFr,fIn,Pr | 6 | 101 | 62 | 2434 | 9 | 0.14 | 13.99472 | 0.02849 | 0.53115 | 0.00100 | 0.958 | 0.19110 | 0.00011 | 2746.3 | 8.4 | 2749.4 | 3.9 | 2751.6 | 1.9 | 0.2 |
| F1 (1) | Z,Co,Clr,rIn,St | 6 | 37 | 22 | 2004 | 3 | 0.15 | 13.17358 | 0.04096 | 0.51516 | 0.00163 | 0.931 | 0.18547 | 0.00022 | 2678.6 | 13.9 | 2692.2 | 5.9 | 2702.4 | 3.9 | 1.1 |
| T1 (20) | T,Br,Clr,An | 91 | 66 | 40 | 1601 | 122 | 0.17 | 13.21763 | 0.01739 | 0.51822 | 0.00049 | 0.890 | 0.18499 | 0.00012 | 2691.6 | 4.2 | 2695.3 | 2.5 | 2698.1 | 2.1 | 0.3 |
| T2 (23) | T,Br,Clr,An | 113 | 52 | 29 | 1638 | 118 | 0.06 | 13.21590 | 0.01811 | 0.51809 | 0.00053 | 0.901 | 0.18501 | 0.00012 | 2691.1 | 4.5 | 2695.2 | 2.6 | 2698.3 | 2.1 | 0.3 |
| T3 (22) | T,Br,Clr,An | 142 | 57 | 32 | 1692 | 156 | 0.07 | 13.18790 | 0.01814 | 0.51738 | 0.00054 | 0.900 | 0.18487 | 0.00012 | 2688.1 | 4.6 | 2693.2 | 2.6 | 2697.0 | 2.1 | 0.4 |
| (9)SNB00-5130A (Z6517): Granodiorite dike[9] | | | | | | | | | | | | | | | | | | | | | |
| T1 (24) | T,Br,Clr,An,Fg | 110 | 39 | 22 | 683 | 207 | 0.05 | 13.15075 | 0.02438 | 0.51663 | 0.00059 | 0.7956 | 0.18462 | 0.00022 | 2684.9 | 5.0 | 2690.5 | 3.5 | 2694.8 | 3.9 | 0.5 |
| T2 (27) | T,Br,Clr,fFr,An,Fg | 78 | 43 | 24 | 711 | 155 | 0.07 | 13.13706 | 0.02263 | 0.51579 | 0.00049 | 0.7844 | 0.18472 | 0.00021 | 2681.3 | 4.2 | 2689.5 | 3.3 | 2695.7 | 3.8 | 0.7 |
| T3 (33) | T,pBr,fFr,fdIn, oIn,An,Fg | 103 | 48 | 27 | 833 | 193 | 0.06 | 13.16046 | 0.02159 | 0.51671 | 0.00049 | 0.7882 | 0.18473 | 0.00020 | 2685.2 | 4.1 | 2691.2 | 3.1 | 2695.8 | 3.5 | 0.5 |

Notes: % Disc refers to Discordance relative to origin = 100 * (1-($^{206}Pb/^{238}U$ age)/($^{207}Pb/^{206}Pb$ age))

[1] Fraction identifier; number in brackets refer to number of grains in analysis; all zircon fractions were abraded following the method of Krogh (1982); titanite fractions were also lighted air abraded

[2] Fraction descriptions: An = anhedral, Br = brown, Clr = clear, Co = colorless, El = elongate, fdIn = fluid inclusions, fFr = few fractures, Fg = fragment, fIn = few inclusions, oIn = opaque inclusions, Osc = oscillatory zoning, pBr = pale brown, Pr = prismatic, rIn = rare inclusions, rFr = rare fractures, St = stubby prism, T = titanite, Tip = tip, Z = zircon

[3] Radiogenic Pb

[4] Measured ratio, corrected for spike and fractionation; the error on the calibration of the GSC $^{205}Pb$-$^{233}U$-$^{235}U$ spike utilized in this study is 0.22% ($2\sigma$)

[5] Total common Pb in picograms in the analysis, corrected for fractionation and spike

[6] Corrected for blank Pb and U and common Pb, errors quoted are $1\sigma$ absolute; procedural blank values for this study ranged from 0.1 to 0.3 pg for U, 2 to 3 pg for Pb for zircon analyses, and 1 to 2 pg U, 8 pg Pb for titanite analyses; Pb blank isotopic composition is based on the analysis of procedural blanks; corrections for common Pb were made using Cumming-Richards compositions (Cumming and Richards, 1975)

[7] Correlation coefficient

[8] Corrected for blank and common Pb, errors quoted are $2\sigma$ in Ma

[9] NAD 1983,UTM 15 easting 433467 northing 564441

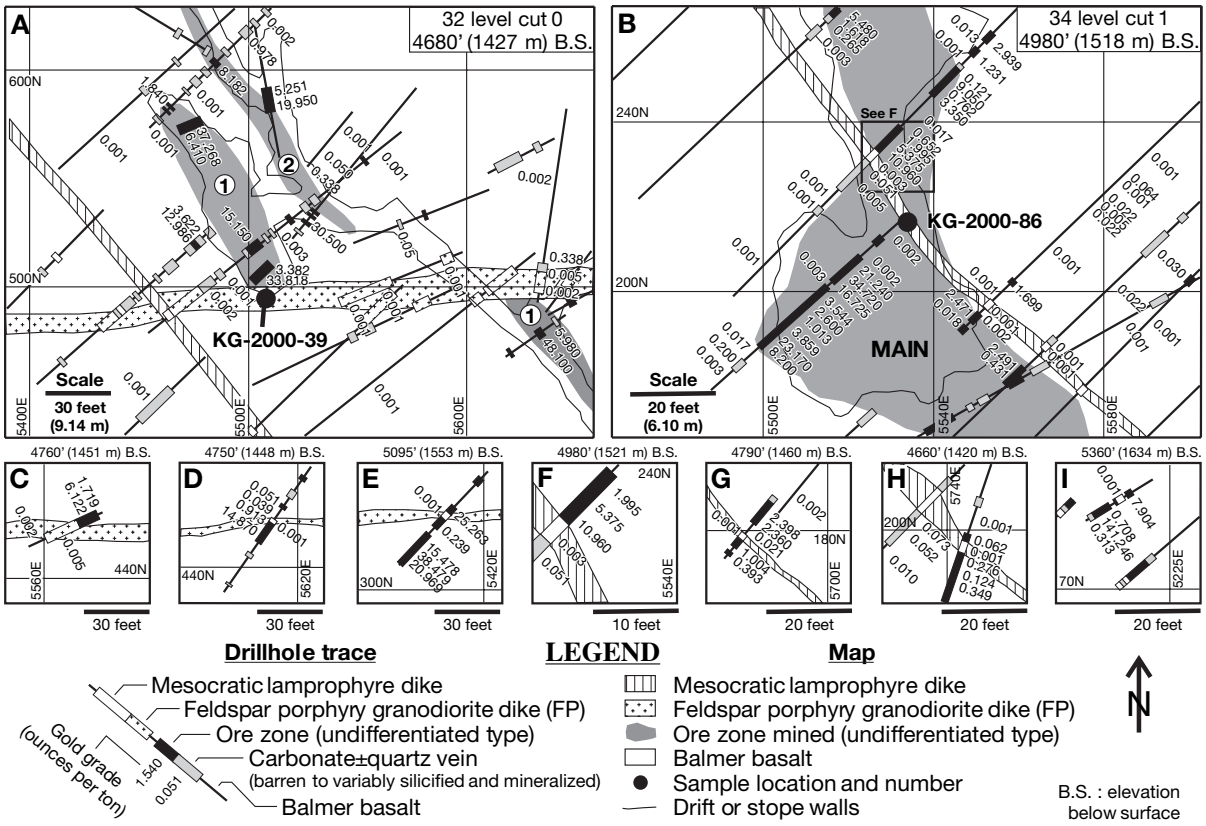


FIG. 13. Simplified geologic maps and drill hole data showing feldspar porphyry granodiorite and/or lamprophyre dike cutting high-grade ore zones. Mine grid is in feet. Modified from Goldcorp Inc. geologic data. A. Feldspar porphyry granodiorite dike cutting high-grade ore in MAIN/MAIN A zone, level 32, stope 32-826-8 cut 0 area, 4,680 ft below surface. B. Mesocratic lamprophyre dike cutting ore in MAIN zone, level 34, stope 34-786-1 cut 1 area, 4,980 ft below surface. Note that the geochronology sample KG-2000-86 was taken in the same area but on cut 0, 10 ft below the shown level plan. C. Same as (A) but 4,760 ft below surface. D. Same as (A) but 4,750 ft below surface. E. Same as (A) but 5,095 ft below surface. F. Close-up of lamprophyre dike cutting high-grade ore as seen in (B). G. Same as (B) but 4,790 ft below surface. H. Same as (B) but 4,660 ft below surface. I. Lamprophyre dike cutting high-grade ore in Hanging-Wall Shear zone area, 5,360 ft below surface. The purpose of all these different plan views is to show that the dikes cut the ore and that there is no gold in the dikes.

weighted average of the $^{207}Pb/^{206}Pb$ ages of the three fractions is 2702 ± 1 Ma (MSWD = 0.88, POF = 0.42), which is interpreted to be the crystallization age of the dike.

*Sample KG-03-32A (z7985), steeply dipping mesocratic lamprophyre dike:* Sample KG-03-32A is a 50-cm-wide, east-striking nonfoliated mesocratic lamprophyre dike. It contains up to 50 percent hornblende and tschermakitic amphibole with plagioclase, biotite, and traces of carbonate. The abundance of amphibole accounts for the lower silica content, whereas the Zr, Y, and $TiO_2$ concentrations indicate that the sampled dike is similar to the other mesocratic dikes (Table 1). The dike and host basalt contain fractures with spectacular coatings and fillings of visible gold without any silicification or arsenopyrite in the dike (Fig. 8A-C). Geochemical analysis of the dated dike (KG-03-32B) demonstrates that, despite the spectacular visible gold filling the late brittle fractures, the dike is otherwise barren (Table 1). The high $CO_2$ content of the dike is interpreted as due to autometasomatism or deuteric carbonate alteration both known to be common features of lamprophyres (Rock, 1991), contamination of the magma during its intrusion through mineralized structures, or late carbonate veinlets. The sample was collected in the Red Lake mine on level 32, in the 32-806-3, cut 5 (mine grid: 5900E, 200N, elevation: 5,400 ft; Fig. 9D).

The sample contains a moderate amount of fair- to good-quality zircon; five zircon fractions were analyzed by TIMS (Fig. 12C, Table 3). Fractions H1 and A2 are comprised of two prismatic zircon crystals and three fragments of larger crystals, respectively. Figure 14F shows BSE and CL images of a prismatic zircon from this sample with a possible inherited core, the boundary of which is marked by inclusions and at least one phase of overgrowth. Fractions H1 and A2 have $^{207}Pb/^{206}Pb$ ages of 2792 to 2793 Ma and are interpreted to be inherited. This inheritance age is the same as that obtained for KGOLD-2000-86 (z6886), the other sample of a steeply dipping lamprophyre dike described above. Fractions E1 and E2 are comprised of single stubby prismatic grains. SEM images of a grain of this morphology with oscillatory zoning are presented in Figure 14G. Fraction C1 is a single tip of a zircon crystal. A linear regression (MSWD = 1.02, POF = 0.30) including fractions C1, E1, and E2 that is anchored at the origin has an upper intercept age of 2702 ± 1 Ma, which is interpreted to be the crystallization age of the dike. This age is in agreement with the age of the lamprophyre dike (sample KG-2000-86) described above.

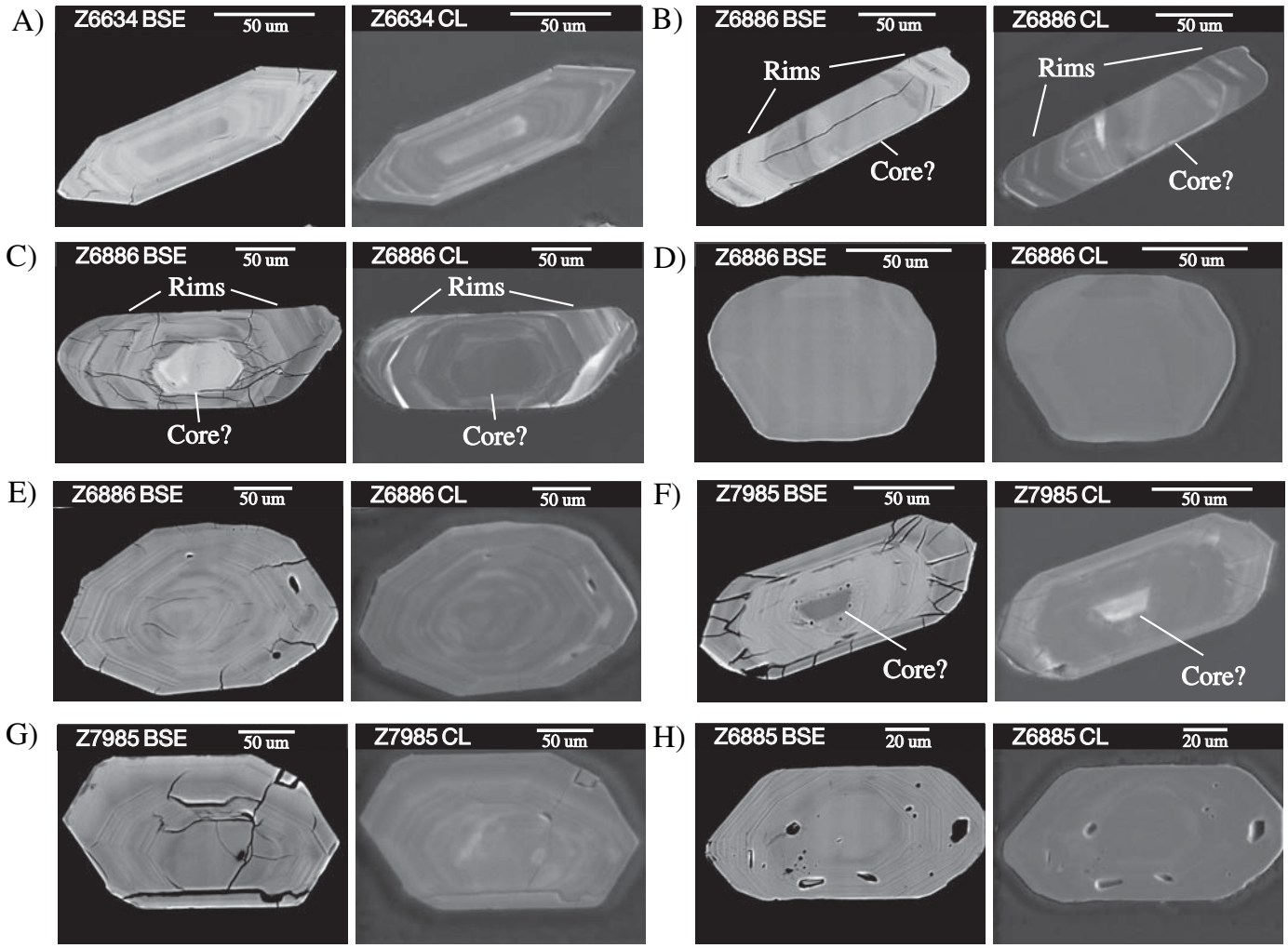


FIG. 14. A. Backscattered electron image (BSE) and cathodoluminescence (CL) images of representative zircons from sample KG-2000-39 (z6634), showing magmatic oscillatory zoning. B. BSE and CL images of an elongated zircon, representative of fraction A1 from sample KG-2000-86 (z6886), with a possible core and overgrowths. C. BSE and CL images of a prismatic zircon, representative of fraction A1 from sample KG-2000-86 (z6886), with a possible core and overgrowths. D. BSE and CL images of an unzoned equant zircon, representative of fraction D, from sample KG-2000-86 (z6886). E. BSE and CL images of a stubby prismatic zircon with fine-oscillatory zoning, representative of fraction C, from sample KGOLD-2000-86 (z6886). F. BSE and CL images of a prismatic zircon, representative of fraction A from sample KG-03-32A (z7985), with a possible inherited core marked by a trail of inclusions at the boundary and at least one phase of overgrowth. G. BSE and CL images of a stubby prismatic zircon with oscillatory zoning, representative of fractions C and E, from sample KG-03-32A (z7985). H. BSE and CL images of a stubby prismatic zircon with fine oscillatory zoning, representative of the zircons analyzed from sample KG-2000-47 (z6885).

*Sample KG-2000-47 (z6885), shallowly dipping melanocratic lamprophyre dike:* Sample KG-2000-47 is a dark gray-colored, massive, homogeneous lamprophyre dike that is representative of a set of shallowly dipping lamprophyre dikes that cut across all units and mineralized zones. The lamprophyre is nonfoliated, composed of abundant feldspar and biotite, and contains a small amount (less than 1%) of disseminated, very fine grained sulfides with a few thin carbonate veinlets cutting through the rock. Geochemical analysis of the dated dike (KG-2000-48B) demonstrates that it is barren and unaltered (Table 1). The sample was collected on level 30 of the Red Lake mine, at the intersection between the 30-844-1 SCX and 30-S959 WDR drifts (mine grid: 4212E, 2287N, elevation: 5603 ft; Figs. 7D, 9E).

The sample contains a small number of euhedral zircon crystals of fair quality, ranging from equant to stubby prismatic in morphology. Figure 14H shows SEM images of representative zircon from this rock with fine-scale oscillatory zoning, interpreted to be magmatic in origin. TIMS analyses of four zircon fractions, ranging from one to eight grains, are 2.2 to 0.3 percent discordant (Fig. 12D, Table 3). A linear regression including all four analyses (MSWD = 0.25, POF = 0.78) has an upper intercept of $2699^{+2}_{-1}$ Ma and a lower intercept near the origin (55 ± 170 Ma). The upper intercept age of $2699^{+2}_{-1}$ Ma is interpreted to be the crystallization age of the lamprophyre dike.

Sample *KG-02-81 (z7501), "pinky" granodiorite dike:* Sample KG-02-81 is a 1.5-m-wide weakly foliated pinky granodiorite

dike. It contains abundant plagioclase, partially altered to sericite, 5 percent biotite, and traces of quartz. The dike cuts across komatiitic basalt and carbonate veins (Fig. 7E-F). Geochemical analysis of the dated dike (KG-03-21B) demonstrates that it is barren and without any sulfide (<0.01 wt % S) or arsenic (Table 1). The sample was collected on level 37 of the Red Lake mine in the 37-735-1SXC exploration drift (mine grid: 4625E, 204S, elevation: 4,580 ft; Fig. 9F).

This sample contains abundant euhedral zircon ranging from stubby prismatic grains to elongated crystals. Seven fractions of single and multiple grains were analyzed by TIMS (Fig. 12E, Table 3). A linear regression including all of the fractions except Z3 has an upper intercept age of $2701^{+2}_{-1}$ Ma and a lower intercept near the origin (354 ± 127 Ma; MSWD = 1.12, POF = 0.34). The upper intercept age of $2701^{+2}_{-1}$ Ma is interpreted to be the crystallization age of the feldspar porphyry dike and provides a minimum age for the carbonate veins. Fraction Z3, which comprises of a large number of grains ($n$ = 11), is interpreted to contain an inherited component.

*MD-39-99 (z7201), postore granodiorite dike from the Madsen mine:* Sample MD-39-99 is a postore, medium- to dark-gray, massive, fine-grained, 1- to 2-m-wide granodiorite dike collected underground at the Madsen mine (shaft 2, level 4; 8290N, 13980E; Fig. 8E).

The granodiorite contains abundant zircon with a range of morphologies including stubby prismatic to elongated euhedral crystals, subrounded to rounded grains, and zircons with apparent inherited cores. Single and multigrain zircon fractions (fractions A1, B2, C1, D1, and E1) analyzed by TIMS range in age from about 2815 to 2752 Ma and are all interpreted to be inherited zircons (Fig. 12F, Table 3). Three fractions of clear, brown, anhedral titanite were also analyzed (T1-T3) and range from 0.4 to 0.3 percent discordant. A weighted average of the $^{207}Pb/^{206}Pb$ ages of the three titanite analyses is 2698 ± 1 Ma (MSWD = 0.44, POF = 0.64). Zircon fraction F1, comprised a single stubby prismatic grain with a $^{207}Pb/^{206}Pb$ age of 2702 ± 4 Ma, which is within error of the age of the titanite analyses. The date of 2698 ± 1 Ma is interpreted to represent the minimum crystallization age for the granodiorite dike based on the ages of the titanite.

*Sample SNB00-5130A (z6517), granodiorite dike from Creek zone near Starratt-Olsen:* The granodiorite dike is 1.5 m wide and cuts quartz-sericite-pyrite schist hosting gold-bearing quartz veins and foliation-parallel biotite-diopside-actinote-epidote metasomatic layering hosted by highly strained basalt and gabbro of the Balmer assemblage (Fig. 8F). The latter alteration style is very similar to the proximal alteration at the Madsen mine (Dubé et al., 2000). The dike is at a high angle to the main east-southeast–trending foliation and it is only slightly buckled. It contains a very weak $S_3$ foliation and postdates alteration.

Three fractions of light-brown to brown, anhedral fragments of titanite were analyzed from this dike. Data from all three analyses overlap and range between 0.5 to 0.7 percent discordant (Fig. 12G, Table 3). A weighted average of the $^{207}Pb/^{206}Pb$ ages of all three fractions has an age of 2696 ± 2 Ma (MSWD = 0.08, POF = 0.92). This age is interpreted to represent a minimum age for the crystallization of the granodiorite dike.

## Discussion and Implications

A minimum age for main-stage high-grade gold mineralization is established at 2712 ± 2 Ma, the age of the feldspar porphyry dike that cuts the Goldcorp High-Grade zone. This age is within error of a 2714 ± 4 Ma quartz-feldspar porphyry dike that cuts sulfide-rich and replacement-style mineralization (ESC-type mineralization; Corfu and Andrews, 1987). The maximum age of the high-grade mineralization is unknown. Therefore, it is unclear whether these two styles of mineralization were contemporaneous and precipitated from the same large-scale hydrothermal system. However, taking into account their analogous geologic characteristics (Dubé et al., 2002), these ages make it permissible that these two types of mineralization, although extremely diverse in terms of grade, were formed at the same time from a single large-scale hydrothermal system, locally focused in extremely rich ore zones such as the High-Grade zone. The main difference between the two styles of mineralization is their structural setting (Dubé et al., 2002). Both types of gold mineralization were present in mafic-dominated rocks prior to 2712 Ma, significantly earlier than lode gold mineralization in other parts of the Superior province (cf. Kerrich and Cassidy, 1994).

In the High-Grade zone, crosscutting relationships suggest that gold-rich silicification is contemporaneous with deformation of the iron-carbonate ± quartz veins, and this deformation is interpreted as the regional $D_2$ event (Dubé et al. 2001a, 2002; Twomey and McGibbon, 2001). Consequently, we propose that the high-grade mineralization probably formed between ca. 2723 and 2712 Ma, the interpreted age of $D_2$ deformation (Fig. 15). This age interval is similar to the intervals proposed by Corfu and Andrews (1987; 2720–2714 Ma) and Penczak and Mason (1997; 2722–2710 Ma) for the entire Campbell-Red Lake deposit. This was a time of extensive magmatic and tectonic activity in the Red Lake belt, during which the Dome, McKenzie, and Abino granodiorite stocks and the Hammell Lake pluton were emplaced and the belt was penetratively deformed and metamorphosed ($D_2$). The maximum age of 2747 Ma for polymictic conglomerate from the Red Lake mine confirms correlation with other conglomeratic rocks of the Huston assemblage. In the Campbell-Red Lake deposit area, the conglomerate of the Huston assemblage coincides with the interface between the Balmer or Bruce Channel assemblages and the Confederation assemblage. The presence of the conglomerate implies that, at least locally, the upper portion of the Bruce Channel and locally Balmer assemblages were exposed at surface by 2747 Ma. Exhumation of these assemblages was caused by significant uplift and erosion, possibly in response to $D_1$ deformation, as proposed by Sanborn-Barrie et al. (2001). Presence of local andalusite-rich clasts and clasts of carbonate vein material in an unaltered matrix demonstrates that there was at least some carbonate and aluminous alteration prior to deposition of the conglomerate. The position of a large amount of colloform-crustiform iron-carbonate ± quartz veins in the Campbell-Red Lake deposit underneath the interpreted subaerial unconformity may partly explain their epithermal-epizonal (near-surface) character. The conglomerate is deformed by $D_2$ deformation, metamorphosed, and locally strongly altered (Dubé et al., 2003). These relationships indicate protracted

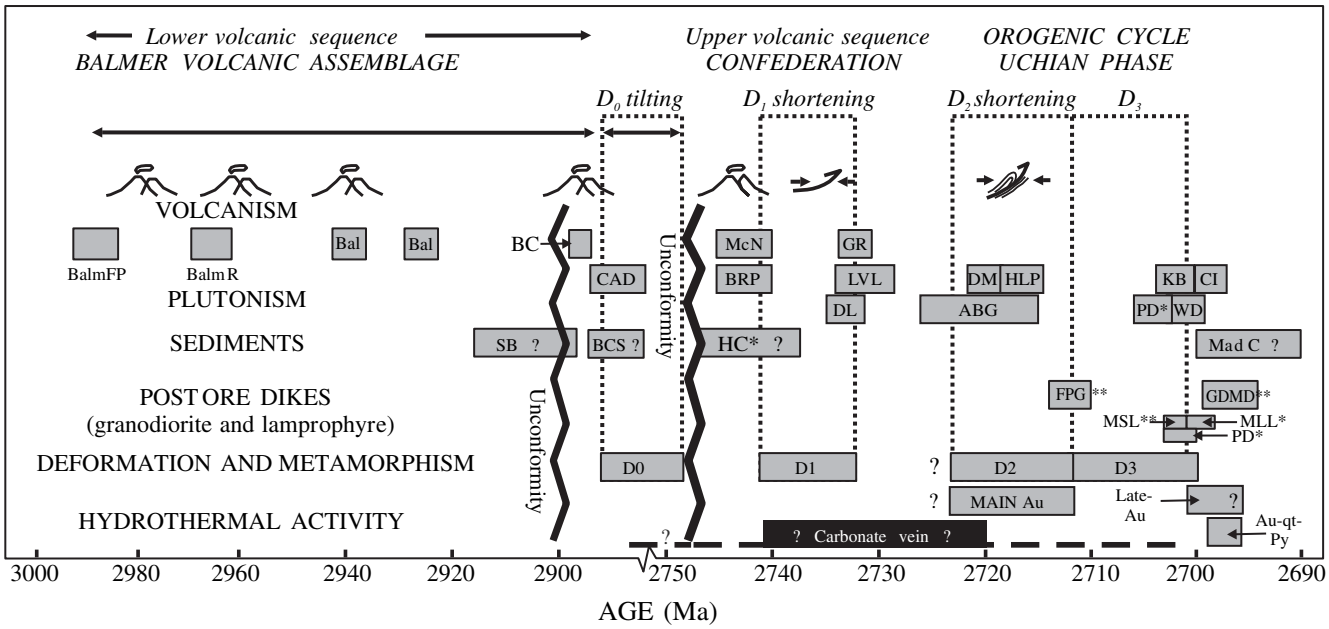


FIG. 15. Schematic representation of the timing and nature of the geologic events in relationship to gold mineralization in the Red Lake district. The width of the boxes represents the age and associated error. ABG = albino granodiorite; Au-qt-Py = late gold, quartz, pyrite mineralization; BalmFP = 2989 ± 3 Ma Balmer rhyolite (zircon age, Corfu and Andrews, 1987), Bal = Ball 2940 ± 2 and 2925 ± 3 Ma felsic volcanics (zircon ages, Corfu and Wallace, 1986); BalmFP = 2989 ± 3 Balmer rhyolite (zircon age, Corfue and Andrews, 1987); BalmR = $2964^{+5}_{-1}$ Ma Balmer rhyolite (zircon age, Corfu and Andrews, 1987); BC = 2894 ± 2 Ma Bruce Channel volcaniclastics (zircon age, Corfu and Wallace, 1986; Corfu and Andrews, 1987); BCS? = <2894 Bruce Channel assemblage sedimentary rocks (zircon age, Sanborn-Barrie et al., 2001); BRP = $2742^{+3}_{-2}$ Ma Brewis Porphyry (zircon age, Corfu and Andrews, 1987); CAD = 2870 ± 15 Ma Campbell-Dickenson diorite (zircon and baddeleyite ages, Corfu and Andrews, 1987); CI = 2699 ± 1 and 2697 ± 2 Ma Cat Island pluton (zircon ages, Noble et al., 1989; Sanborn-Barrie et al., 2004); DL = Douglas Lake pluton; DM = 2718.2 ± 1.1 Ma Dome and $2720^{+3}_{-2}$ Ma McKenzie Island stocks (zircon ages, Corfu and Andrews, 1987); FPG* = 2712 ± 2 Ma Ma feldspar porphyry granodiorite dikes (two zircon ages, this paper) and 2714 ± 4 Ma quartz-feldspar porphyry (zircon age, Corfu and Andrews, 1987); GDMD** = 2698 ± 2 Ma granodiorite dike from Madsen (titanite and zircon ages, this paper), and 2696 ± 1 Ma granodiorite dike from Creek zone (titanite age, this paper), GR = $2732.8^{+1.4}_{-1.2}$ Ma Graves assemblage (zircon age, Corfu and Wallace, 1986); HC* = <2747 Ma conglomerate (zircon ages, this paper), <2743 Ma conglomerate (zircon ages, Sanborn-Barrie et al., 2002) ; HLP = 2717 ± 2 Ma Hammell Lake pluton (titanite age, McMaster, 1987); KB = 2704 ± 1.5 Ma Killala-Baird batholith (zircon age, Corfu and Andrews, 1987); Late Au = late-stage gold mineralization; LVL = 2731 ± 3 Ma Little Vermillion Lake batholith (zircon age, Corfu and Andrews, 1987); Mad C = <2700 ± 6 Ma English River assemblage (Austin tuff) conglomerate (zircon ages, Sanborn-Barrie et al., 2002); Main Au = main-stage gold mineralization; McN = $2742^{+5}_{-2}$ and $2742^{+3}_{-2}$ Ma McNeely volcanics (zircon ages, Sanborn-Barrie et al., 2001); MLL* = $2699^{+2}_{-1}$ Ma shallow-dipping melanocratic lamprophyre dike (zircon age, this paper); MSL** = 2702 ± 1 Ma mesocratic lamprophyre dikes (two zircon ages, this paper); PD* = $2701^{+2}_{-1}$ Ma pinky granodiorite dike; SB = <2916 Ma Slate Bay assemblage sedimentary rocks (zircon ages, Corfu et al., 1998); WD = Wilmar granodiorite dike.

multistage iron-carbonate ± quartz and aluminous alteration and veining event(s) prior to and after deposition of the conglomerate, thus expanding the range of hydrothermal alteration to more than 35 m.y.

The minimum age of the colloform-crustiform, barren to low-grade carbonate ± quartz veins and cockade breccias is also constrained by the 2712 ± 2 Ma feldspar porphyry granodiorite dike cutting the high-grade silicified and arsenopyrite-rich carbonate ± quartz veins. Their minimum age might even be ca. <2732 Ma, the age of a quartz-feldspar porphyry dike at the Campbell mine (Sanborn-Barrie et al., 2004), which is late- to postiron carbonate veining. The maximum age of these veins and breccias remains unknown. Dubé et al. (2002, 2003) have presented evidence that iron-carbonate ± quartz veins and/or breccias have accommodated a significant part of the $D_2$ strain and are either early- or pre-$D_2$. Their geometry and cavity-filling textures are, at least in part, compatible with the east-west–directed $D_1$ shortening. There is also evidence of carbonate alteration and/or veining before and after deposition of the conglomerate of the Huston assemblage at 2747 Ma. It remains possible that at least some of the carbonate ± quartz veins were emplaced at ca. 2732 Ma, coincident with the volcanic rocks of the Graves assemblage. The geologic setting associated with these calc-alkaline subaerial volcanic rocks would be compatible with the low-sulfidation epithermal style (e.g. Cooke and Simmons, 2000) of the carbonate ± quartz veins and breccias. However, the isochores of carbonic fluid inclusions combined with the homogenization temperatures of limited aqueous inclusions suggest depths >5 km (Chi et al., 2003), an environment atypical for an epithermal setting, although these authors mentioned that a more accurate estimation of the depth is precluded by the uncertainty in the fluid temperature. Based on their cavity-filling textures and geologic setting, the veins have probably formed between 2 to 5 km below surface under conditions of high fluid pressure in an epizonal crustal setting

(e.g., Groves et al., 2003). They have many features in common with the ankerite veins at the Dome mine in Timmins (Dubé et al., 2003).

The local presence of a significant amount of visible gold in steep- and shallowly dipping mesocratic lamprophyre dikes (Fig. 8A-D) indicates that late-stage gold mineralization (or remobilization) occurred after 2702 ± 1 Ma. The timing of this late-stage gold mineralization relative to the emplacement of the melanocratic lamprophyre dikes ($2699^{+2}_{-1}$ Ma) is unknown, because these dikes are not present in the area of the High-Grade zone. The local presence of visible gold in the mesocratic lamprophyre dikes could suggest that there is only one stage of gold mineralization and that it postdates these 2702 Ma dikes. However, in a scenario involving post-2702 Ma main-stage gold mineralization, it would be impossible to explain how a barren 2712 Ma feldspar porphyry dike could cut across siliceous arsenopyrite-rich high-grade ore (Fig. 6C). Such a scenario would also imply that despite all the paragenetic and chronologic relationships documented, the main stage of mineralization is not related to the arsenopyrite-rich silicic silicification of the carbonate ± quartz veins and selvages (Fig. 4C-D) as there is no such alteration in the lamprophyre dike. Furthermore, it would also imply that the mineralization has no relationship to $F_2$ folding, the main foliation or the faults within the Red Lake mine trend, as the feldspar porphyry dikes cut across the fold limbs and the structural corridor (Figs. 2–3A). More importantly, it would be impossible to explain how lamprophyre dikes could be barren, chilled against, and cut across the high-grade ore but still be premineralization (Figs. 6F, 7A-B, Table 1). The collective arguments presented here indicate that there are two stages of gold mineralization: a pre-2712 Ma main stage related to silicification of iron-carbonate ± quartz veins with associated arsenopyrite and a second stage that is post-2702 Ma and is associated with filling of late brittle fractures, to form a smaller amount of very high grade gold mineralization.

The minimum gap of 10 m.y. between the main stage of gold mineralization (pre-2712 Ma) and emplacement of the mesocratic lamprophyre dikes is significantly larger than the observed space-time relationships between late-kinematic lamprophyric magmatism and gold mineralization elsewhere in the Superior province and worldwide (e.g., Wyman and Kerrich, 1988, 1989; Rock et al., 1989; Kerrich and Cassidy, 1994). Despite the fact that both the gold mineralization and the lamprophyre dikes are late in the geologic evolution of the district, crosscutting relationships and high-precision U-Pb dating argue against a direct genetic and temporal relationship between the main stage of gold mineralization and the lamprophyre dikes at the Campbell-Red Lake deposit. The maximum age of the local late-stage gold mineralization (2702 ± 1 Ma) is coincident with significant magmatic activity in the southern and eastern parts of the district (Figs. 1, 15). However, the minimum age of this second-stage gold mineralization is unknown. It could be related to either the thermal gradient and deformation associated with the emplacement of the Cat Island pluton (Walsh Lake), approximately 7 km east of the deposit, or the ca. 2.63 to 2.66 Ga postorogenic regional thermal event indicated by the hornblende, muscovite, and biotite Ar-Ar cooling ages from the Uchi subprovince (York et al., 1991; Hanes and Archibald, 1998).

The 2712 ± 2 Ma feldspar porphyry dikes cut the Red Lake mine trend at a high angle and are significantly less deformed than the supracrustal packages (Fig. 2), suggesting that the main $D_2$ deformation responsible for the mine trend was pre-2712 Ma. The $2699^{+2}_{-1}$ Ma age of the unstrained shallowly to moderately dipping, melanocratic lamprophyre dike defines the minimum age of the brittle-ductile deformation ($D_2$-$D_3$), at least in the Campbell-Red Lake deposit area.

A post-2702 ± 1 Ma age for the second-stage gold mineralization is consistent with the maximum age of gold-bearing quartz-tourmaline veins that cut the 2701 ± 1.5 Ma Wilmar granodiorite dated by Corfu and Andrews (1987). Although these are two totally different styles of gold mineralization, the possibility that some gold within the Campbell-Red Lake deposit was added, and not just remobilized, around 2700 Ma cannot be ruled out because there are postlamprophyre quartz-tourmaline veins in the deposit as well. However, the quartz-tourmaline veins are barren and the lamprophyre dikes are known to contain significant gold mineralization only where they cut high-grade ore, so remobilization of gold from sites of the main-stage gold mineralization appears to be the most reasonable late-mineralizing process at the Campbell-Red Lake deposit.

The age of the flat-lying melanocratic lamprophyre dike is identical to the age of a steep granodiorite dike at the Madsen mine, dated at 2698 ± 1 Ma (MD-39-99), and similar to the diorite dike that cuts the alteration and deformed rocks at the Creek zone near the former Starratt-Olsen mine (2696 ± 2 Ma; SNB00-5130A; Fig. 15). The dated granodiorite dike at Madsen cuts the mineralization and is weakly deformed compared to the ore zone. The minimum age of this dike is similar to the 2699 ± 4 Ma titanite age from a granodiorite dike collected at surface by Corfu and Andrews (1987). The crosscutting relationships between the dated dike and the ore demonstrate that the main-stage gold mineralization at Madsen predates 2698 Ma and corresponds to the main stage of gold mineralization in the district (Andrews et al., 1986; Corfu and Andrews., 1987). The age of the dike also indicates that the deformed and metamorphosed conglomerate of the English River assemblage from the Madsen mine, dated at <2700 ± 6 Ma by Sanborn-Barrie et al. (2002, 2004), is not part of the same Austin tuff horizon that hosts the bulk of the Madsen deposit, which is older than 2698 Ma, and must be part of a younger sedimentary sequence.

## Conclusions

Main-stage high-grade mineralization in the High-Grade zone of the Red Lake mine formed before 2712 Ma, whereas the less abundant but spectacular second-stage gold mineralization likely formed by remobilization after 2702 Ma. The extremely high gold grades of the Goldcorp High-Grade zone are the result of a combination of factors (Dubé et al., 2002). One of these factors is the local late-stage mineralization and remobilization of highly concentrated gold in fractures at least 10 m.y. after the main stage of mineralization. The minimum age of the brittle-ductile regional deformation in the deposit area is $2699^{+2}_{-1}$ Ma, the age of unfoliated shallowly dipping lamprophyre dikes. This date, combined with the 2698 ± 1 Ma age of the late-deformation granodiorite dike at Madsen and the 2696 ± 2 Ma age of the diorite dike

from the Starratt-Olsen mine area, indicate that the bulk of the ductile strain in the Red Lake district predates ca. 2698 Ma.

The minimum age of gold mineralization at Madsen, the second largest deposit in the district, is 2698 Ma and the maximum age is 2744 ± 1 Ma, the age of an altered and deformed quartz porphyritic unit, interpreted to be a lapilli-crystal tuff in the immediate hanging wall of the main orebody (e.g., Corfu and Andrews, 1987; Dubé et al., 2000). It is possible that the Madsen mineralization formed between 2700 and 2698 Ma, based on the ages of the deformed and metamorphosed Austin tuff conglomerate and the postore dike. However, as the Madsen deposit has been interpreted as early- or pre-$D_2$ deformation (Dubé et al., 2000), it is probable that the mineralization at Madsen was formed between ca. 2723 and 2712 Ma, the interpreted age of $D_2$ in the district, and is similar in age to the mineralization in the Campbell-Red Lake deposit. This would explain the similarities in terms of geologic setting, style of alteration, and mineralization between the Madsen and Campbell-Red Lake deposits (cf. Andrews et al., 1986; Dubé et al., 2000).

According to Sanborn-Barrie et al. (2004), the collisional stage of the Uchian phase of the Kenoran orogeny occurred in the Red Lake belt between ca. 2720 to 2715 Ma. Therefore, the main stage of gold mineralization at the Campbell-Red Lake deposit was likely contemporaneous with and related to large-scale tectonometamorphic event(s) during the collision between the North Caribou and Winnipeg River terranes. Furthermore, the main-stage gold mineralization at Red Lake is older than the main gold event in the Abitibi subprovince (ca. 2680–2670 Ma; Kerrich and Cassidy, 1994). The different ages of penetrative tectonometamorphism across the Superior province are attributed to successive collisional events from north (e.g., Uchian phase of the Kenoran orogeny between 2720–2704 Ma; Stott, 1997) to south (e.g., Abitibi at ca. 2690 Ma; Percival et al., 2003). The main stage of gold mineralization at Red Lake, between ca. 2723 and 2712 Ma, clearly demonstrates that major gold deposits in the Superior province are not restricted to the waning stage of the Archean era. It also illustrates the potential for large gold deposits in Archean greenstone belts in the central and northern portions of this geologic province.

Crosscutting relationships and high-precision U-Pb zircon dating indicate that the formation of the High-Grade zone resulted from protracted multistage hydrothermal event(s) including mainly pre- to early main-stage deformation and iron carbonate ± quartz veining, syndeformation high-grade arsenopyrite-rich silicification, and some late carbonatization and late-stage gold mineralization, all focused in a single hydrothermal and/or structural corridor (Red Lake mine trend). The Red Lake mine trend also was the focus of numerous granodiorite and lamprophyre dikes. Several of these factors have been identified by Groves et al. (2003) as key to the formation of world-class orogenic gold deposits.

Lamprophyre dikes commonly show a spatial relationship with large orogenic gold deposits (Wyman and Kerrich, 1988, 1989; Rock et al., 1989; Kerrich and Cassidy, 1994; Groves et al., 2003). However, this study illustrates that such dikes postdate main-stage gold mineralization at Red Lake by at least 10 m.y. Despite their spatial relationship, a genetic link between the main-stage gold mineralization and the lamprophyre dikes is not supported, although the mineralizing and magmatic systems may have used the same pathways to higher crustal levels, as proposed by Wyman and Kerrich (1988, 1989). The presence of these lamprophyre dikes indicates that the structural corridor (Red Lake mine trend) hosting the Campbell-Red Lake deposit has deep roots that facilitated the emplacement of lamprophyric magmas to higher crustal levels.

In terms of exploration, the main stage of gold mineralization clearly postdates volcanism of the Balmer assemblage at 2990 to 2960 Ma and is contemporaneous with emplacement of the ca. 2718 Ma Dome and McKenzie stocks as well as the Hammell Lake pluton. The <2747 Ma conglomerate from the Huston assemblage in the Red Lake mine occurs at an important interface between Mesoarchean and Neoarchean strata and highlights the proximity of the Campbell-Red Lake deposit to a folded regional unconformity, supporting the empirical spatial and genetic (?) relationship between large gold deposits and regional unconformities in the district (Dubé et al., 2000, 2003; Percival et al., 2000; Sanborn-Barrie et al., 2000; D. Adamson, Rubicon, pers. commun., 2000) and in greenstone belts elsewhere (Hodgson, 1993, Robert, 2000, 2001; Dubé et al., 2003). These regional unconformities result from, or are associated with, large-scale protracted tectonic (faulting and uplift), magmatic, and hydrothermal event(s) to which large gold deposits are empirically related. The unconformities may also provide a first-order guide to the favorable erosion levels for mineralization (Robert., 2001). In Red Lake, this paleosurface represents a key first-order exploration target, as 25.9 Moz (94%) of the 27.6 Moz Au found so far in the district (production, reserves, and resources) is contained in three deposits adjacent to the unconformity (Dubé et al., 2003) . It is proposed that areas of high potential for gold exploration in Red Lake occur in the rocks of the Balmer assemblage within 500 m to 1 km of the unconformity.

## Acknowledgments

Goldcorp Inc., in particular Gilles Filion, Stephen McGibbon, Rob Penczak, John Kovala, Matt Ball, Mark Epp, Michael Dehn, Kimberley DaPatro, and the entire production staff at the mine are thanked for their scientific contribution, logistical and financial support, critical review, and permission to publish. The staff at Placer Dome Inc. is sincerely thanked for numerous underground visits at the Campbell mine and for sharing their knowledge of gold mineralization at Red Lake. Claude Resources Inc. and Placer Dome Inc. are thanked for permission to publish this work. We benefited from and are grateful for the numerous discussions and field visits with Jack Parker of the Ontario Geological Survey. The Ontario Geological Survey and its regional office in Red Lake are thanked for their support and collaboration. Howard Poulsen, François Robert, Vic Wall, Phil Olsen, Walter Balmer, and Jean-François Couture are thanked for constructive discussions. K. Williamson would like to acknowledge INRS-ETE for a scholarship. We thank the staff of the Geological Survey of Canada Geochronology laboratory for their assistance in generating the U-Pb data. Critical reviews by H.K. Poulsen, Rob Penczak, Sebastien

Castonguay, and Patrice Gosselin improved the manuscript. We acknowledge Natural Sciences and Engineering Research Council (NSERC), which has provided a grant through a Partnership Agreement with the Earth Sciences Sector of Natural Resources Canada and Goldcorp mine. Careful constructive reviews for the journal by R. Stern, M. Gauthier, and N. Vielreicher led to substantial improvements.

*January 13, September 2, 2004*

## REFERENCES

Andrews, A.J., Hugon, H., Durocher, M., Corfu, F., and Lavigne, M., 1986, The anatomy of a gold-bearing greenstone belt: Red Lake, northwestern Ontario, *in* Macdonald, A.J., ed., Gold '86 Symposium: Toronto, PDM Digital Publication, p. 3–22.

Chi, G., Dubé, B., and Williamson, K., 2002, Preliminary fluid inclusion microthermometry study of fluid evolution and temperature-pressure conditions in the Goldcorp High-Grade zone, Red Lake mine, Ontario: Geological Survey of Canada Current Research 2002-C27, 14 p.

——2003, Fluid evolution and pressure regimes in the Campbell-Red Lake gold deposit, Red Lake mine trend, Red Lake, Ontario: Fluid-inclusion evidence for a protracted, highly dynamic hydrothermal system: Geological Survey of Canada Current Research 2003, 16 p.

Christie, B.J., 1986, Alteration and gold mineralization associated with a sheeted veinlet zone at the Campbell Red Lake mine, Balmertown, Ontario: Unpublished M.Sc. thesis, Kingston, Ontario, Queen's University, 334 p.

Cooke, D.R., and Simmons, S.F., 2000, Characteristics and genesis of epithermal gold deposits: Society of Economic Geologists Reviews, v. 13, p. 221–244.

Corfu, F., and Andrews, A.J., 1987, Geochronological constraints on the timing of magmatism, deformation, and gold mineralization in the Red Lake greenstone belt, northwestern Ontario: Canadian Journal of Earth Sciences, v. 24, p. 1302–1320.

Corfu, F., and Wallace, H., 1986, U-Pb zircon ages for magmatism in the Red Lake greenstone belt, northwestern Ontario: Canadian Journal of Earth Sciences, v. 23, p. 27–42.

Corfu, F., Davis, D.W., Stone, D., and Moore, M., 1998, Chronostratigraphic constraints on the genesis of Archean greenstone belts, northwestern Superior province, Ontario, Canada: Precambrian Research, v. 92, p. 277–295.

Cowan, P., 1979, The gold content of interflow metasedimentary rocks in the Red Lake area: Unpublished M.Sc. thesis, Hamilton, Ontario, McMaster University, 121 p.

Cumming, G.L., and Richards, J.R., 1975, Ore lead isotope ratios in a continuously changing earth: Earth and Planetary Science Letters, v. 28, p. 155–171.

Damer, G.C., 1997, Metamorphism of hydrothermal alteration at the Red Lake mine, Balmertown, Ontario: Unpublished M.A.thesis, Kingston, Ontario, Queen's University, 195 p.

Davis, W.J., McNicoll, V.J., Bellerive, D.R., Santowski, K., and Scott, D.J., 1997, Modified chemical procedures for the extraction and purification of uranium from titanite, allanite and rutile in the Geochronology Laboratory, Geological Survey of Canada: Radiogenic Age and Isotopic Studies Report 10, Geological Survey of Canada Current Research 1997-F, p. 33–35.

Dubé, B., Balmer, W., Sanborn-Barrie, M., Skulski, T., and Parker, J. 2000, A preliminary report on amphibolite-facies, disseminated-replacement-style mineralization at the Madsen gold mine, Red Lake, Ontario: Geological Survey of Canada Current Research 2000-C17, 12 p.

Dubé, B., Williamson, K., and Malo, M., 2001a, Preliminary report on the geology and controlling parameters of the Goldcorp Inc. High-Grade zone, Red Lake mine, Ontario: Geological Survey of Canada Current Research 2001-C18, 31 p.

——2001b, The Goldcorp High-Grade zone, Red Lake mine, Ontario: A photographic atlas of the main geological features [poster]: Geological Survey of Canada Open File 3890.

——2002, Geology of the Goldcorp Inc. High-Grade zone, Red Lake mine, Ontario: An update: Geological Survey of Canada Current Research 2001-C26, 13 p.

——2003, Gold mineralization within the Red Lake mine trend: Example from the Cochenour-Willans mine area, Red Lake, Ontario, with some new key information from the Red Lake mine and potential analogy with the Timmins camp: Geological Survey of Canada Current Research 2003-C21, 15 p.

Goldcorp Inc., 2003, Annual Report: Toronto, Ontario, 36 p. <http://www.goldcorp.com/mfset.asp>.

Groves, D.I., Goldfarb, R.J., Robert, F., and Hart, C.J.R., 2003, Gold deposits in metamorphic belts: Overview of current understanding, outstanding problems, future research, and exploration significance: Economic Geology, v. 98, p. 1–30.

Gulson, B.L., Mizon, K.J., and Atkinson, B.T., 1993, Source and timing of gold and other mineralization in the Red lake area, northwestern Ontario, based on lead-isotope investigations: Canadian Journal of Earth Sciences, v. 30, p. 2366–2379.

Hanes, J.A., and Archibald, D.A., 1998, Post-orogenic tectonothermal history of the Archean western Superior province of the Canadian Shield as determined by conventional and laser Ar-Ar dating: Western Superior Lithoprobe Transect Annual Workshop, 4th, March 23-24, 1998, University of British Columbia, Vancouver, British Columbia, Lithoprobe Report 65, p. 12–16.

Hodgson, C.J., 1993, Mesothermal lode-gold deposits: Geological Association of Canada Special Paper 40, p. 635–678.

Hugon, H., and Schwerdtner, W.M., 1984, Structural signature and tectonic history of gold-bearing deformed rocks in northwestern Ontario: Ontario Geological Survey Miscellaneous Paper 127, p. 62–72.

Kerrich, R., and Cassidy, K.F., 1994, Temporal relationships of lode gold mineralization to accretion, magmatism, metamorphism and deformation—Archean to present: A review: Ore Geology Reviews, v. 9, p. 263–310.

Kerrich, R., Fryer, B.J., Milner, K.J., and Pierce, M.G., 1981, The geochemistry of gold-bearing chemical sediments, Dickenson Mines, Red Lake Ontario: A reconnaissance study: Canadian Journal of Earth Sciences, v. 18, p. 624–637.

Krogh, T.E., 1982, Improved accuracy of U-Pb zircon ages by the creation of more concordant systems using an air abrasion technique: Geochimica et Cosmochimica Acta, v. 46, p. 637–649.

Kusmirski, T.T.M., 1981, Metallogeny of the "East South C" ore zone in the Dickenson mine, Red Lake Ontario: Unpublished M.Sc. thesis, Hamilton, Canada, McMaster University, 187 p.

Ludwig, K.R., 2001, User's manual for Isoplot/Ex rev. 2.49: A geochronological toolkit for Microsoft Excel: Berkley Geochronology Center Special Publication 1a, 55 p.

MacGeehan, P., And Hodgson, C.J., 1982, Environments of gold mineralization in the Campbell Red Lake and Dickenson mines, Red Lake district, Ontario: Canadian Institute of Mining and Metallurgy Special Volume 24, p. 184–207.

Mathieson, N.A., and Hodgson, C.J., 1984, Alteration, mineralization, and metamorphism in the area of the East South C ore zone, 24th level of the Dickenson mine, Red Lake, northwestern Ontario: Canadian Journal of Earth Sciences, v. 21, p. 35–52.

McMaster, N.D., 1987, A preliminary $^{40}Ar/^{39}Ar$ study of the thermal history and age of gold in the Red Lake greenstone belt: Unpublished M.Sc. thesis, Toronto, Ontario, University of Toronto, 107 p.

Menard, T., and Pattison, D., 1998, Correlation of multiple alteration events with successive tectonic and metamorphic events in the Red Lake gold belt, northwestern Ontario: Western Superior Transect Annual Workshop, 4th, University of British Columbia, Vancouver, British Columbia, Lithoprobe Report 65, p. 63–69.

Menard, T., Pettigrew, N., and Spray, J., 1999, A joint industry-Lithoprobe project on the tectonic history of gold deposits in the Red Lake greenstone belt, Red Lake Ontario, 2740–2700 Ma: Western Superior Transect Annual Workshop, 5th, University of British Columbia, Vancouver, British Columbia, Lithoprobe Report 70, p. 97–103.

Noble, S.R., Grogh, T.E., and Evensen, N.M., 1989, U-Pb age constraints on the evolution of the Trout Lake-Uchi-Confederation Lakes granite-greenstone terrane, Superior province, Canada [abs.]: Geological Association of Canada-Mineralogical Association of Canada, Joint Annual Meeting, Program with Abstracts, v. 14, p. 56.

Parker, J.R., 2000, Gold mineralization and wall rock alteration in the Red Lake greenstone belt: A regional perspective: Ontario Geological Survey Open File Report 6032, p. 22-1 and 22-28.

Parrish, R.R., Roddick, J.C., Loveridge, W.D., and Sullivan, R.W., 1987, Uranium-lead analytical techniques at the Geochronology Laboratory, Geological Survey of Canada: Radiogenic Age and Isotopic Studies Report 1, Geological Survey of Canada Paper 1988-2, p. 3–7.

Penczak, R.S., 1996, The geological context of alteration and gold mineralization at the Campbell mine, Red Lake district, Ontario: Unpublished M.Sc. thesis, Kingston, Canada, Queen's University, 334 p.

Penczak, R.S., and Mason, R., 1997, Metamorphosed Archean epithermal Au-As-Sb-Zn-(Hg) vein mineralization at the Campbell mine, northwestern Ontario: ECONOMIC GEOLOGY, v. 92, p. 696–719.

——1999, Characteristics and origin of Archean premetamorphic hydrothermal alteration at the Campbell gold mine, northwestern Ontario: ECONOMIC GEOLOGY, v. 94. p. 507–528.

Percival, J.A., Bailes, A.H., Corkery, M.T., Dubé, B., Harris, J.R., McNicoll, V., Panagapko, D., Parker, J. Rogers, N., Sanborn-Barrie, M., Skulski, T., Stone, D., Stott, G.M., Thurston, P.C., Tomlinson, K.Y., Whalen, J.B., and Young, M.D., 2000 , Project unit 95-034. An integrated view of western Superior crustal evolution: Highlights of 2000 Natmap studies: Ontario Geological Survey Open File Report 6032, p. 13-1–13-17.

Percival, J.A., Bleeker, W., Cook, F.A., Rivers, T., Ross, G., and van Staal, C., 2003, PanLithopobe Workshop IV: Intra-orogen correlations and comparative orogenic anatomy: Geoscience Canada, v. 30, p. 23–39.

Pirie, J., 1981, Regional geological setting of gold deposits in the Red Lake area, northwestern Ontario: Ontario Geological Survey Miscellaneous Paper 97, p. 71–93.

Ramsay, J.G., and Huber, M.I., 1987, The techniques of modern structural geology. Volume 2: Folds and fractures: London, Academic Press, 700 p.

Rigg, D., and Helmsteadt, H., 1981, Relationships between structures and gold mineralization in Campbell Red Lake and Dickenson mines, Red Lake area, Ontario: Ontario Geological Survey Miscellaneous Paper 97, p.111–127.

Robert, F., 2000, World-class greenstone gold deposits and their exploration [abs.]: International Geological Congress, 31st, Rio de Janeiro, Brasil, August 2000, Vol. De Presentacionnes, CD-ROM, doc. SG304e, 4 p.

——2001, Syenite-associated disseminated gold deposits in the Abitibi greenstone belt, Canada: Mineralium Deposita, v. 36, p. 503–516.

Rock, N.M.S., 1991, Lamprophyres: With additional invited contributions from D.R. Bowes and A.E. Wright: Glasgow and London, Blackie and Son Ltd., 285 p.

Rock, N.M.S., Groves, D.I., and Perring, C.S., 1989, Gold, lamprophyres and porphyries: What does their association mean?: ECONOMIC GEOLOGY MONOGRAPH 6, p. 609–625.

Roddick, J.C., Loveridge, W.D., and Parrish, R.R., 1987, Precise U-Pb dating of zircon at the sub-nanogram Pb level: Chemical Geology, v. 66, p. 111–121.

Rogers, J.A., 1992, The Arthur W. White mine, Red Lake area, Ontario: Detailed structural interpretation the key to successful grade control and exploration: Canadian Mining and Metallurgical Bulletin, v. 85, p. 37–44.

Sanborn-Barrie, M., Skulski, T., Parker, J., and Dubé, B., 2000, Integrated regional analysis of the Red Lake belt and its mineral deposits, western Superior province, Ontario: Geological Survey of Canada Current Research 2000C-18, 12 p.

Sanborn-Barrie, M., Skulski, T., and Parker, J., 2001, 300 m.y. of tectonic history recorded by the Red Lake greenstone belt: Ontario Geological Survey of Canada Current Research 2001-C19, 32 p.

Sanborn-Barrie, M., Skulski, T., Rayner, N., and Parker, J.R, 2002, 300 m.y. evolution of the Red Lake greenstone belt, western Superior province, Ontario: A synthesis of current constraints on volcanism, sedimentation, deformation, metamorphism and gold mineralization [ext. abs.]: Institute on Lake Superior Geology Annual Meeting, 48th, May 12–16, 2002, Kenora, Ontario, Proceedings Volume 48, Part 1-Program and Abstracts, p. 43–45.

Sanborn-Barrie, M., Skulski, T., and Parker, J.R., 2004, Geology, Red Lake greenstone belt western Superior province, Ontario: Gelogical Survey of Canada Open File 4594, 1:50,000 scale color map.

Stern, R.A. 1997, The GSC sensitive high resolution ion microprobe (SHRIMP): Analytical techniques of zircon U-Th-Pb age determinations and performance evaluation: Radiogenic Age and Isotopic Studies Report 10, Geological Survey of Canada Current Research 1997-F, p. 1–31.

Stern, R.A., and Amelin, Y., 2003, Assessment of errors in SIMS zircon U-Pb geochronology using a natural zircon standard and NIST SRM 610 glass: Chemical Geology, v. 197, p. 111–142.

Stott, G.M., 1997, The Superior province, Canada: Oxford Monograph on Geology and Geophysics, v. 35, p. 480–507.

Stott, G.M., and Corfu, F., 1991, Uchi subprovince: Ontario Geological Survey Special Volume 4, part 1, p. 145–236.

Stott, G.M., Corfu, F., Breaks, F.W., and Thurston, P.C., 1989, Multiple orogenesis in northwestern Superior province [abs.]: Geological Association of Canada-Mineralogical Association of Canada Annual Meeting, Montreal, May 15–17, 1989, Program with Abstracts, v. 14, p. A56.

Tarnocai, C., 2000, Gold mineralization at the Campbell mine, Red Lake greenstone belt, Uchi subprovince Ontario: Unpublished Ph.D. thesis, Ottawa, Ontario, University of Ottawa, 227 p.

Thompson, P.H., 2003, Toward a new metamorphic framework for gold exploration in the Red Lake greenstone belt: Ontario Geological Survey Open File Report 6122, 51 p.

Twomey, T., and McGibbon, S., 2001, The geological setting and estimation of gold grade of the High-Grade zone, Red Lake mine, Goldcorp Inc.: Exploration and Mining Geology, v. 10, p. 19–34. (published in 2002).

Wallace, H., Thurston, P.C., and Corfu, F. 1986, Developments in stratigraphic correlation: Western Uchi subprovince: Ontario Geological Survey Miscellaneous Paper 129, p. 88–102.

Wyman, D., and Kerrich, R., 1988, Alkaline magmatism, major structures, and gold deposits: Implications for greenstone belt gold metallogeny: ECONOMIC GEOLOGY, v. 83, p. 454–461.

——1989, Archean shoshonitic lamprophyres associated with Superior province gold deposits: Distribution, tectonic setting, noble metal abundances, and significance for gold mineralization: ECONOMIC GEOLOGY MONOGRAPH 6, p. 651–657.

York, D., Layer, P.W., McMaster, N.D., Hall, C.M., and Masliwec, A., 1991, The dating of Ontario's gold deposits: Ontario Geological Survey Open File Report 5738, 161 p.

Zhang, G., Hattori, K., and Cruden, A., 1997, Structural evolution of auriferous deformation zones at the Campbell mine, Red Lake greenstone belt, Superior province: Precambrian Research, v. 84, p. 83–103.